CHARACTERISTICS OF A FAMILY OF MICROWAVE LUNEBERG LENSES

A Thesis submitted to

the Faculty of Graduate Studies

The University of Manitoba

In Partial Fulfillment

of the Requirements for the Degree of

Doctor of Philosophy

by

Mohamed Atef Barakat

February 1982

CHARACTERISTICS OF A FAMILY OF MICROWAVE LUNEBERG LENSES

BY

MOHAMED ATEF BARAKAT

A thesis submitted to the Faculty of Graduate Studies of the University of Manitoba in partial fulfillment of the requirements of the degree of

DOCTOR OF PHILOSOPHY

To Samia

ABSTRACT

A solution for the electromagnetic field in the presence of a radially stratified spherical lens is used to study the radiation characteristics of the Luneberg lens. It is shown that for a Huygens' source excitation the directivity of a Luneberg lens increases smoothly with the size of the lens and approaches asymptotically that of a uniformly illuminated aperture. On the other hand, the performance of the lens as a focusing element deteriorates continuously at low frequencies and its directivity fall below that of a homogeneous spherical lens.

To enhance the directivity of the lens at low frequencies a new class of modified Luneberg lenses are then introduced. The electromagnetic field of these modified lenses, for a Huygens' source excitation are also obtained by utilizing the spherical wave expansion method. Their radiation characteristics indicate a better focusing property at low frequencies, which are examined for various parameters of the lens profile.

To study the performance of a lens with a practical source antenna, the excitation is represented by an array of Huygens' sources. A rectangular array is used to model the radiated field of an open-ended rectangular waveguide. This source array is then used to generate the desired radiation fields. The effect of a Luneberg lens on the polarization of the field is also studied and for both Huygens and dipole sources the computed data of the co-polar and the cross-polar radiated fields of the lens are presented.

ACKNOWLEDGEMENTS

I want to express my gratitude to Professor L. Shafai for his invaluable guidance, encouragement and patience during all phases of this work. Special thanks are due to Mr. C.G. Saunders of the National Research Council of Canada for his continuous support.

I wish to thank the advisory committee members; Professors E. Bridges and F. Zeiler for their invaluable discussions.

The financial support by the National Research Council of Canada during the early stages of this work and their continuing support during the last two years is deeply appreciated.

TABLE OF CONTENTS

LIST OF FIGURES

LIST OF TABLES

LIST OF SYMBOLS

Unless otherwise stated, the symbols most commonly used in this thesis have the following meaning.

Latin Alphabet:

a	radius of a sphere
a	broad dimension of a rectangular waveguide
C_e	electric dipole current moment
D	diameter of a sphere
dB	decibel
e	subscripts denote even
$\bar{E}$	electric field vector
${}_1F_1$	confluent Hypergeometric function
$\bar{H}$	magnetic field vector
$h_n^{(1)}, h_n^{(3)}$	spherical hankel functions of the first and third kind of order n.
i	$\sqrt{-1}$
j_n	spherical Bessel function
k	propagation constant
$\bar{M}_{\substack{e\\o}mn}$, $\bar{N}_{\substack{e\\o}mn}$	spherical vector wave functions
$P_n^m(\cos\theta)$	associated Legendre polynomial of first kind of order m and degree n
r	radial distance from the origin
$\hat{r}$	unit vector of spherical coordinate system
R	radial distance between the origin and an arbitrary point in space
S_n, T_n	solutions of the radial equation for inhomogeneous sphere

Greek Alphabet:

ϵ	permittivity
η	intrinsic impedance
θ	polar angle
$\hat{\theta}$	unit vector of spherical coordinate system
κ	dielectric constant
λ	wavelength
μ_o	free space permeability
π	pi (3.141592654)
ρ	κr
ϕ	Azimuthal angle
$\hat{\phi}$	unit vector of the spherical coordinate system
ψ	scalar wave function
ω	angular frequency

CHAPTER 1

INTRODUCTION

Recent advances in the communications field, particularly satellite communications, have renewed the need for economical high gain antenna systems. This has resulted in additional efforts towards more thorough investigation of some of the existing antenna designs that has been previously considered impractical due to their complexity. In addition, the availability of new dielectric materials and recent advances in manufacturing techniques have provided economical means of fabricating new antennas.

High gain antennas can be classified into two categories, phase arrays and reflector or lens systems. Phase arrays are normally made of simple radiating elements with a complex feeding system to supply proper input signal to each element. Their characteristics can be controlled easily by the feed system electronics, but are too costly to fabricate and less reliable due to the complexity of their electronics. On the other hand, the reflector and lens systems have a simple feed system and the reflector or lens is used to correct the phase of the feed radiation to provide a uniform phase distribution over the antenna aperture to increase the directivity. Their geometry is therefore simpler than that of a phase array and since the unit operates as a passive phase corrector, they are more reliable. In this thesis we are concerned primarily with the lens antennas and thus, the reflector antennas will not be discussed.

Among the lens antennas, one of the most widely investigated

system is the Luneberg lens. A Luneberg lens [20] is a variable-index, spherically symmetric refracting structure which will form perfect geometrical images of two given concentric spheres on each other. If one of the spheres is of infinite radius, the lens will focus a parallel beam of rays from any direction exactly at a point on the other sphere, or will form a perfectly parallel beam out of rays from a point source on the local sphere. Considerable interest has developed in microwave applications of Luneberg lenses, because of their advantages as wide angle scanners and passive reflectors.

The perfect focusing property of the luneberg lens may be achieved in many number of ways. Luneberg [20] found a particular solution for the index of refraction of a lens which has two given points outside the lens as conjugate foci. His solution takes a simple explicit form if one of the points is at infinity and the other is at the surface of the lens. Brown [3] and Gutman [12] have designed lenses with one focal point at infinity and the other inside the lens. Gutman has shown that it is theoretically possible to build a large diameter Luneberg lens antenna, with which a pencil beam can be scanned over the entire volume of space by moving a point source over a small diameter sphere.

A general expression for the index of refraction of a lens which will focus between two given conjugate points has been presented by Morgan [22]. One of the foci is taken to be outside the lens or at its surface; the other may be outside, inside, or at the surface. Daniele et al [7] and Kay [17], and Huynen [14] have presented general solutions and properties for a certain class of spherically symmetrical lenses with indices of refraction which vary with the radius only.

Their study put great emphasis on the Luneberg lens case.

Several Luneberg lens fabrication techniques have been investigated. Peeler and Coleman [21] and Buckley [18], have presented the stepped-index Luneberg lens and measured the radiation patterns for the prototypes. The lenses were constructed by assembling several molded hemispherical shells of expanded polystyrene material.

Gunderson and Holmes [10] and Gunderson and Kaufman [11] have fabricated two dimensional and three dimensional Luneberg lenses out of foamed borosilicate glass. They indicated that a lens fabricated from glass would have a significant advantage with regard to the environmental effects. Also it will handle six times the power density that a lens fabricated from expanded polystyrene can normally handle.

Several researchers have dealt with the theoretical radiation characteristics of Luneberg lens. Braun [2] has derived an expression for the radiation characteristics of the spherical Luneberg lens. He assumed that the amplitudes of the electric and magnetic fields are arbitrarily known functions of position over the surface of the lens, and the phases are such as to result in a plane phase front perpendicular to the axis of the lens.

An exact theory of the cylindrical or the two-dimensional Luneberg lens has been obtained by Jasik [15]. Tai [33] starting with a general discussion of the electromagnetic field in a radially stratified medium, applied the solution to the spherical Luneberg lens. He also derived the general expression for the electromagnetic field due to a dipole outside and on the surface of the lens. Rozenfeld [29] used the dyadic Green's functions to derive an expression for the electric fields generated by the Huygens source in the presence of a

Luneberg lens.

The scattering of the electromagnetic waves by a Luneberg lens has also received considerable attention by numerous investigators. Garbacz [9] determined the bistatic scattering cross-section of the Luneberg lens of small diameter. The coefficients of the scattered fields were expressed in terms of the TE and TM impedance and admittance functions. This method has a disadvantage due to the fact that both the impedance and admittance functions are rapidly varying functions. These functions can become very large and even unbounded in the region of anti-resonances. A more convenient method from the computational point of view is described by Shafai [32]. The vector potentials are expressed in terms of two auxiliary functions, namely the phase and amplitude functions. The scattered field is given completely by the phase functions and they were found to be relatively smooth and well behaved. Therefore, their computation is more efficient than that of the impedance and admittance functions used by Garbacz. Hizal and Tosun [13] used the state-space formulation for the same purpose. Their results are in good agreement with those of Shafai.

A comparison between the radiation patterns of a Luneberg lens and a homogeneous sphere of small diameter using geometrical optics is reported by Ryan and Cain [30]. They found that the homogeneous lens compares favorably with the Luneberg lens with regard to directivity, beam width and sidelobes. Rozenfeld [29] has computed the directivity of the Luneberg lens and compared it to the directivity of the homogeneous lens. He found that the directivity of small diameter Luneberg lenses is in general lower than that of the homogeneous lens.

The directivity of homogeneous lenses deteriorates while the directivity of Luneberg lenses improves as their diameter increases. Also, Luneberg lens does not present the resonance phenomenon experienced in the homogeneous lenses. This indicates that a Luneberg lens is a more frequency independent antenna than a homogeneous lens. Recently, Onoe et al [23] have introduced a Luneberg lens controllable reflector. The reflection of such a reflector can be modulated by slowly varying data such as temperature and wind velocity.

To enhance the performance of the Luneberg lens at microwave frequencies, we will introduce a new class of modified Luneberg lenses. We will show that the new lens designs will improve all the radiation characteristics of a Luneberg lens, especially, when the lens diameter is in the order of a few wavelengths.

We will also investigate the performance of a Luneberg lens as a wideband antenna. To analyse such antennas a new model of a waveguide radiator as an array of Huygens sources will also be introduced.

Prior to the introduction of the new lens design, a review of the existing lens designs, characteristics, and methods of fabrication are presented in Chapter 2. Chapter 3 presents the spherical vector wave function solution for a radially stratified sphere and hence for the Luneberg lens. The Luneberg lens radiation pattern, directivity and modal power distributions are also presented. Chapter 4 is dedicated to the investigation of the new classes of modified lenses. Starting with the dielectric constant profile of the new lens, we will derive an expression for the radiated field and the radiation characteristics.

The radiation characteristics of Luneberg lenses excited by a

rectangular waveguide and the quality of their radiated field are discussed in Chapter 5. Normally, a waveguide radiator is modelled by a single Huygens source. However, a single Huygens source does not describe adequately the radiation of a waveguide with arbitrary cross-sectional dimensions. We have therefore modelled an open ended rectangular waveguide by a rectangular array of Huygens sources, located at its aperture. It is shown that such an array represents the radiation of the open ended waveguide more accurately and is therefore used to simulate the excitation of a Luneberg lens by a waveguide. The radiation characteristics of both standard and modified Luneberg lenses are then studied using the arrays of Huygens sources. The quality of the radiated fields is also examined by investigating the cross-polar radiation of the lens.

Chapter 6 summarizes the results and presents concluding remarks on the characteristics of Luneberg lenses. It also includes recommendations for future work.

CHAPTER 2

SPHERICALLY SYMMETRIC LENSES

2.1 Introduction

Historically, considerable interest has been shown in scattering by spheres with continuously variable but rotationally symmetric refractive index, due to their ability to focus microwave radiation. According to the geometric optics, radially symmetric spheres can behave as perfectly focusing lenses when they have an appropriate variation of the refractive index.

A classical example of spherically symmetric lenses is the Maxwell "fish-eye" for which the refractive index variation is [1]

$$n(r) = \frac{n_o}{\left[1 + \left(\frac{r}{e}\right)^2\right]} \tag{2.1}$$

where n_o and e are constants and r is the distance from the center of symmetry to an arbitrary point. In such a medium, all rays emanating from this point will be focused elsewhere in the medium. When the medium is a finite sphere, with r the radial distance relative to the radius of the sphere $(0 < r < 1)$, it behaves as a lens, which brings the rays emanating from a point source on the surface, p_o, to focus at the opposite surface point, p. The ray paths are shown in Fig. 2.1 .

A Luneberg lens [15,17,22] is a spherically symmetric structure with a variable refractive index, which will form perfect geomet-

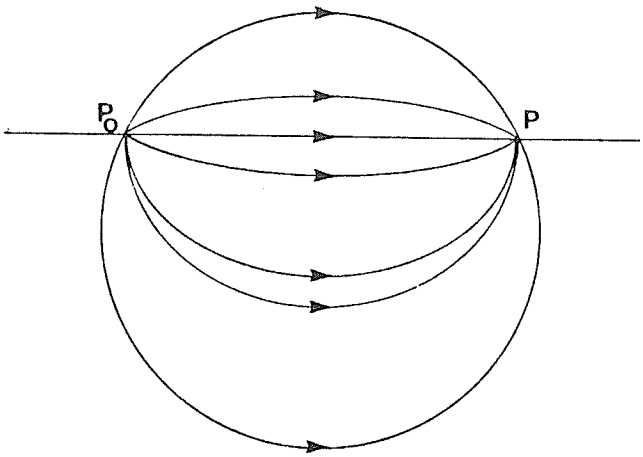

Fig. 2.1 Spherical Maxwell "fish -eye" lens

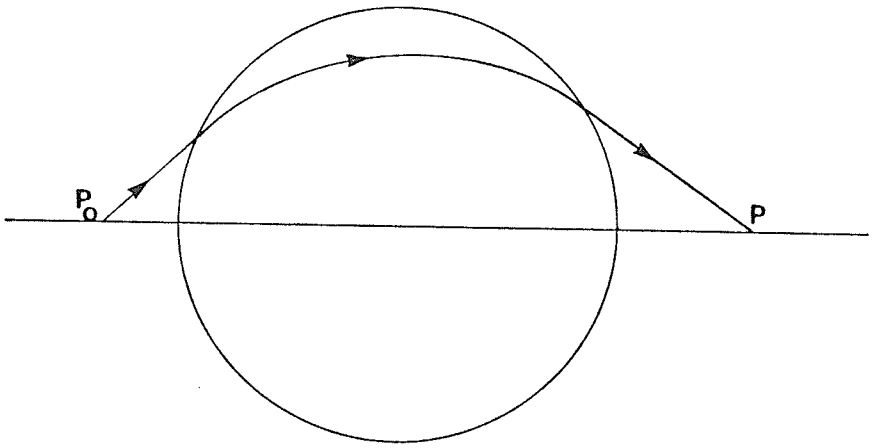

Fig. 2.2 Luneberg lens with two external foci

rical images of two given concentric spheres on each other. Fig. 2.2 and 2.3 illustrate schematic Luneberg lenses, respectively, with two external foci and with one external and one internal focus. When one of the foci is placed on the surface of the lens and the other is moved to infinity, the refractive index profile takes on the following form

$$n(r) = (2 - r^2)^{1/2} \tag{2.2}$$

with the ray path shown in Fig. 2.4. A plane parallel incident beam is brought to a focus at p or the rays from a source at p emerges as a parallel beam at the opposite surface. If the Luneberg lens is now fitted with a spherical cap reflector, it becomes a Luneberg reflecter. Such a lens will behave as a perfect back-scatterer, returning all the incident energy into the backward direction except for the rays lost at the front surface reflection. In a higher order Luneberg lens or reflector [14], the rays reverse within the sphere before coming to a focus as shown in Fig. 2.5.

The isotropic or Eaton lens first proposed as a perfect back-scattering device, which obviates the need for a metallic reflecter. The refractive index variation is

$$n(r) = \left(\frac{2 - r}{r}\right)^{1/2} \tag{2.3}$$

The elliptical path of a ray through an Eaton lens emerges in the backward direction as shown in Fig. 2.6.

Luneberg has developed the theory for the stratified spheres

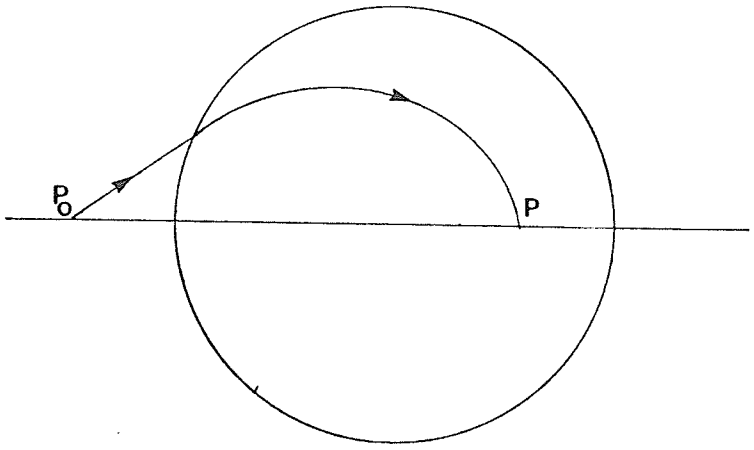

Fig. 2.3 Luneberg lens with one external focus and one internal focus

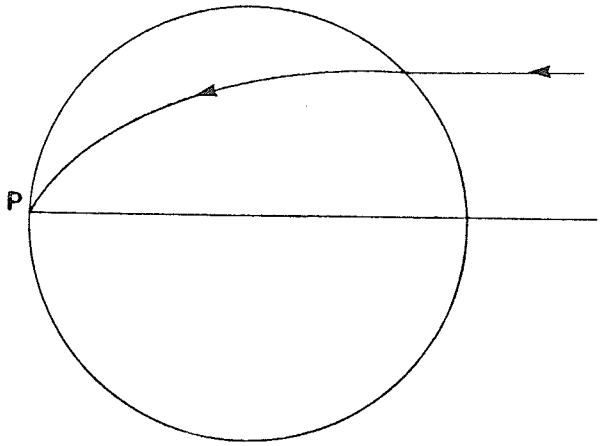

Fig. 2.4 Luneberg lens with one focus at infinity and one on the surface of the lens

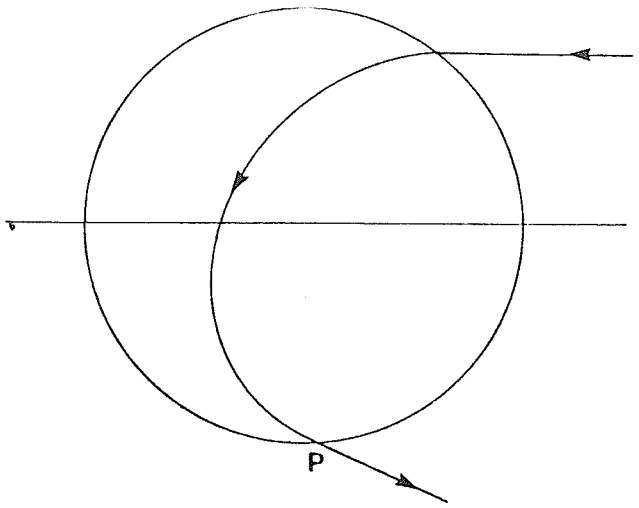

Fig. 2.5 Higher order Luneberg lens with one focus at infinity and the other on the near-side surface of the lens

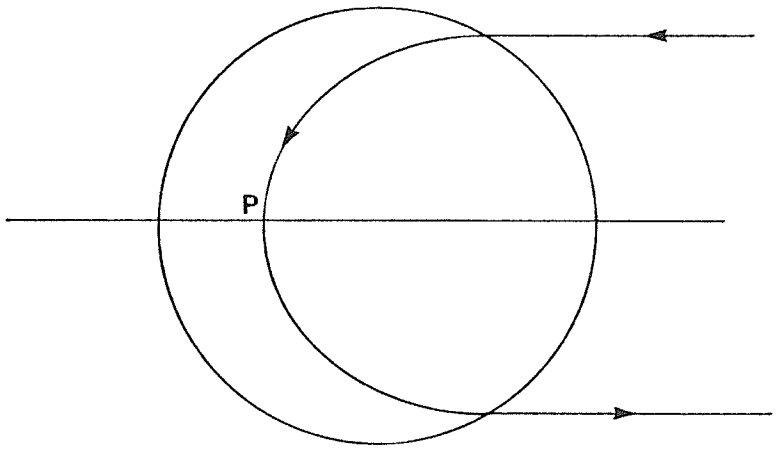

Fig. 2.6 Eaton lens

as an academic exercise in classical optics. However radar workers immediately recognized their utility.

2.2 Luneberg Lens

Luneberg lenses are the most commonly used among all the above classes of lenses. In its complete form, the lens is a sphere with the property that energy from a feed source at any point on the spherical surface, which is propagated through the sphere is focused into parallel rays emerging from the other side of the sphere. Perfect focusing is obtained for all feed positions on the surface.

As presented above the lens is formed as an inhomogeneous medium in which the index of refraction n varies with the lens radius r according to the expression in equation (2.2). A central cross-section of the sphere is shown in Fig. 2.7, together with typical ray paths through the lens. The ray paths are sections of ellipses which are given in polar coordinates by the expression [16]

$$r^2 = \frac{\sin^2\alpha}{1 - \cos\alpha \cos(2\theta-\alpha)} \qquad (2.4)$$

where α is the feed angle defining a particular ray. Because the lens is a symmetrical structure, certain relationships between angles in the system are evident from Fig. 2.7. The most important is the equiangular relationship between the angle formed between the ray and the radius vector at the point where the ray leaves the lens, the polar angle defined by the radius vector to the point at which the ray leaves the lens, and the feed angle. The feed angle is measured at the source

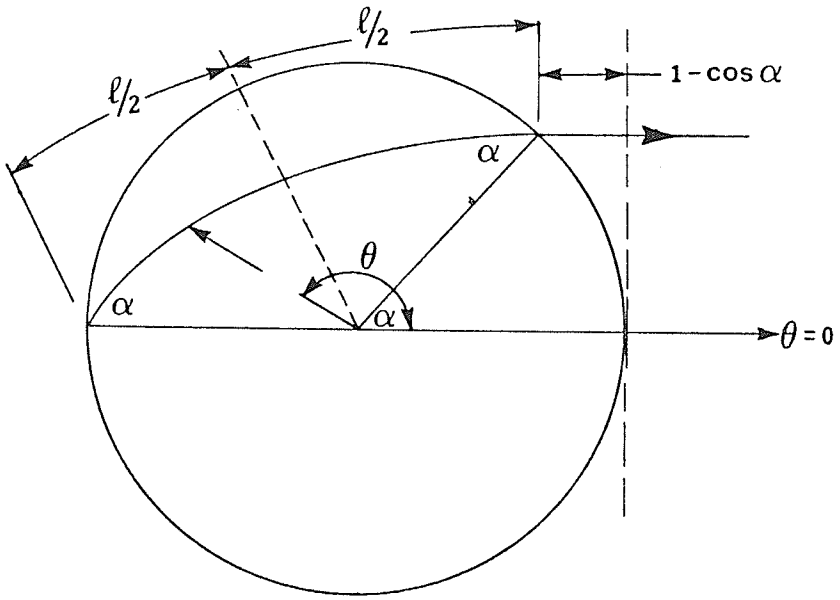

Fig. 2.7 Geometry of Luneberg lens cross-section

point between the central ray and the general ray. This equiangle is designated α in Fig. 2.7.

Another point of interest is the fact that the radius vector normal to the ray path bisects the ray path within the lens. Further geometrical information obtained from Fig. 2.7 shows that the path length of a ray within the lens can be obtained as a function of the feed angle. For a maximum feed angle of 90°, the ray travels along the lens periphery for a distance of $\pi/2$. Other path lengths within the lens can be determined from the fact that the optical path length equals $\pi/2 + \cos\alpha$. From the path length variations, it is possible to give an expression for the variation in the phase across the output arc of the lens cross section as $1 - \cos\alpha$, where α is the polar angle.

Another significant property of the Luneberg lens is the fact that the rays emerging from a feed horn do not appear in a uniform manner across the aperture, but instead tend to spread out in the center and approach a theoretically infinite concentration at the edges. Because of this fact, the analytical aperture illumination is obtained from the original feed pattern multiplied by the factor $\sec\alpha$.

2.2.1 Two-dimensional Luneberg lens

Many variations of the Luneberg lens have been analyzed. The simplest to consider is one in which only a plane section of the lens is utilized [21]. The ray paths through this section are identical to those of Fig. 2.7. However, the emerging wave front is not a plane but a saddle-shaped surface. This surface is the envelope of the Huygens' wavelets, with centres on the semicircular aperture. In rectangular

coordinates, this surface is given by the parametric expression

$$x = \beta$$

$$y = \frac{\sqrt{1 - \alpha^2}}{\alpha} (1 - \beta - \alpha)$$

$$z = \left[(1-\alpha^2)^2 - (\beta-\alpha)^2 - \frac{1-\alpha^2}{\alpha^2} (1-\beta-2\alpha)^2 \right]^{1/2}$$

Because of this distorted wave-front, certain limitations exist in the radiation pattern. This pattern has been analyzed by Peeler and Archer [24], where it is shown that a side-lobe level of 17 to 18 dB exists for all normal feed-horn illuminations. This problem can be circumvented by introducing a linear aperture, as shown in Fig. 2.8. A cylindrical wavefront is produced by this system, and the expected pattern is similar to that obtained from an ordinary line source. It should be pointed out that the introduction of the linear aperture destroys the symmetry of the lens and limits the system to narrower angle of scan.

2.2.2 Virtual-source Luneberg lens

A variation of the Luneberg lens involves the addition of plane metallic reflectors passing through the centre of the lens [26]. The addition of such reflectors produces virtual sources where positions depend on the orientation of the real feed source and the metallic reflector. Fig. 2.9 shows a lens cross-section with a single reflector in place. From a consideration of the ray paths, it is evident that a perfect virtual image of the real source is formed. It should be noted from the figure that not all the energy from the real

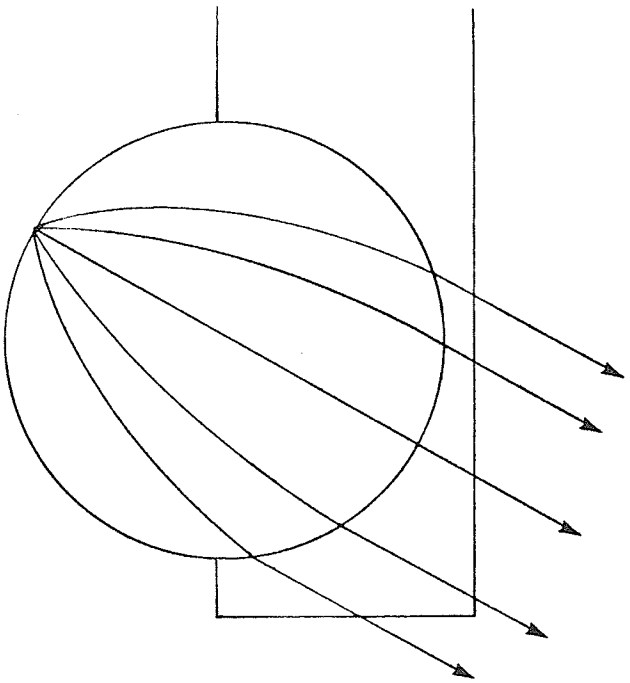

Fig. 2.8 Luneberg lens with linear aperture

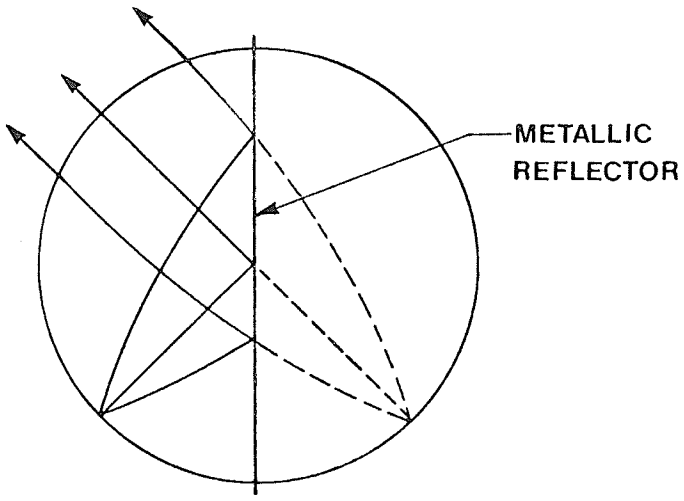

Fig. 2.9 Virtual-source Luneberg lens

source which passes through the lens strikes the reflector. Therefore this antenna will produce two focused beams, one from the real source and one from the virtual source.

It is possible to add more plane reflectors and create a complexity of virtual sources.

2.2.3 Small-feed-circle Luneberg lens

Another variation of the spherical Luneberg lens has produced a system with smaller radius of the feed circle and with limited angle of scan. It is interesting to see that the requirements for a smaller feed circle and perfect focusing does not produce a unique expression for the variations in the index of refraction.

The first expression was obtained by Eaton [8]. He considered a sphere of unit radius, with refractive index equal to unity on the surface and with a feed position at any distance, less than or equal to unity, from the center of the sphere. If the radius of the feed circle is denoted by a then the variation in refractive index is given by the following expression

$$n^2 = \frac{2a - r^2}{a} \qquad \text{for} \quad 0 \leq r \leq a \tag{2.5}$$

$$n^2 = \frac{2 - a}{r} \qquad \text{for} \quad a \leq r \leq 1 \tag{2.6}$$

from the expression it can be seen that if the feed circle radius is one-half the radius of the sphere, the refractive index at the centre is 2 , at the feed circle is 1.7 , and at the edge of the lens it

decreases to unity.

The second expression for a small-feed-circle Luneberg lens was derived by J. Brown [3]. He indicated that the problem could be attacked by assuming a certain variation in the index of refraction between the feed circle and the outer surface and then computing its variation within the feed circle which would yield the desired focusing properties. He considered the problem of bringing all rays incident upon the lens surface into the feed point and displayed two solutions to this problem. The first solution involves choosing a refractive index which is constant in the outer region. In terms of the variables used above, the refractive index was chosen $1/a$. With this constant value of the refractive index, the index variation in the inner region was found by a numerical integration process. For a feed circle of one half the lens radius, the results showed that the index had a maximum value of 2.34 at the lens centre and decreased monotonically to the value 2 at the feed circle. The index in the outer region had the constant value 2 . The variation in the index is then continuous, but the slope of the variation is discontinuous at the feed circle.

Since there is an abrupt discontinuity in the index of refraction at the lens surface, a ray passing from the region in which the index is 2 into free space, where the index is 1 , suffers both reflection and refraction. In order to avoid this problem, Brown considered a lens with index of unity at the surface. He showed that it was impossible under this condition to select a constant index in the outer region. He found one permissible index variation to be

$$r^2 n^2 = 1 + \gamma(1-r)(r-a) \tag{2.7}$$

where γ is a positive constant. Using this value of the index of refraction for the outer region, it was possible to evaluate the index in the inner region from the following expression

$$4an^2 = (1+P)\frac{\left\{\sqrt{\gamma}\ (1+a) + \left[4p^2 + \gamma(1-a)^2\right]^{1/2}\right\}^2}{(p + \sqrt{\gamma}a)^2} \tag{2.8}$$

where $p^2 = 1 - r^2 n^2$.

Brown selected a value of γ equal to $4/a$, since such a value minimized the refractive index required at the lens center. The refractive index varied continuously from 2.2 at the center to 2.0 at the feed circle, and hence to unity at the surface. The slope of the refractive index vs. radius curve was discontinuous at the feed circle.

A third small-feed-circle Luneberg was obtained by Gutman [12]. He selected an index variation given by the expression

$$n^2 = (1 + a^2 - r^2)/a^2$$

He then showed that with the feed at a distance a from the lens center, the outgoing rays would be parallel. It is obvious from this expression that the index and its slope are continuous functions of the radius. For a feed-circle radius equal to one-half the lens radius, the index varies from 2.24 at the lens center to 2 at the feed-circle radius and to unity at the surface.

It is evident, then, that many expressions are available for the design of a small feed-circle Luneberg lens. A comparison of the various designs can be made for feed-circle radius one-half the lens radius on the basis of the maximum refractive index required and the maximum effective aperture obtained. This is shown in Table 2.1, where it can be seen that Eaton's design provides a minimum in the required index but Brown's design provides a maximum effective aperture with only a small increase in refractive index.

TABLE 2.1

Comparison of Small-feed-circle Luneberg Lenses

	Maximum refractive index	Effective Aperture, %
Eaton	2.0	86.6
Brown	2.2	100
Gutman	2.24	100

It should be noted that although all above designs have theoretically produced a small feed circle, the practical utilization of such designs is physically difficult. Also the introduction of the feed and feed mechanism to these designs for practical use may seriously affect their performance.

2.3 Methods of Constructing Luneberg Lenses

Many different methods have been proposed for constructing the Luneberg lens. Several schemes have been attempted in a spherical lens to satisfactorily approximate the variation of the dielectric constant. No practicable scheme for smoothly varying the relative

dielectric constant from two at the centre to one at the surface has been achieved.

Lenses have been made with void-type dielectrics in which a series of flat circular plates of different radii are stacked on one another to approximate a sphere. These plates have a relative dielectric constant of 2 or greater. Holes, 1/8 to 1/2 inch in diameter, are drilled in each plate to reduce the "effective" dielectric constant to more or less the correct value at each point in the sphere. Such dielectrics are neither homogeneous nor isotropic, however, the resulting lenses may be severely sensitive to polarization unless very small holes in very thin plates are employed.

Artificial dielectrics, in which conducting particles are dispersed uniformly in a low-κ medium, are frequency-sensitive, unless the dimensions of the loading elements are either very small with respect to wavelength or in the order of magnitude of a wavelength. In most cases, adequate polarizability requires other than spherical loading elements, with the larger elements of the order of one wavelength, isotropicity then requires complicated and expensive shapes. One reasonable artificial dielectric appears to be one in which very tiny (micron dimesioned) conducting flakes of a metal such as aluminum are randomly dispersed in a low-κ, low density, foam base. Isotropicity and homogeneity are fair to good, but the dissipation factor is too large for many applications in the microwave region [18].

A strait forward approach involves an approximation to the sphere by a central sphere and several spherical shells [21]. The central sphere has a dielectric constant of about 2, while the shells will have decreasing values of dielectric constant with increasing

radius. Through the use of a sufficient number of dielectric shells, a sufficiently close approximation to the required lens can be obtained.

If a two dimensional model of the lens is considered, all the previous methods of construction are applicable. Another construction method involves obtaining the required refractive index by using the concept that the phase velocity of a wave can be varied by varying the spacing between parallel plates [24]. If the electric field vector is parallel to the plates, the required refractive index is obtained by varying plate spacing a according to the following formula

$$a = \frac{\lambda}{(\kappa_e - 2 + r^2)^{1/2}} \qquad (2.10)$$

where κ_e = dielectric constant for medium between parallel plates

r = radial coordinate, $0 \leq r \leq 1$.

Thin metalic cylinders can be used between parallel plates to produce the variation in the refractive index required in the Luneberg lens. If the pins are mounted between the plates so that they are perpendicular to, but do not contact either plate, the desired variation can be obtained by varying the length and spacing of the pins.

The most used technique for the construction of Luneberg lenses is the stepped index technique [18]. In the following section we will review this technique in detail.

2.3.1 Stepped-index Luneberg lenses

In this technique the desired continuous variation of index of refraction with radius is approximated by a number of constant index

spherical shells. The most practical dielectrics for use in such a type are adjustable density foam materials in which the relative dielectric constant can be held within a tolerance of about ± 0.02 for dielectric constant between 1 and 2. These foams can be considered void-type dielectrics, but the voids are very small and random in both size and shape so the isotropicity is reasonably good. The dissipation factor can be kept to less than 0.0005.

The following factors influence the choice of the actual number of steps in any particular case:

a) The maximum required frequency of operation places a limitation on maximum shell thickness of the order of a half wavelength. If shells are much thicker than a half wavelength, a type of wave-trapping phenomenon appears to be possible. It tends to reduce the transmission of energy from one shell to the next.

b) The degree of production-line control over the dielectric constant (± 0.02) may limit the number of steps.

c) Individual shells cannot be made arbitrarily thin because of molding difficulties and the relatively fragile nature of very low-density, low-κ foams. At the outside of a large lens ($\kappa \approx 1$), it is not feasible to make shells much less than 1/8 inch in thickness. The step-wise approximation of the smooth κ versus r curve permits the use of an outermost step which is actually air, and the focal point can be located just outside the surface of the ball. this in turn, permits optimum adjustment of the position of the feed antenna or the cap reflector. Stepped-index Luneberg lenses has been made in practically any diameter from 3 to 48 in. The number of steps varies from a minimum of 10 in small size lenses to 50 in larger units.

2.4 Applications of Luneberg Lenses

Luneberg lenses are commonly used in lens antennas and passive reflectors. If a small broad beamed feed antenna is placed with its effective phase centre at the focal radius of the lens, all energy will radiate into the forward hemisphere. Neglecting the scattering due to finite size of the source and the lens, this radiation will be collimated along the axis of the lens as shown in Fig. 2.10. In practice the feed can be made lightweight, so that it can be moved radially over the surface of the sphere to provide a convenient means of scanning a radiation beam. A series of fixed feeds, electrically switched, is also possible for scanning. The lens does not impose any limitation on the scanning angle, since it can remain stationary while the lightweight feed is moved over its surface.

Typical feed devices are small-aperture waveguide horns, open-end waveguides or dielectric loaded waveguides, the prime requirment being a satisfactory approximation to a point source. The directivity, beam width and side-lobe level of the resulting feed-plus-lens antenna system can be controlled to some extent by modifying the illumination taper and by radial adjustment of the effective phase center of the feed with respect to the focal point.

The majority of Luneberg lenses are used as passive reflectors in conjunction with appropriate cap reflecting surfaces. These are widely used as radar cross-section enhancement devices in target drones or other test vehicles. They are also applied as tow targets, runway markers and seaway channel markers, and in test installation for radar equipment [18].

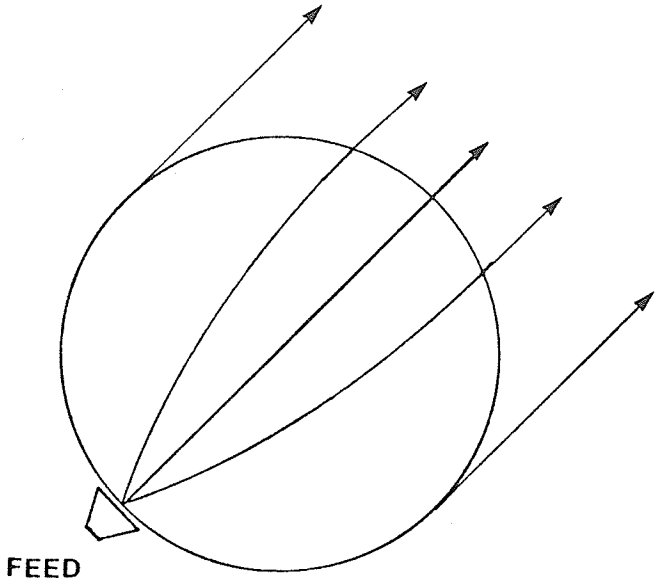

Fig. 2.10 Luneberg lens antenna

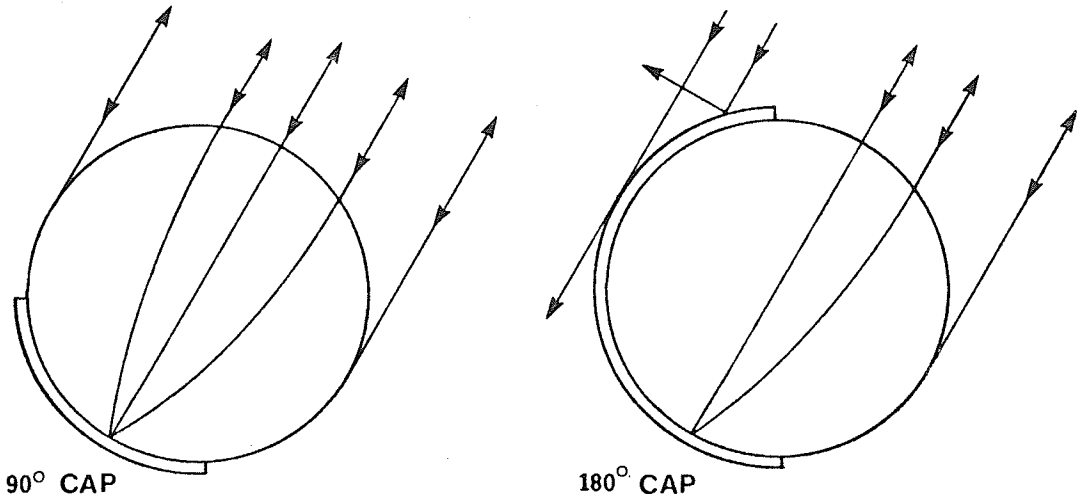

Fig. 2.11 Luneberg lens reflector

If a metallic reflector cap is used to cover a portion of the surace of the lens, the combination will serve as a passive reflector of microwave energy throughout a solid angle equal to that subtended by the cap as shown in Fig. 2.11. If the reflecting cap is circular and subtends a conical angle of 90° at the centre of the sphere, as shown in Fig. 2.11a, the reflector will have a uniform response over a conical angle of 90°. With a 180° cap, the conical response angle will be increased beyond 90° but the response pattern will not be uniform because, as the incident angle changes, a variable portion of the incident radiation will be diverted by the outside surface of the cap. This effect is shown in Fig. 2.11b.

The theoretical scattering cross-section of the Luneberg lens reflector at the angle of maximum response is equal to the scattering cross-section of a circular flat plate whose radius is equal to that of the sphere

$$\sigma = \frac{4\pi^3 R^4}{\lambda^2}$$

where $R \gg \lambda$. In practice, however, σ may be as much as 1.5 db below the theoretical value, due to losses and imperfections in the lens.

Recently a Luneberg controllable reflector [23], which can send information about slowly varying data such as temperature, wind velocity, etc, has been manufactured. The system is achieved by placing half wavelength slots in two overlapping plates with DC bias isolation on the focal phase of a Luneberg lens. The lens reflection can be

controlled by a switching diode inserted at the feed point of the slot.

An experimental reflector consisting of 6 x 48 slots mounted on a Luneberg lens has produced a modulation depth of more than 10 dB over a range of 180 degrees incident angle.

CHAPTER 3

VECTOR WAVE FUNCTIONS FOR THE SPHERICALLY SYMMETRIC LENSES

3.1 Introduction

An electromagnetic field within a volume may be specified in terms of its distribution over the surface enclosing the volume or, by its source distribution. In either case the field generated at any point in space may be represented in terms of certain integrals over the surface and source distributions or, in terms of an appropriate series of wave functions. In the latter case the expansion coefficients are normally determined from the boundary conditions and the source distributions.

The representation of the field in terms of the surface and source distributions provides a simple and general formulation for the field. However, while such an integral formulation is convenient for certain numerical computations it requires the evaluation of the integrals for every field point. On the other hand, the expansion method using appropriate wave functions, represents the field in terms of an infinite series, but its coefficients need to be determined only once. Although, its form is more complex, and the appropriate wave functions, satisfying the boundary condition, can be determined for certain simple geometries, it provides a convenient form for understanding the field behaviour and its computation. For field computation, in this method, the infinite series are usually truncated after a certain number of terms. The required number of terms depends on the type of the field distribution and the size of the object in scattering or antenna

problems.

In the present work the expansion function method is used to formulate the problem of a spherical Luneberg lens. Because of the spherical geometry of the lens, spherical wave functions are utilized. Within the lens the region has a permittivity which is a function of the radial coordinate and appropriate wave functions must be utilized. The form of these functions are discussed first and the total fields both inside and outside the lens are represented by proper series form, with unknown expansion coefficients. These coefficients are determined by utilizing the boundary conditions on the lens surface. For excitation both electric and magnetic dipole sources are considered and the expected field equations are generated. The results are also obtained for a Huygens source, which is simulated by a combination of an electric and a magnetic dipole.

3.2 Vector Wave Functions for a Radially Stratified Medium

The electromagnetic field associated with a radially stratified medium has been discussed by several writers [7, 22, 32, 33, 36].

In a radially stratified medium where the dielectric constant is a function of the radial distance r, measured from the origin of a coordinate system, Maxwell equations in a source-free region can be written in the form

$$\nabla \times \bar{E} = i\omega\mu_o \bar{H} \quad , \tag{3.1}$$

$$\nabla \times \bar{H} = - i\omega\varepsilon_o \kappa(r)\bar{E} \ , \qquad (3.2)$$

$$\nabla \cdot [\kappa(r)\bar{E}] = 0 \ , \qquad (3.3)$$

$$\nabla \cdot \bar{H} = 0 \ , \qquad (3.4)$$

where $\kappa(r)$ denotes the relative dielectric constant with respect to ε_o , and assuming a time dependence of the form $e^{-i\omega t}$.

By eliminating either $\bar{E}$ or $\bar{H}$ from (3.1) and (3.2) one obtains the following two vector equations:

$$\nabla \times \nabla \times \bar{E} - k^2\kappa\bar{E} = 0 \ , \qquad (3.5)$$

$$\nabla \times \nabla \times \bar{H} - \frac{\nabla\kappa}{\kappa} \times \nabla \times \bar{H} - k^2\kappa\bar{H} = 0 \ , \qquad (3.6)$$

where $k^2 = \omega^2\mu_o\varepsilon_o$.

The general solution of (3.5) and (3.6) can be defined by two sets of wave functions.

3.2.1 The magnetic or transverse electric modes

These types of fields are derived by assuming the electric field to be proportional to a vector wave function defined by:

$$\bar{M}^{(m)} = \nabla \times (\psi^{(m)}\hat{r}) \ , \qquad (3.7)$$

where the superscript (m) denotes the magnetic type and $\hat{r}$ denotes

the unit vector in the radial direction (Fig. 3.1). From equations (3.5) and (3.7) $\bar{M}^{(m)}$ is found to be a solution of the wave equation if $\psi^{(m)}$ satisfies

$$\frac{\partial^2\psi^{(m)}}{\partial r^2} + \frac{1}{r^2\sin\theta}\frac{\partial}{\partial\theta}\left(\sin\theta\,\frac{\partial\psi^{(m)}}{\partial\theta}\right) + \frac{1}{r^2\sin^2\theta}\frac{\partial^2\psi^{(m)}}{\partial^2\phi^2} + k^2\kappa\psi^{(m)} = 0 \qquad (3.8)$$

The general solutions for the above equation are

$$\psi^{(m)}_{\substack{e\\o}mn} = S_n(r)P^m_n(\cos\theta)\begin{matrix}\cos\\\sin\end{matrix} m\phi \qquad (3.9)$$

where $P^m_n(\cos\theta)$ denotes the associated Legendre function, and e, 0 for even and odd functions respectively.

The radial function $S_n(r)$ satisfies the differential equation

$$\frac{d^2S_n}{dr^2} + \left[k^2\kappa - \frac{n(n+1)}{r^2}\right]S_n = 0\ . \qquad (3.10)$$

The vector wave functions corresponding to the magnetic field are given by

$$\bar{N}^{(m)}_{\substack{e\\o}mn} = \frac{1}{k}\nabla\times\bar{M}^{(m)}_{\substack{e\\o}mn} \qquad (3.11)$$

where by definition

$$\bar{M}^{(m)}_{\substack{e\\o}mn} = \nabla\times(\psi^{(m)}_{\substack{e\\o}mn}\hat{r})\ . \qquad (3.12)$$

which can be written as

$$\bar{M}^{(m)}_{\substack{e\\o}mn} = \frac{S_n}{r}\left(\mp \frac{mP^m_n}{\sin\theta} \begin{matrix}\sin\\\cos\end{matrix} m\phi\ \hat{\theta} - \frac{\partial P^m_n}{\partial\theta} \begin{matrix}\cos\\\sin\end{matrix} m\phi\ \hat{\phi}\right) = \frac{S_n}{r}\bar{m}_{\substack{e\\o}mn} \qquad (3.13)$$

$$\bar{N}^{(m)}_{\substack{e\\o}mn} = \frac{1}{k}\left[\frac{n(n+1)}{r^2} S_n P^m_n \begin{matrix}\cos\\\sin\end{matrix} m\theta\ \hat{r} + \frac{1}{r}\frac{\partial S_n}{\partial r}\left(\frac{\partial P^m_n}{\partial\theta} \begin{matrix}\cos\\\sin\end{matrix} m\phi\ \hat{\theta} \mp \frac{mP^m_n}{\sin\theta} \begin{matrix}\sin\\\cos\end{matrix} m\phi\ \hat{\phi}\right)\right]$$

$$= \frac{1}{k}\left[\frac{S_n}{r^2}\bar{l}_{\substack{e\\o}mn} + \frac{1}{r}\frac{\partial S_n}{\partial r}\left(\hat{r} \times \bar{m}_{\substack{e\\o}mn}\right)\right] \quad . \qquad (3.14)$$

where $\bar{m}_{\substack{e\\o}mn} = \mp \frac{mP^m_n}{\sin\theta} \begin{matrix}\sin\\\cos\end{matrix} m\phi\ \hat{\theta} - \frac{\partial P^m_n}{\partial\theta} \begin{matrix}\cos\\\sin\end{matrix} m\phi\ \hat{\phi}$

and

$$\bar{l}_{\substack{e\\o}mn} = n(n+1)\ P^m_n \begin{matrix}\cos\\\sin\end{matrix} m\phi\ \hat{r}$$

3.2.2 The electric or transverse magnetic modes

The electric or the transverse magnetic modes are derived by assuming the magnetic field to be proportional to a vector wave function defined by

$$\bar{M}^{(e)} = \nabla \times (\psi^{(e)}\hat{r}) \ , \qquad (3.15)$$

where the superscript (e) denotes the electric type. By the same procedure used in section 3.2.1, $\bar{M}^{(e)}$ is a solution for the wave

equation if $\psi^{(e)}$ satisfies

$$\frac{\partial \psi^{(e)}}{\partial r^2} - \frac{1}{\kappa}\frac{d\kappa}{dr}\frac{\partial \psi^{(e)}}{\partial r} + \frac{1}{r^2 \sin\theta}\frac{\partial}{\partial \theta}\left(\sin\theta \frac{\partial \psi^{(e)}}{\partial \theta}\right) +$$

$$+ \frac{1}{r^2 \sin^2\theta}\frac{\partial^2 \psi^{(e)}}{\partial \phi^2} + k^2 \kappa \psi^{(e)} = 0 \ . \qquad (3.16)$$

The general solutions for 3.16 are given by

$$\psi^{(e)}_{\substack{e \\ o}mn} = T_n(r) P_n^m(\cos\theta) \begin{matrix}\cos \\ \sin\end{matrix} m\phi \ , \qquad (3.17)$$

where $T_n(r)$ satisfies the differential equation

$$\frac{d^2 T_n}{dr^2} - \frac{1}{\kappa}\frac{d\kappa}{dr}\frac{dT_n}{dr} + \left[k^2 \kappa - \frac{n(n+1)}{r^2} \right] T_n = 0 \ . \qquad (3.18)$$

Equation (3.18) differs considerably from equation (3.10) when κ is a function of r, but they become the same when κ is a constant. The vector wave function representing the electric field in this case is given by

$$\bar{N}^{(e)}_{\substack{e \\ o}mn} = \frac{1}{k\kappa} \nabla \times \bar{M}^{(m)}_{\substack{e \\ o}mn} \ , \qquad (3.19)$$

where

$$\bar{M}^{(e)}_{\substack{e \\ o}mn} = \nabla \times (\psi^{(e)}_{\substack{e \\ o}mn} \hat{r}) \ . \qquad (3.20)$$

The electromagnetic field associated with a radially stratified medium

in a source-free region can in general be represented by

$$\bar{E} = \sum_n \left(A_n \bar{M}_n^{(m)} + B_n \bar{N}_n^{(e)}\right) \quad , \tag{3.21}$$

$$\bar{H} = \frac{k}{i\omega\mu_o} \sum_n \left(A_n \bar{N}_n^{(m)} + B_n \bar{M}_n^{(e)}\right) \quad , \tag{3.22}$$

3.3 Solution for the Spherical Luneberg Lens

The spherical Luneberg lens is characterized by a dielectric constant which varies according to the relation

$$\kappa = 2 - \left(\frac{r}{a}\right)^2 \quad , \quad 0 \leq r \leq a \quad , \tag{3.23}$$

where a is the lens radius. When equation (3.23) is substituted into equation (3.10) the resultant equation is transformable into the confluent hypergeometric equation [33]. One solution for that equation, which is finite at $r = 0$ is given by

$$S_n = \rho^{n+1} \; e^{-\rho^2/2\rho_a} \; {}_1F_1(\alpha, \gamma, \rho^2/\rho_a) \quad , \tag{3.24}$$

where

$$\rho = kr \quad , \quad \rho_a = ka$$
$$\alpha = \frac{1}{2}(n + \frac{3}{2} - \rho_a) \quad , \quad \gamma = n + \frac{3}{2}$$

${}_1F_1(\alpha, \gamma, z)$ denotes the confluent hypergeometric function or Kummer's function that satisfies the differential equation

$$\frac{d^2w}{dz^2} + \left(\frac{\gamma}{z} - 1\right) \frac{dw}{dz} - \frac{\alpha}{z} w = 0 \ . \qquad (3.25)$$

when equation (3.23) is substituted into equation (3.18) the resultant equation becomes

$$\frac{d^2T_n}{d\rho^2} + \frac{2\rho}{2\rho_a^2 - \rho^2} \frac{dT_n}{d\rho} + \left[2 - \frac{\rho^2}{\rho_a^2} - \frac{n(n+1)}{\rho^2}\right] T_n = 0 \qquad (3.26)$$

where

$$T_n = (2\rho_a^2 - \rho^2)^{1/2} \rho^{n+1} e^{-\rho^2/2\rho_a} U_n \qquad (3.27)$$

and

U_n satisfies the equation .

$$\frac{d^2U_n}{d\rho^2} + 2\left(\frac{n+1}{\rho} - \frac{\rho}{\rho_a}\right) \frac{dU_n}{d\rho} + \left[2 - \frac{2n+3}{\rho_a}\right.$$

$$\left. - \frac{1}{2\rho_a^2 - \rho^2} - \frac{3\rho^2}{(2\rho_a^2 - \rho^2)^2}\right] U_n = 0 \ . \qquad (3.28)$$

A further transformation of the independent variable $z = \rho^2/\rho_a$ converts (3.28) into

$$\frac{d^2U_n}{dz^2} + \left(\frac{\gamma}{z} - 1\right) \frac{dU_n}{dz} - \left[\frac{\alpha_1}{z} + \frac{2\alpha_2}{z - a_2} - \frac{2a_2\alpha_3}{(z - a_2)^2}\right] U_n = 0$$

with

$$\gamma = n + \frac{3}{2}$$

$$\alpha_1 = \frac{1}{2}\left(n + \frac{3}{2} - \rho_a + \frac{1}{4\rho_a}\right)$$

$$\alpha_2 = -\frac{1}{16\rho_a}$$

$$\alpha_3 = -\frac{3}{16\rho_a}$$

$$a_2 = 2\rho_a$$

Tai [33] has found that the differential equation for T_n is basically different from the differential equation for S_n, and he called it the generalized confluent hypergeometric function.

3.4 Radiation from an Electric Dipole in the Presence of a Spherical Luneberg Lens

A horizontal electric dipole of moment P_x is located parallel to x-direction at r = b, θ = o, φ = o, Fig. 3.1. The field due to the dipole in free space is given by

$$\bar{E}^i = \frac{ik^3 p_x}{4\pi\varepsilon} \sum_{n=1}^{\infty} \frac{2n+1}{n(n+1)}$$

$$h_n^{(1)}(\rho_b)\, \bar{M}_{oln}^{(1)} + \frac{[\rho_b h_n^{(1)}(\rho_b)]'}{\rho_b} \bar{N}_{eln}^{(1)} \qquad r \leq b$$

$$j_n(\rho)\, \bar{M}_{oln}^{(3)} + \frac{[\rho_b j_n(\rho_b)]'}{\rho_b} \bar{N}_{eln}^{(3)} \qquad r \geq b \tag{3.29}$$

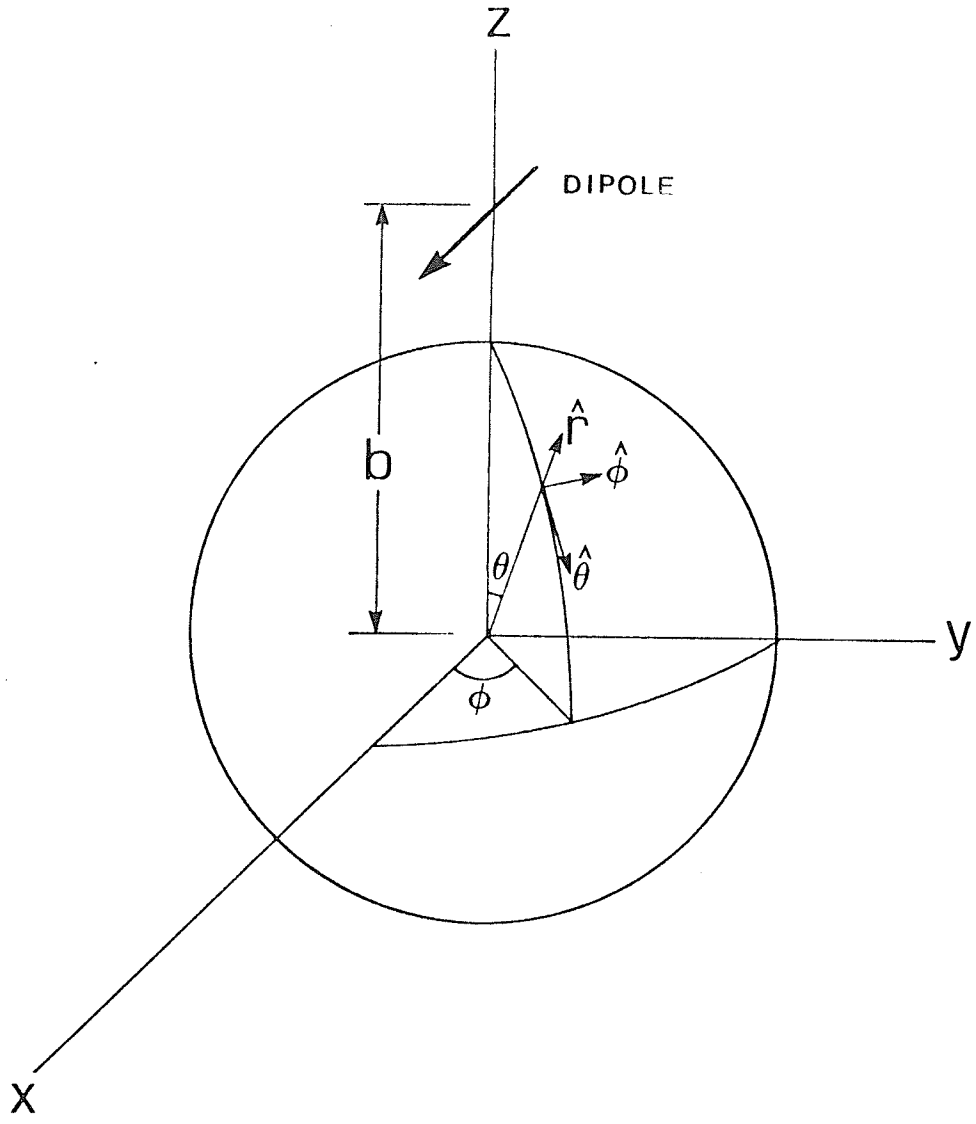

Fig. 3.1 Spherical coordinate system

$$\bar{H}^i = \frac{\omega k^2 p_x}{4\pi} \sum_{n=1}^{\infty} \frac{2n+1}{n(n+1)}$$

$$h_n^{(1)}(\rho_b)\,\bar{N}_{oln}^{(1)} + \frac{[\rho_b h_n^{(1)}(\rho_b)]'}{\rho_b}\,\bar{M}_{eln}^{(1)} \qquad r \leq b \tag{3.30}$$

$$j_n(\rho_b)\,\bar{N}_{oln}^{(3)} + \frac{[\rho_b j_n(\rho_b)]'}{\rho_b}\,\bar{M}_{eln}^{(3)} \qquad r \geq b$$

where

$$\rho_b = kb \ ,$$

$$\bar{M}_{\substack{e\\o}ln}^{(1)} = \nabla \times [r j_n(kr) P_n^1(\cos\theta) \begin{matrix}\cos\\ \sin\end{matrix} \phi\, \hat{r}] \ ,$$

$$\bar{N}_{\substack{e\\o}ln}^{(1)} = \frac{1}{k} \nabla \times \bar{M}_{\substack{e\\o}ln}^{(1)} \ .$$

The vector wave functions of the third kind $\bar{M}_{oln}^{(3)}$, $\bar{N}_{eln}^{(3)}$, $\bar{M}_{eln}^{(3)}$, $\bar{N}_{oln}^{(3)}$ can be obtained by replacing $j_n(kr)$ by $h_n^{(1)}(kr)$. The primes denote derivative with respect to the argument ρ_b .

The scattered field in the presence of the lens and transmitted fields inside the lens may be shown to be in the form

$$\bar{E}^s = \frac{ik^3 p_x}{4\pi\epsilon} \sum_{n=1}^{\infty} \frac{2n+1}{n(n+1)} \{\alpha_n^{(m)} h_n^{(1)}(\rho_b) \bar{M}_{oln}^{(3)}$$

$$+ \alpha_n^{(e)} \frac{[\rho_b h_n^{(1)}(\rho_b)]'}{\rho_b} \bar{N}_{eln}^{(3)}\} \ , \tag{3.31}$$

$$\bar{H}^s = \frac{k^2 p_x \omega}{4\pi} \sum_{n=1}^{\infty} \frac{2n+1}{n(n+1)} \{\alpha_n^{(m)} h_n^{(1)}(\rho_b) \bar{N}_{oln}^{(3)}$$

$$+ \alpha_n^{(e)} \frac{[\rho_b h_n^{(1)}(\rho_b)]'}{\rho_b} \bar{M}_{eln}^{(3)}\} \quad , \quad r \geq a \quad , \tag{3.32}$$

$$\bar{E}^t = \frac{ik^3 p_x}{4\pi\epsilon} \sum_{n=1}^{\infty} \frac{2n+1}{n(n+1)} \{\beta_n^{(m)} h_n^{(1)}(\rho_b) \bar{M}_{oln}^{(m)}$$

$$+ \beta_m^{(e)} \frac{[\rho_b h_n^{(1)}(\rho_b)]'}{\rho_b} \bar{N}_{eln}^{(e)}\} \quad , \tag{3.33}$$

$$\bar{H}^t = \frac{k^2 p_{x\omega}}{4\pi} \sum_{n=1}^{\infty} \frac{2n+1}{n(n+1)} \{\beta_n^{(m)} h_n^{(1)}(\rho_b) \bar{N}_{oln}^{(m)}$$

$$+ \beta_n^{(e)} \frac{[\rho_b h_n^{(1)}(\rho_b)]'}{\rho_b} \bar{M}_{eln}^{(e)} \} \quad , \quad r \leq a \quad . \tag{3.34}$$

The coefficients $\alpha_n^{(m)}$, $\alpha_n^{(e)}$, $\beta_n^{(m)}$ and $\beta_n^{(e)}$ can be determined by applying the boundary conditions that $\hat{r} \times \bar{E}$ and $\hat{r} \times \bar{H}$ are continuous at the surface of the sphere. This gives

$$\alpha_n^{(m)} = \frac{R_1}{R_3}\left(\frac{R_1'}{R_1} - \frac{S_a'}{S_a}\right) \Big/ \left(\frac{S_a'}{S_a} - \frac{R_3'}{R_3}\right) ,$$

$$\beta_n^{(m)} = \frac{R_1}{S_a}\left(\frac{R_1'}{R_1} - \frac{R_3'}{R_3}\right) \Big/ \left(\frac{S_a'}{S_a} - \frac{R_3'}{R_3}\right) , \qquad (3.35)$$

$$\alpha_n^{(e)} = \frac{R_1}{R_3}\left(\frac{R_1'}{R_1} - \frac{T_a'}{T_a}\right) \Big/ \left(\frac{T_a'}{T_a} - \frac{R_3'}{R_3}\right) ,$$

$$\beta_n^{(e)} = \frac{R_1}{T_a}\left(\frac{R_1'}{R_1} - \frac{R_3'}{R_3}\right) \Big/ \left(\frac{T_a'}{T_a} - \frac{R_3'}{R_3}\right) . \qquad (3.36)$$

where

$$R_1 = \rho_a j_n(\rho_a) , \quad R_1' = \frac{d}{d\rho}\left[\rho\, j_n(\rho)\right]\Big|_{\rho=\rho_a} ,$$

$$R_3 = \rho_a h_n^{(1)}(\rho_a) , \quad R_3' = \frac{d}{d\rho}\left[\rho\, h_n^{(1)}(\rho)\right]\Big|_{\rho=\rho_a} ,$$

$$S_a = S_n(\rho_a) , \qquad S_a' = \frac{d}{d\rho} S_a(\rho)\Big|_{\rho=\rho_a} ,$$

$$T_a = T_n(\rho_a) , \qquad T_a' = \frac{d}{d\rho} T_n(\rho)\Big|_{\rho=\rho_a} ,$$

$$\rho_a = Ka$$

For the Luneberg lens case the source should be situated at the surface of the sphere corresponding to $b = a$. The total electric field due to the dipole in the presence of the lens is therefore

$$\bar{E}_e = \frac{k^2 p_x}{4\pi\epsilon a} \sum_{n=1}^{\infty} \frac{2n+1}{n(n+1)} \cdot$$

$$\cdot \frac{1}{R_3} \left[\frac{\bar{M}^{(3)}_{oln}}{\left(\frac{R'_3}{R_3} - \frac{S'_a}{S_a}\right)} + \frac{\bar{N}^{(3)}_{eln}}{\left(\frac{T_a}{T'_a}\frac{R'_3}{R_3} - 1\right)} \right] \cdot \qquad (3.37)$$

The far-zone expression for $\bar{E}_e$ can be obtained using the asymtotic expression for $\bar{M}^{(3)}_{oln}$, $\bar{N}^{(3)}_{eln}$ given by

$$\bar{M}^{(3)}_{oln} \simeq (-i)^{n+1} \frac{e^{i\rho}}{\rho} \bar{m}_{oln} ,$$

$$\bar{N}^{(3)}_{eln} \simeq (-i)^{n} \frac{e^{i\rho}}{\rho} (\hat{r} \times \bar{m}_{eln}) ;$$

$$\rho = kr$$

resulting in the far electric field of the form

$$\bar{E}_e = \frac{k^2 p_x}{4\pi\varepsilon a}\left(\frac{e^{i\rho}}{\rho}\right)\sum_{n=1}^{\infty}(-i)^n\frac{2n+1}{n(n+1)}$$

$$\cdot\frac{1}{R_3}\left[\frac{-i\bar{m}_{oln}}{\left(\frac{R_3'}{R_3}-\frac{S_a'}{S_a}\right)}+\frac{r\times\bar{m}_{eln}}{\left(\frac{T_a R_3'}{T_a' R_3}-1\right)}\right]. \qquad (3.38)$$

3.5 Radiation from a Magnetic Dipole in the Presence of a Luneberg Lens

When considering the radiation of a magnetic dipole it is convenient to use the duality principle [6, 33]. To change from a system of fields excited by an electric source to one excited by the magnetic source, or vice versa, it is only necessary to replace the quantities by their duals as presented in Table 3.1.

TABLE 3.1

Duality Relationship

Electric source	E	H	μ	ε	k
Magnetic source	H	-E	ε	μ	k

The expression for the magnetic field due to a magnetic dipole located on the surface of the sphere in the negative y direction can then be written as [6]

$$\bar{H}_m = \frac{-k^2 p_y}{4\pi a} \sum_{n=1}^{\infty} \frac{2n+1}{n(n+1)} \frac{1}{R_3} \left[\frac{\bar{M}_{eln}^{(3)}}{\frac{R_3'}{R_3} - \frac{T'}{T_a}} + \frac{\bar{N}_{oln}^{(3)}}{\frac{S_a}{S_a'} \frac{R_3'}{R_3} - 1} \right] \tag{3.39}$$

since

$$\bar{E}_m = \frac{1}{i\omega\varepsilon_o} \bar{\nabla} \times \bar{H}_m$$

The electric field radiated by the magnetic dipole is given by

$$\bar{E}_m = \frac{ik^2 p_y}{4\pi a} \sum_{n=1}^{\infty} \frac{2n+1}{n(n+1)} \frac{1}{R_3} \left[\frac{\bar{M}_{oln}^{(3)}}{\frac{R_3' S_a}{R_3 S_a'} - 1} + \frac{N_{eln}^{(3)}}{\frac{R_3'}{R_3} - \frac{T_a'}{T_a}} \right] \tag{3.40}$$

3.6 Radiation from a Huygens Source in the Presence of a Luneberg Lens

In many practical situations a Luneberg lens may be excited by an aperture radiator, such as an open ended waveguide. An exact solution for a lens illuminated by a waveguide radiator is not feasible, but may be simulated by a combination of an electric and a magnetic dipole forming a Huygens source. This representation is approximate and neglects the diffraction effects at the waveguide open end. However, it provides a convenient means of approximating the waveguide radiator and investigation of lens radiation characteristics. In this section, we therefore, first define a Huygens source and present its field and properties.

3.6.1 Elementary Huygens source

Assume that a constant electric and magnetic current source $J_x = \bar{J}_o$ and $M_y = -\bar{M}_o$ of equal length $L \ll \lambda$ are simultaneously placed at the origin of the spherical coordinate system, Fig. 3.1.

If the currents are adjusted such that

$$\eta \bar{J}_o L = \bar{M}_o L$$

then the far fields of this source are given by

$$E_\theta = \frac{-ik \exp(iKr)}{4\pi r} \cos\phi(1 - \cos\theta) J_o L \qquad (3.41)$$

$$E_\phi = \frac{-ik \exp(iKr)}{4\pi r} \sin\phi(1 - \cos\theta) J_o L \, . \qquad (3.42)$$

The unique feature of this fictitious source compared to the electric or the magnetic current elements is the factor $(1 - \cos\theta)$ which tends to cancel the far field radiation pattern in the region $0 \leq \theta \leq \pi/2$. Figure 3.2 shows the radiation pattern for a Huygens' source in free space. Due to this cardoid shape, aperture antennas which have similar field distributions can be represented by Huygens' source elements.

3.6.2 Huygens source in the presence of a Luneberg lens

To obtain the electric field due to a Huygens source located at the surface of a sphere, combine equation (3.37) with equation (3.40), the resulting field equation is given by

$$\bar{E}_H(r) = \frac{ik^3 P_x}{4\pi\varepsilon} \sum_{n=1}^{\infty} \frac{2n + 1}{n(n + 1)} \left\{ (A_n + D_n) \bar{M}_{oln} + (B_n + C_n) \bar{N}_{eln} \right\} \qquad (3.43)$$

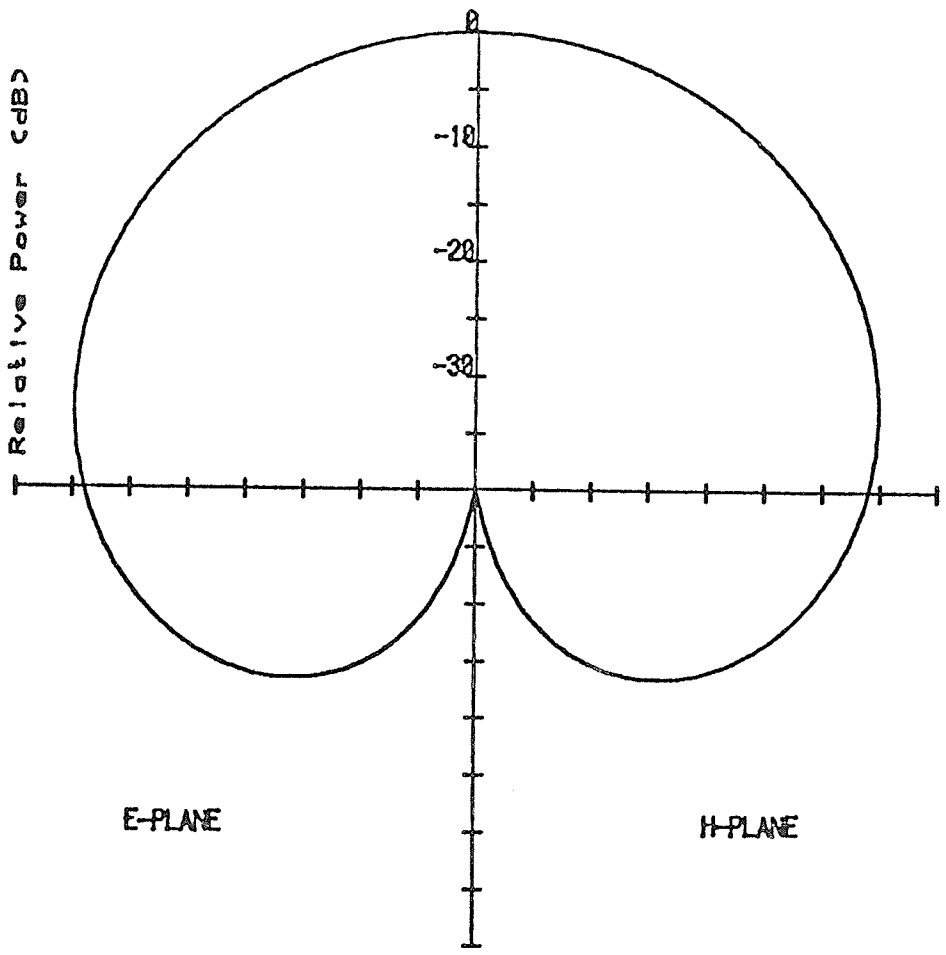

Fig. 3.2 Radiation pattern of a Huygens' source

where

$$A_n = j_n(\rho_a) + \alpha_n^{(m)} h_n^{(1)}(\rho_a) \tag{3.44}$$

$$B_n = \frac{R_1'}{\rho_a} + \alpha_n^{(e)} \frac{R_3'}{\rho_a} \tag{3.45}$$

$$C_n = i j_n(\rho_a) + i\, \alpha_n^{(e)}\, h_n^{(1)}(\rho_a) \tag{3.46}$$

$$D_n = - i \frac{R_1'}{\rho_a} - i\, \alpha_n^{(m)} \frac{R_3'}{\rho_a} \quad . \tag{3.47}$$

From equations (3.35), (3.36) and the equation

$$R_1 R_3' - R_1' R_3 = \rho j_n(\rho)\, [\rho h_n^{(1)}(\rho)]' - \rho h_n^{(1)}(\rho)[\rho j_n(\rho)]' = i \tag{3.48}$$

and after some algebraic manipulation it is found that

$$A_n = \frac{i}{\rho_a} \cdot \frac{1}{R_3} \cdot \frac{1}{\left(\frac{R_3'}{R_3} - \frac{S_a'}{S_a} \right)} \tag{3.49}$$

$$B_n = \frac{i}{\rho_a} \cdot \frac{1}{R_3} \cdot \frac{\frac{T_a'}{T_a}}{\left(\frac{R_3'}{R_3} - \frac{T_a'}{T_a} \right)} \tag{3.50}$$

$$C_n = -\frac{1}{\rho_a} \cdot \frac{1}{R_3} \cdot \frac{1}{\left(\frac{R_3'}{R_3} - \frac{T_a'}{T_a}\right)} \tag{3.51}$$

$$D_n = \frac{1}{\rho_a} \cdot \frac{1}{R_3} \cdot \frac{\frac{S_a'}{S_a}}{\left(\frac{R_3'}{R_3} - \frac{S_a'}{S_a}\right)} \cdot \tag{3.52}$$

Now the far-zone field expressions may be written as

$$\bar{E}_H(r) = \frac{ik^2 P_x}{4\pi\epsilon} \frac{e^{ikr}}{r} \sum_{n=1}^{\infty} \frac{2n+1}{n(n+1)} (-i)^n$$

$$\left\{-i\,(A_n + D_n)\,\bar{m}_{oln} + (B_n + C_n)\,\bar{n}_{eln}\right\} \cdot \tag{3.53}$$

3.6.3 Radiated power

An expression for the total radiated power W may be derived by integrating the total power flow across an infinitely large sphere centered at the origin as follows

$$W = \frac{1}{2\eta_o} \int_0^{2\pi} \int_0^{\pi} E \cdot E^* R^2 \sin\theta \, d\theta \, d\phi \tag{3.54}$$

where

$\eta_o = 120\,\pi\,\Omega$ is the intrinsic impedance of free space, and

$*$ denotes the complex conjugate.

The vector wave functions $\bar{m}_{oln}$, $\bar{n}_{eln}$ are given by

$$\bar{m}_{oln} = \frac{P_n^1(\cos\theta)}{\sin\theta} \cos\phi \, \hat{\theta} - \frac{\partial P_n^1(\cos\theta)}{\partial\theta} \sin\phi \, \hat{\phi} \tag{3.55}$$

$$\bar{n}_{eln} = \frac{\partial P_n^1(\cos\theta)}{\partial\theta} \cos\phi \, \hat{\theta} - \frac{P_n^1(\cos\theta)}{\sin\theta} \sin\phi \, \hat{\phi} \quad . \tag{3.56}$$

Using the following orthogonality properties of the associated Legendre functions

$$\int_0^\pi \frac{P_n^1(\cos\theta)}{\sin\theta} \cdot \frac{\partial P_n^1(\cos\theta)}{\partial\theta} \sin\theta \, d\theta = 0 \tag{3.57}$$

and

$$\int_0^\pi P_n^m(\cos\theta) \; P_n^K(\cos\theta) \; d\theta = 0 \quad m \neq K \tag{3.58}$$

and also using the formula

$$\int_0^\pi \left(\frac{\partial P_n^m}{\partial\theta} \frac{\partial P_\ell^m}{\partial\theta} + m^2 \frac{P_n^m P_\ell^m}{\sin\theta} \right) \sin\theta \, d\theta$$

$$= \frac{2n(n+1)(n+m)!}{(2n+1)(n-m)!} \delta_{n\ell} \quad . \tag{3.59}$$

the radiated power can be expressed as

$$W = \frac{15}{2} k^2 C_e^2 \sum_{n=1}^{\infty} (2n+1)(\alpha_n \alpha_n^* + \beta_n \beta_n^*) \tag{3.60}$$

where

$C_e = -i\ P_x$ is the dipole current moment

$\alpha_n = -i\ (A_n + D_n)$

$\beta_n = B_n + C_n$

3.6.4 Directivity

The directivity in the forward direction relative to an isotropic source is defined by

$$D = \frac{4\pi(\text{radiated intensity in } \theta = 180^\circ \text{ direction})}{\text{total radiated power}} \tag{3.61}$$

the wave functions $\bar{m}_{oln}$, $\bar{n}_{eln}$ at $\theta = \pi$ and $\phi = 0$ can be written as

$$\bar{m}_{oln}\Big|_{\substack{\theta=\pi \\ \phi=0}} = (-1)^{n+1}\ \frac{n(n+1)}{2}\ \hat{\theta} \tag{3.62}$$

and

$$\bar{n}_{oln}\Big|_{\substack{\theta=\pi \\ \phi=0}} = (-1)^{n}\ \frac{n(n+1)}{2}\ \hat{\theta} \tag{3.63}$$

Using the above equations and equation (3.53), an expression for the radiated power intensity in the negative z direction is

$$\frac{R^2}{2\eta_o} E \cdot E^*\Big|_{\theta=\pi} = \frac{15k^2C_e^2}{4\pi}\left|\sum_{n=1}^{\infty}\ \frac{2n+1}{2}\ (i)^n(\alpha_n + \beta_n)\right|^2 \tag{3.64}$$

the directivity can therefore be written as

$$D = \frac{\left| \sum_{n=1}^{\infty} \frac{2n+1}{2} (i)^n (\alpha_n + \beta_n) \right|^2}{\sum_{n=1}^{\infty} \frac{2n+1}{2} (\alpha_n \alpha_n^* + \beta_n \beta_n^*)} \quad . \tag{3.65}$$

3.7 Results and Discussion

Using the field equations developed in the preceding sections, relevant numerical data are computed to investigate the focusing and radiation characteristics of a Luneberg lens. The exciting source is assumed to be a Huygens source located on the surface of the lens. Representative computed radiation fields, directivity and the mode power distributions are presented in the following sections.

3.7.1 Radiation pattern

The normalized power pattern of a Huygens source in the presence of a Luneberg lens of diameters from $D = 2\lambda$ to $D = 10\lambda$ are calculated in both E and H planes, corresponding to the $\phi = 0$ and $\phi = \frac{\pi}{2}$ planes respectively. Figures 3.4 and 3.5 show the patterns corresponding to $D = 5\lambda$ and $D = 10\lambda$. It should be noted that, with the source oriented as shown in Fig. 3.3, a maximum radiation occurs in the negative z-direction, and hence the top of the computed patterns correspond to $\theta = 180$ degrees. Comparing the two patterns, we see that the lens presents more directivity for larger diameters as predicted by geometrical optics. The side lobe levels are also decreased. The radiation pattern characteristic for Luneberg lens are

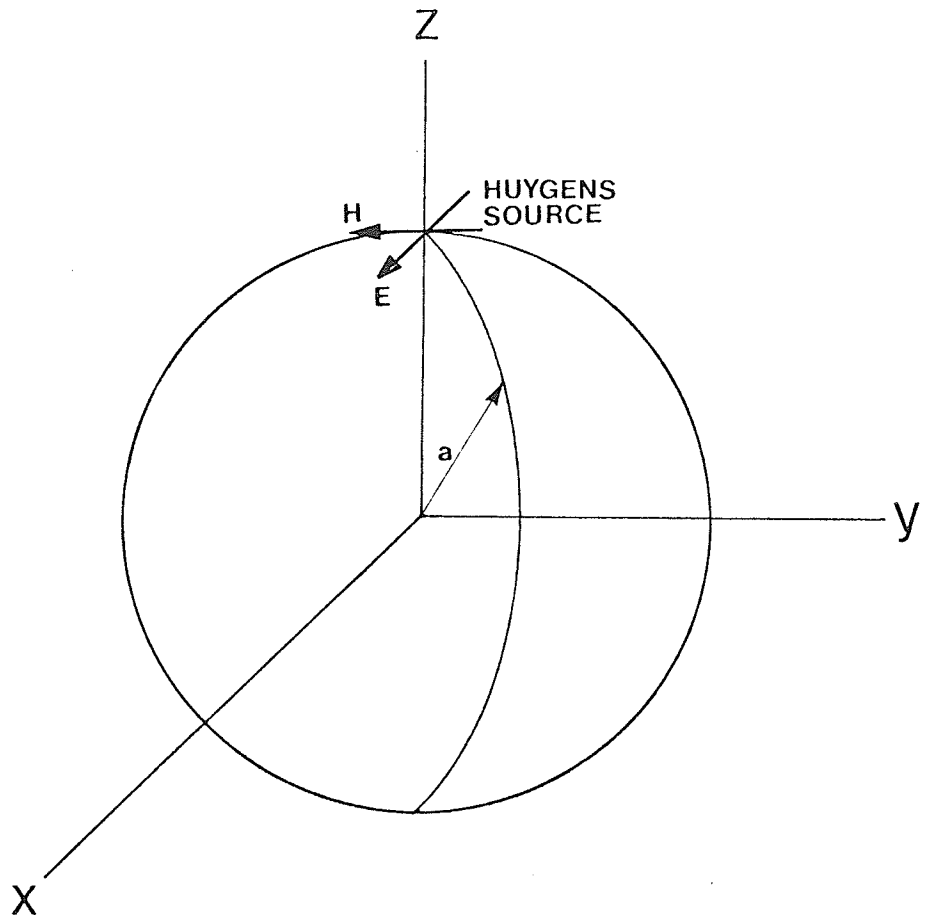

Fig. 3.3 Huygens' source on the surface of a Luneberg lens

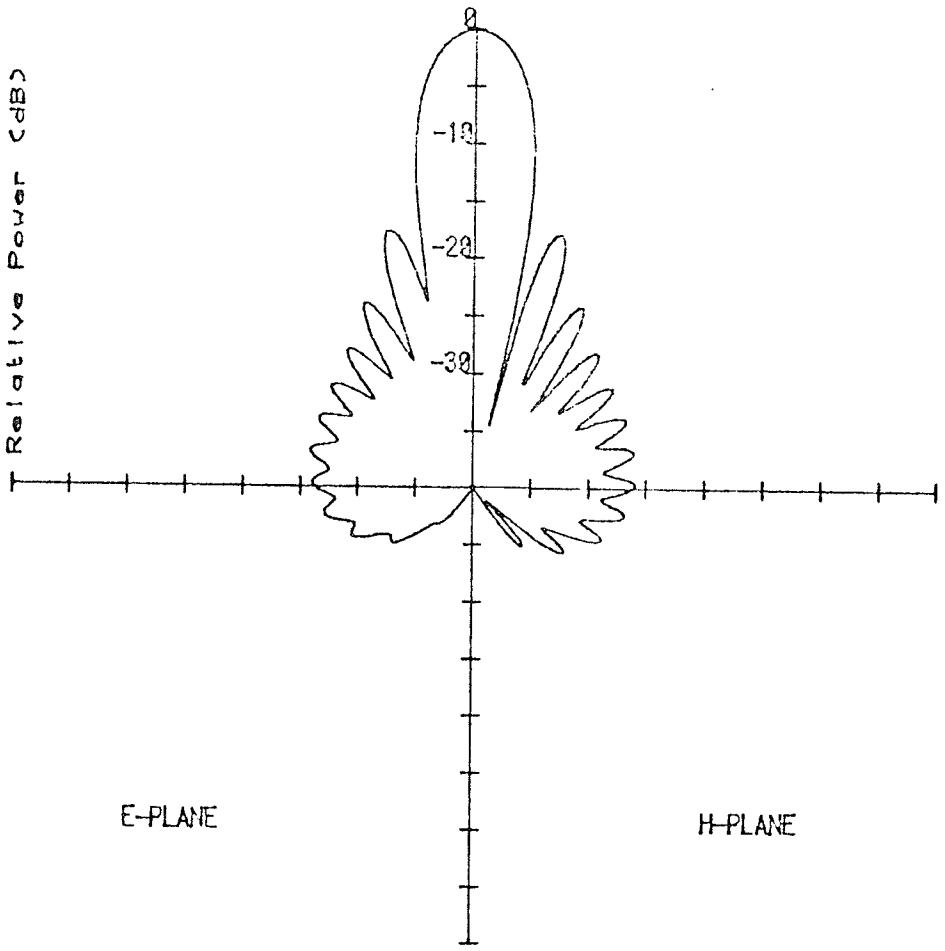

Fig. 3.4 Radiation pattern of a Huygens' source on the surface of a Luneberg lens; Diameter D = 5λ

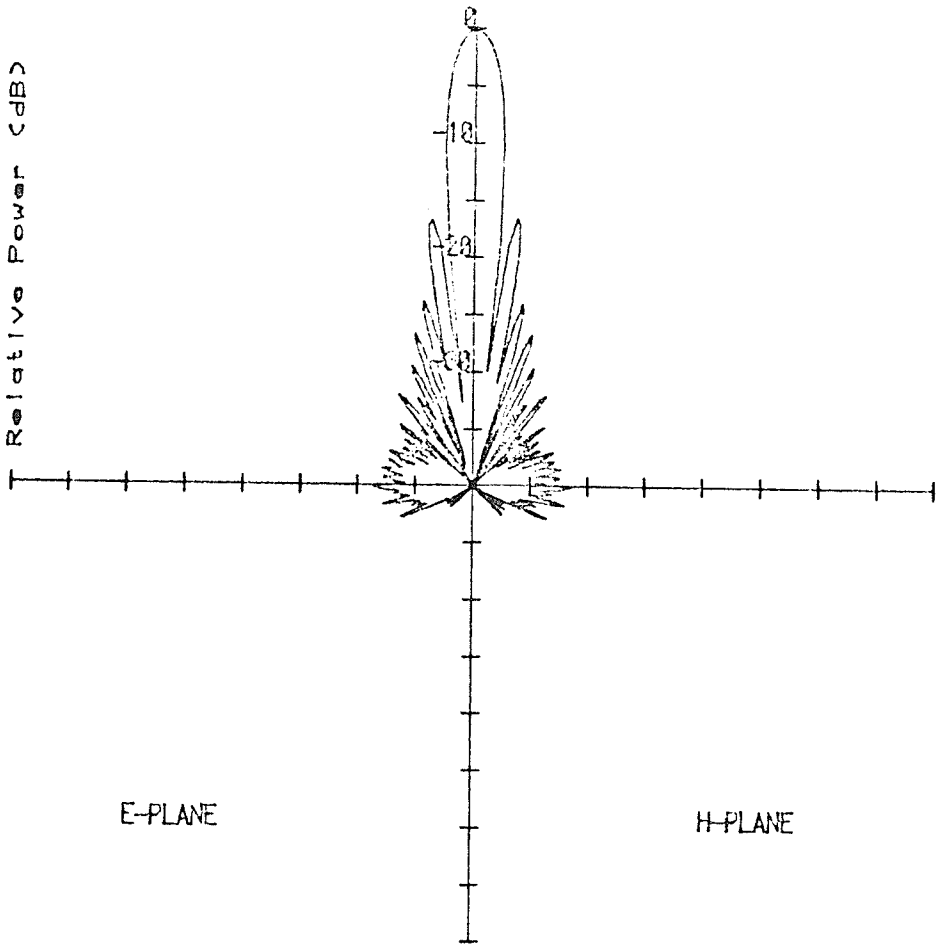

Fig. 3.5 Radiation pattern of a Huygens' source on the surface of a Luneberg lens; Diameter D = 10λ

summarized in Table 3.1. To compare this characteristic with the radiation characteristics of a uniformly illuminated circular aperture [34], the half power beam width and the level of the first side lobe for the circular aperture are also presented in Table 3.1. For small lenses the radiation pattern characteristic for the Luneberg lens differ slightly from that of a circular aperture particularly for the level of the side lobe. However, both patterns become almost identical at large diameters.

TABLE 3.2

Luneberg Lens Radiation Pattern Characteristic

Luneberg Lens				Circular Aperture		
Diameter	Gain	Beam Width	Level of 1st	Gain	Beam Width	Level of 1st
(λ)	(dB)	(degrees)	Side lobe	(dB)	(degrees)	Side lobe
2	14.785	30.16	-14.41	15.96	29.20	-17.6
3	18.240	19.87	-15.78	19.48	19.48	-17.6
4	20.758	15.00	-16.05	21.98	14.61	-17.6
5	22.725	11.79	-16.74	23.92	11.68	-17.6
6	24.339	9.80	-16.90	25.50	9.74	-17.6
7	25.708	8.37	-17.00	26.84	8.35	-17.6
8	26.895	7.31	-17.07	28.00	7.30	-17.6
9	27.940	6.48	-17.10	29.02	6.49	-17.6
10	28.776	5.8	-16.28	29.94	5.84	-17.6

3.7.2 Directivity

Using equation (3.65), the radiation pattern directivity of Luneberg lenses were calculated for the same diameters of section 3.7.1. The results are presented in Table 3.2 and Fig. 3.6. The directivity increases monotonicaly with increasing the lens diameter. The differential increase in the directivity, on the other hand, decreases for larger lens diameters, as can be seen from the 'saturation' behaviour of the curve in Fig. 3.6. This behaviour is expected since for large diameters compared to wave length, the lens behaviour will approach the theoretical behaviour explained by the geometrical optics. Comparing the directivity of the Luneberg lens as presented in Fig. 3.6 with the directivity of a homogeneous sphere with $\kappa = 3.00$ as presented by Rozenfeld [29], it is seen that the directivity of small Luneberg lens is lower than that of the homogeneous sphere. However, for a Luneberg lens the directivity characteristics does not present the resonance phenomena experienced in the case of a lossless homogeneous lenses [6]. From the above result, it is evident that a Luneberg lens when excited by a Huygens' source has a behaviour similar to a uniformly illuminated aperture. Since a uniformly illuminated circular aperture provides an optimum gain, a Luneberg lens is therefore an ideal lens to focus the radiation field of elementary radiators with a radiation pattern similar to a Huygens source, such as waveguides and horn antennas. The focusing properties of a Luneberg lens, however, deteriorates as its diameter decreases. In Chapter 4 we, therefore, will attempt to study new lens profiles that will improve its performance at low frequencies.

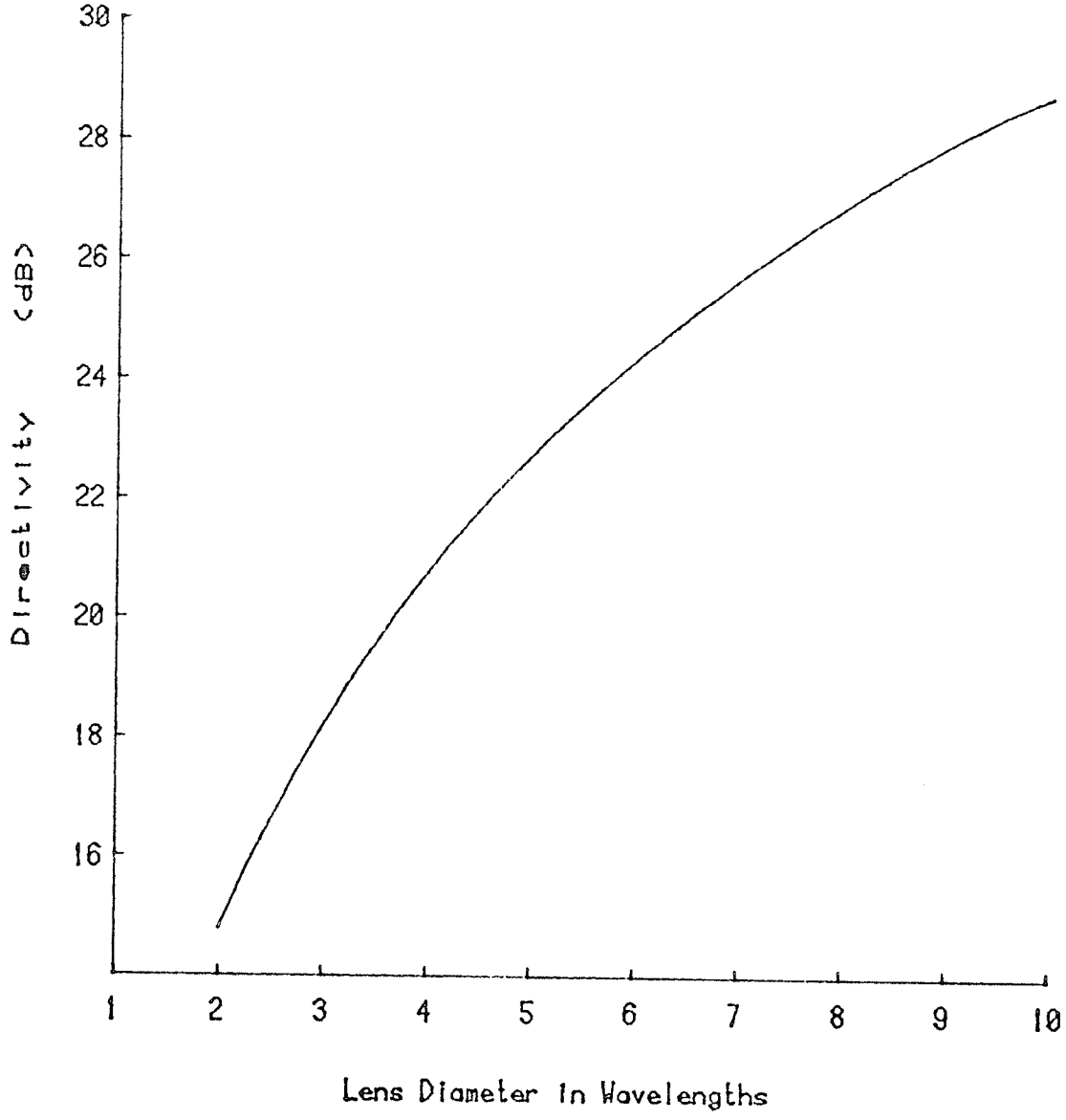

Fig. 3.6 Directivity of a Luneberg lens

3.7.3 Modal power distribution

The power distribution among different spherical wave modes presents a useful means of investigating the behaviour of the radiation characteristic. A resonance behaviour, for example, may be expected if one of the modes is carrying most of the radiated power. Also, modal distribution is a good indication of the convergence of the summation in equation (3.43). For this reason, we shall attempt to evaluate the percentage of power distribution among various modes in the spherical wave expansions. The results will be used to determine the resonance behaviour of the modes and the rate of the convergence for the series.

The total radiated power may be expressed as the summation of the powers radiated by each mode, which may be written as $W = \sum_{n=1}^{\infty} P_n$. The quantity $\frac{P_n}{W} \times 100$ represents, therefore, the percentage of the total power contributed by each mode. The percentage power distribution among the modes for diameter $D = 5\lambda$ to $D = 10\lambda$ are presented in Table 3.3 and the power distributions for $D = 5\lambda$ and $D = 10\lambda$ are shown in Fig. 3.7. Although the modes are discrete, their contributed power levels are connected to form a continuous curve for identification.

From the distribution of the percentage powers among various modes shown in Table 3.3, it is evident that, for a Luneberg lens the power content of the modes continuously increase with the mode number until the mode n, where $n = |ka| - 1$, beyond which the contribution of the higher order modes decreases rapidly. Thus unlike a homogeneous lens a Luneberg lens does not manifest a resonance phenomena. In addition, the series representing the lens field converges rapidly

TABLE 3.3

Modal Power Distribution

% contribution/ Mode #	D = 5λ	D = 6λ	D = 7λ	D = 8λ	D = 9λ	D = 10λ
1	0.88	0.61	0.45	0.35	0.28	0.22
2	1.48	1.02	0.75	0.58	0.46	0.37
3	2.00	1.43	1.07	0.81	0.64	0.53
4	2.75	1.83	1.33	1.05	0.84	0.67
5	3.05	2.30	1.70	1.26	1.00	0.83
6	4.06	2.54	1.9	1.55	1.21	0.96
7	4.29	3.33	2.31	1.66	1.37	1.15
8	4.82	3.11	2.58	2.10	1.56	1.23
9	6.65	4.40	2.75	2.06	1.79	1.48
10	4.6	4.04	3.52	2.61	1.83	1.51
11	9.18	4.62	2.97	2.60	2.30	1.77
12	8.18	6.44	4.51	2.84	2.07	1.89
13	5.01	3.89	3.74	3.54	2.78	1.95
14	19.13	8.29	4.3	2.77	2.50	2.38
15	14.47	7.91	6.23	4.50	2.87	2.02
16	6.22	3.65	3.36	3.48	3.48	2.87
17	2.25	16.31	7.37	3.94	2.56	2.37
18	0.71	14.12	7.82	6.05	4.42	2.85
19	0.19	6.44	2.87	3.01	3.29	3.4
20	0.05	2.50	13.62	6.43	3.54	2.36
21	0.01	0.86	13.89	7.82	5.90	4.3
22	0.00	0.26	6.69	2.51	2.8	3.16
23		0.07	2.75	11.02	5.50	3.13
24		0.02	1.01	13.73	7.81	5.75
25		0.00	0.34	6.97	2.48	2.73
26			0.10	2.99	8.56	4.59
27			0.03	1.17	13.55	7.76
28			0.01	0.41	7.27	2.67
29			0.00	0.38	3.25	6.33
30				0.01	1.33	13.28
31				0.00	0.5	7.58
32					0.17	3.50
33					0.05	1.50
34					0.01	0.59
35					0.00	0.21
36						0.07
37						0.02
38						0.06

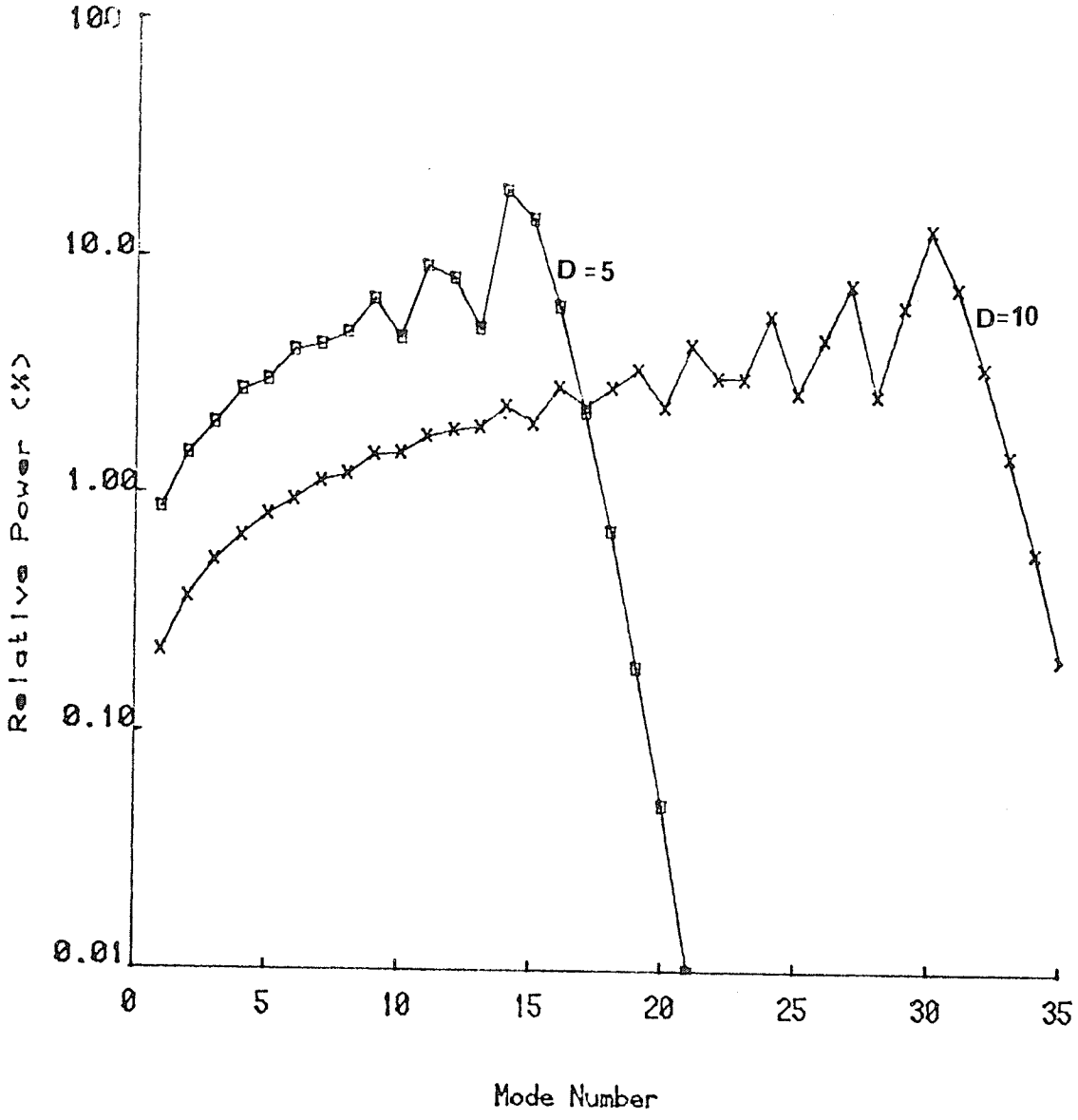

Fig. 3.7 Modal power distribution

beyond a mode number $n = |ka| - 1$. This upper limit in the number of modes, with a significant power content, provides a useful limit for truncation of the series for an accurate evaluation of the infinite series.

CHAPTER 4

MODIFIED LUNEBERG LENSES

4.1 Introduction

From a practical point of view lens antennas are normally used to increase the directivity of a radiating source. From the computed data of the last chapter it is clear that a Luneberg lens is a good candidate for focusing the radiation field of elementary radiators, such as open-ended waveguides or horns. However, it was also found in the last chapter that a Luneberg lens performs satisfactorily only at higher frequencies, where the lens diameter is several wavelengths in size. At low frequencies the directivity of a Luneberg lens deteriorates and a modification in the lens profile may be necessary to improve its focusing properties. However before introducing our modification of the lens profile, we present some of the previously proposed modifications.

Since the wavelength encountered at microwave frequencies are much longer than those in optics, a large diameter Luneberg lens is needed for scanning antennas. The instruments for the radiation, therefore, are correspondingly larger, which makes the rotating of such large instruments for scanning purposes cumbersome, and the speed of rotation has its mechanical limitations.

As previously reviewed in Chapter 2, some investigators [3, 8, 12] have proposed some new expressions for the design of small-feed-circle Luneberg lens. Eaton [8] and Brown [3] expressions have produced an abrupt discontinuity in the slope index of the refraction at

the feed circle. The Gutman [12] design, on the other hand, has produced a continuous function of the index of refraction versus the radius.

Gutman, using the Hamiltonian optics for analysing the rays in the Luneberg lens has presented a formula for the index of a new lens that is spherically symmetric and has a focal point near its centre. The corresponding new index of refraction formula is

$$n = \frac{1}{f}\left(a^2 + f^2 - r^2\right)^{1/2}$$

where r is the radial distance from the origin and n is the index of refraction, f is the distance from the centre to the focus, where a feed may be located, and a is the radius of the new lens as shown in Fig. 4.1.

When $f = a$, the index of refraction is the same as in an ordinary Luneberg lens, i.e.

$$n = \left[2 - \left(\frac{r}{a}\right)^2\right]^{1/2}$$

However, when $f < a$ for this lens the dielectric constant increases more rapidly towards the centre. At the centre its dielectric constant κ is given by

$$\kappa = 1 + \frac{a^2}{f^2}$$

Figure 4.1 illustrates the ray path for some values of f. The smallest feed circle that is possible is determined by the dielectric con-

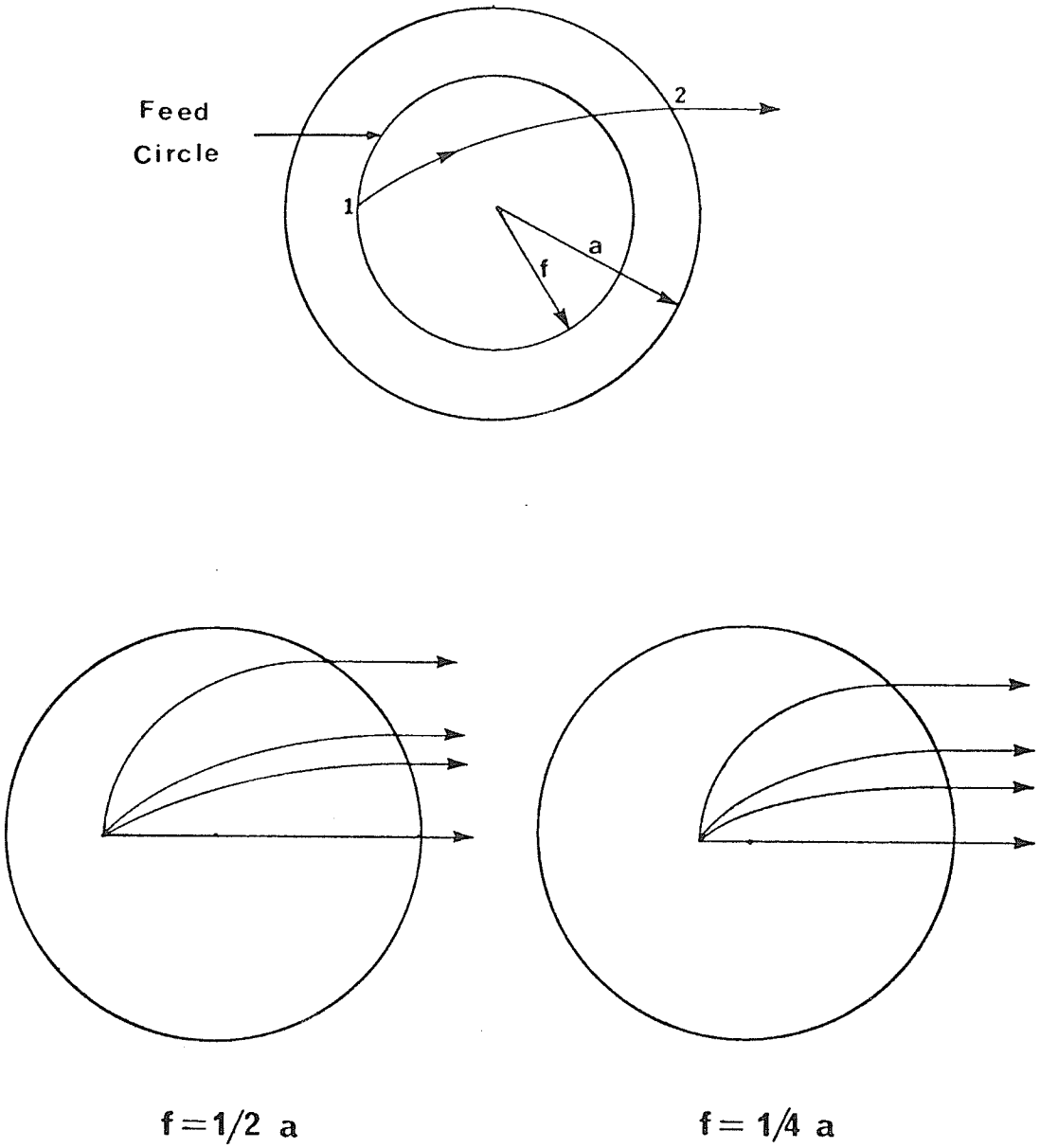

Fig. 4.1 Small-feed-circle Luneberg lens

stant. The highest dielectric constant is at the centre, which limits the minimum size of the feed circle as follows

$$f_{min} = \frac{a}{(\kappa_{max} - 1)^{1/2}}$$

A practical realization of such a lens is difficult since the feed antenna must be located inside the sphere and be allowed to move freely for scanning purposes without disturbing the performance of the lens. It is also impractical to introduce such a sharp gradient in the dielectric constant by stepping techniques frequently used. Also, since Gutman has used geometrical optics, his derivation is only valid for large diameter lenses. It should also be noted that this modification did not reduce the radius of Luneberg lens, which is the main disadvantage of using a Luneberg lens at microwave frequencies.

The radiation characteristics of a Luneberg lens presented in Chapter 3 has indicated that the lens behaviour improves with an increase in the lens diameter, and the deterioration in the lens behaviour at small diameters was attributed to the small diameter lens compared to the wavelength. It was also found that a small homogeneous lens with a dielectric constant $\kappa = 3$, presents a better directivity than a Luneberg lens of the same diameter. This property of a homogenious sphere suggests an alternative means of modifying Luneberg lenses for a better directivity performance at low frequencies. Their geometry is simpler than a Gutman lens and from a practical point of view they are easier to fabricate and use.

4.2 Modified Luneberg Lens

The dielectric constant for the modified Luneberg lens is assumed to have a profile expressed by

$$\kappa = 2B - A^2 \left(\frac{r}{a}\right)^2 \qquad 0 \leq r \leq a \tag{4.1}$$

where B and A are arbitrary constants

a is the radius of the lens

and r is the radial distance measured from the centre of the lens.

Using the same nomenclature used by Tai [33], the differential equation of such lenses for the radial function $S_n(r)$ of the magnetic or transverse electric modes may be represented by

$$\frac{d^2 S_n(r)}{dr^2} + \left[k^2\kappa - \frac{n(n+1)}{r^2}\right] S_n(r) = 0 \tag{4.2}$$

which can be written as

$$\frac{d^2 S_n(\rho)}{d\rho^2} + \left[\kappa - \frac{n(n+1)}{\rho^2}\right] S_n(\rho) = 0 \,, \tag{4.3}$$

$$\rho = kr \quad , \quad \rho_a = ka$$

Substituting equation (4.1) in equation (4.3), we have

$$\frac{d^2 S_n(\rho)}{d\rho^2} + \left[2B - A^2\left(\frac{r}{a}\right)^2 - \frac{n(n+1)}{\rho^2}\right] S_n(\rho) = 0 \tag{4.4}$$

or

$$\frac{d^2 S_n(\rho)}{d\rho^2} + \left[2B - \frac{\rho^2}{\rho_1^2} - \frac{n(n+1)}{\rho^2} \right] S_n(\rho) = 0 \; ; \qquad (4.5)$$

$$\rho_1 = \frac{\rho_a}{A}$$

This is the normal form of the second order differential equation [27] and its soluton can be found by the polynomial method of Sommerfeld [18]. The method consists of defining three functions such that their product is the exact solution of the differential equation. These functions are chosen such that one of them describes the behaviour of the solution around the origin, the second solution describes the behaviour at infinity and the third determines the nature of the solution in the intermediate region.

When $\rho \to \infty$, the differential equation (4.5) can be approximated by

$$\frac{d^2 S_n}{d\rho^2} - \frac{\rho^2}{\rho_1^2} S_n = 0 \qquad (4.6)$$

which has an asymptotic solution proportional to $e^{\pm \rho^2 / 2\rho_1}$, i.e.

$$S_n \alpha e^{\pm \rho^2 / 2\rho_1} \qquad (4.7)$$

In (4.7) only the negative sign will be considered in order that the function vanishes at infinity and therefore

$$S_n \alpha e^{-\rho^2/2\rho_1} \tag{4.8}$$

At the origin, the Frobenius method gives a solution which is a polynomial of power $(n+1)$ or $-n$. To obtain a finite solution at the origin, we select the polynomial with the power $(n+1)$.

The solution of equation (4.5) can then be written as

$$S_n(\rho) = \rho^{n+1} e^{-\rho^2/2\rho_a} F_n(\rho) \tag{4.9}$$

where $F_n(\rho)$ describes the behaviour of S_n in the intermediate region. Differentiating (4.9), we have

$$\frac{dS_n}{d\rho} = S_n\left[\frac{(n+1)}{\rho} - \frac{\rho}{\rho_1} + \frac{F'_n}{F_n}\right] ; \tag{4.10}$$

$$F'_n = \frac{d\,F_n}{d\rho}$$

and

$$\frac{d^2 S_n}{d\rho^2} = S_n\left[\frac{(n+1)}{\rho} - \frac{\rho}{\rho_1} + \frac{F'_n}{F_n}\right]^2$$

$$+ S_n\left[\frac{-(n+1)}{\rho^2} - \frac{1}{\rho_1} + \frac{F''_n}{F_n} - \frac{F'^2_n}{F^2_n}\right] \tag{4.11}$$

$$F_n'' = \frac{d^2 F_n}{d\rho^2}$$

Substituting into equation (4.5), we find that the function F_n must satisfy the following equation

$$\frac{d^2 F_n}{d\rho^2} + 2\left(\frac{n+1}{\rho} - \frac{\rho}{\rho_1}\right) \frac{dF_n}{d\rho} + \left[2B - \frac{1}{\rho_1} - \frac{2(n+1)}{\rho_1} \right] F_n = 0 \qquad (4.12)$$

Now, if we define a new variable z as

$$Z = \rho^2/\rho_1$$

then

$$\frac{dF_n}{d\rho} = \frac{2\rho}{\rho_1} \frac{dF_n}{dZ} \qquad (4.13)$$

$$\frac{d^2 F_n}{d\rho^2} = \frac{4\rho^2}{\rho_1^2} \frac{d^2 F_n}{dZ^2} + \frac{2}{\rho_1} \frac{dF_n}{dZ} \qquad (4.14)$$

Equation (4.12) can now be written as

$$\frac{d^2 F_n}{dZ^2} + \left(\frac{\gamma}{2} - 1\right) \frac{dF_n}{dZ} - \frac{\alpha}{Z} F_n = 0 \qquad (4.15)$$

where

$$\alpha = \frac{1}{2}\left(n + \frac{3}{2} - B\rho_1\right) = \frac{1}{2}\left(n + \frac{3}{2} - \frac{B}{A}\ \rho_a\right)$$

$$\gamma = n + \frac{3}{2}$$

$$\rho_a = ka$$

$$\rho_1 = \rho_a / A$$

Equation (4.15) is the confluent hypergeometric differential equation. The solution of this differential equation is the confluent hypergeometric function (Kummer's function),

$$F_n(Z) = {}_1F_1(\alpha, \gamma; Z) \tag{4.16}$$

The second solution of the confluent hypergeometric equation $Z^{1-\gamma}\ {}_1F_1(\alpha - \gamma+1, 2 - \gamma; Z)$ is not finite at the origin. The confluent hypergeometric function is given by the series

$${}_1F_1(\alpha, \gamma; Z) = 1 + \frac{\alpha}{\gamma} Z + \frac{(\alpha)_2}{(\gamma)_2 2!} Z + \ldots + \frac{(\alpha)_n}{(\gamma)_n n!} Z^n + \ldots$$

where

$$(\alpha)_n = \alpha(\alpha+1)(\alpha+2) \ldots (\alpha+n-1) \quad \text{and} \quad \alpha_o = 1$$

${}_1F_1(\alpha, \gamma; Z)$ is a convergent series for all values of α, γ, Z if $\gamma \neq \ell$ and $\alpha \neq -m$ where ℓ and m are positive integers. Since

$$\alpha = \frac{1}{2}(n + \frac{3}{2} - \frac{B}{A} \rho_a)$$

it can assume negative integer values. When α is negative the

function exhibits an oscillatory behaviour and when α is a negative integer the series terminates and becomes an oscillatory polymomial. Since $\gamma = n + \frac{3}{2}$, then $\gamma \neq -m$.

Therefore, the confluent hypergeometric function is always well-behaved in this case.

The derivative of the confluent hypergeometric function is given by

$$\frac{d_1 F_1(\alpha, \gamma; Z)}{dZ} = \frac{\alpha}{\gamma} {}_1F_1(\alpha + 1, \gamma + 1; Z) \qquad (4.17)$$

The S-function can then be written as

$$S_n(\rho) = \rho^{n+1} e^{-\rho^2/2\rho_1} {}_1F_1(\alpha, \gamma; \rho^2/\rho_1) \qquad (4.18)$$

The differential equation for the radial function $T_n(r)$ for the electric or transverse magnetic modes is

$$\frac{d^2T_n(r)}{dr^2} - \frac{1}{\kappa} \frac{d\kappa}{dr} \frac{d\, T_n(r)}{dr} + \left[k^2\kappa - \frac{n(n+1)}{r^2} \right] T_n(r) = 0 \qquad (4.19)$$

When the expression for the dielectric constant, equation (4.1) is substituted into equation (4.19) we get

$$\frac{d^2 T_n(\rho)}{d\rho^2} + \frac{2\rho}{2\rho_2^2 - \rho^2} \frac{d\ T_n(\rho)}{d\rho} + \left[2B - \frac{\rho^2}{\rho_1^2} - \frac{n(n+1)}{\rho^2} \right] T_n(\rho) = 0 \qquad (4.20)$$

where $\rho_2 = \sqrt{B}\ \rho_1 = \frac{\sqrt{B}}{A} \rho_a$

Equation (4.20) can be transformed to the normal form by the following change to the dependent variable

$$T_n = V_n \exp(-\frac{1}{2} \int p d\rho) ,$$

where p is the coefficient of the first derivative in the differential equation and is

$$p = \frac{2\rho}{2\rho_2^2 - \rho^2}$$

Therefore

$$T_n(\rho) = (2\rho_2^2 - \rho^2)^{1/2} V_n(\rho)$$

The differential equation for the new dependent variable $V_n(\rho)$ thus becomes

$$V_n'' + \left\{ 2B - \frac{\rho^2}{\rho_1^2} - \frac{n(n+1)}{\rho^2} - \frac{2(\rho_2^2 + \rho^2)}{(2\rho_2^2 - \rho^2)^2} \right\} V_n = 0 \qquad (4.21)$$

which is the normal form of the differential equation. Again applying the polynomial method of Sommerfeld [18], we find that

$$V_n(\rho) = e^{-\rho^2/2\rho_a} \; \rho^{n+1} \; W_n(\rho)$$

where W_n satisfies the differential equation

Therefore T_n can be written as

$$T_n(\rho) = (2\rho_2^2 - \rho^2)^{1/2} \; \rho^{n+1} \; e^{-\rho/2\rho_1} \; W_n(\rho) \qquad (4.22)$$

with

$$\frac{dT_n}{d\rho} = T_n \left[\frac{-\rho}{(2\rho_2^2 - \rho^2)} + \frac{(n+1)}{\rho} - \frac{\rho}{\rho_1} + \frac{W_n'}{W_n} \right]^2 \qquad (4.23)$$

where $W_n' = \dfrac{dW_n}{d\rho}$

and

$$\frac{d^2T_n}{d\rho^2} = T_n \left[\frac{-\rho}{(2\rho_2^2 - \rho^2)^2} + \frac{(n+1)}{\rho} - \frac{\rho}{\rho_1} + \frac{W_n'}{W_n} \right]^2$$

$$+ T_n \left[\frac{-2\rho^2}{(2\rho_2^2 - \rho^2)^2} + \frac{1}{(2\rho_2^2 - \rho^2)} - \frac{(n+1)}{\rho^2} - \frac{1}{\rho_1} - \frac{W_n'^2}{W_n} + \frac{W_n''}{W_n} \right]$$

...(4.24)

where $W_n'' = \dfrac{d^2W_n}{d\rho^2}$

Substituting equations (4.22), (4.23), (4.24) into equation (4.20) we get

$$\frac{d^2W_n}{d\rho^2} + 2\left(\frac{n+1}{\rho} - \frac{\rho}{\rho_1}\right)\frac{dW_n}{d\rho} + \left[2B - \frac{2n+3}{\rho_1} - \frac{1}{(2\rho_2 - \rho^2)} - \frac{3\rho^2}{(2\rho_2^2 - \rho^2)^2}\right] W_n = 0$$

...(4.25)

A change of the independent variable to $Z = \rho^2/\rho_1$ reduces (4.25) to

$$\frac{d^2W_n}{dZ^2} + \left(\frac{\gamma}{Z} - 1\right)\frac{dW_n}{dZ} - \left[\frac{\alpha_1}{Z} + \frac{2\alpha_2}{(Z - a_2)} - \frac{2a_2\alpha_3}{(Z - a_2)^2}\right] W_n = 0 \qquad (4.26)$$

where $\gamma = n + \frac{3}{2}$

$$\alpha_1 = \frac{1}{2}\left[n + \frac{3}{2} - \frac{B}{A}\rho_a + \frac{A}{4B\rho_a}\right]$$

$$\alpha_2 = \frac{A}{16B\rho_a}, \quad \alpha_3 = \frac{-3A}{16B\rho_a}, \quad a_2 = \frac{2B}{A}\rho_a$$

Equation (4.26) is the differential equation for the generalized confluent hypergeometric function given by Tai [33]. The two possible series solutions around zero for this function are

$$W_n = \sum_{m=0}^{\infty} A_m Z^m$$

and

$$W_n = Z^{-(n + \frac{1}{2})} + \sum_{m=1}^{\infty} A_m Z^{m-(n + \frac{1}{2})}$$

We will only consider the first solution since the second solution is

not finite at the origin. Substituting the first solution in to the differential equation (4.26) and equating all the coefficients having the same power to zero, we find a four term recurrence relation between the coefficients. This recurrence relation can be further reduced to the relation between the first coefficient and any subsequent term. These relations are:

$$\frac{A_1}{A_0} = \frac{\alpha_1}{\gamma}$$

$$\frac{A_2}{A_0} = \frac{1}{2}\frac{\alpha_1(\alpha_1 + 1)}{\gamma(\gamma + 1)} - \frac{\alpha_2 + \alpha_3}{(\gamma + 1)a_2}$$

$$\frac{A_3}{A_0} = \frac{1}{3!}\frac{\alpha_1(\alpha_1 + 1)(\alpha_2 + 2)}{\gamma(\gamma + 1)(\gamma + 2)} - \frac{1}{3(\gamma + 2)}\left[\frac{(\alpha_1 + 2)(\alpha_2 + \alpha_3)}{(\gamma + 1)\, a_2}\right.$$

$$\left. + \frac{2^{\alpha_1}(\alpha_2 + \alpha_3)}{\gamma\, a_2} + \frac{2(\alpha_2 + 2^{\alpha_3})}{a_2^2}\right]$$

For $m \geq 3$, the coefficients can be obtained from the recurrence relationship

$$a_2^2(m + 1)(m + \gamma)\, A_{m+1} - a_2\left[a_2(m + \alpha) + 2n(\gamma - m + 1)\, A_m\right.$$

$$\left. + \left[2a_2(\alpha_1 + \alpha_2 + \alpha_3 + m-1) + (n-1)(\gamma + m-2)\right] A_{m-1}\right.$$

$$- (\alpha_1 + 2\alpha_2 + m-2)\, A_{m-2} = 0$$

The series solution for W_n converges uniformly and absolutely for $|Z| < a_2$ or $\rho^2 < \frac{2B}{A^2}\rho_a^2$. This condition will always be satisfied in the region $0 \leq \rho \leq \rho_a$ as long as $\frac{2B}{A^2} > 1$. This can easily be satisfied by the choice of the values of the constants A and B as will be explained further in the following sections.

4.3 Dielectric Constant Profile

It is clear from the discussion in section 4.1 that in order to enhance the performance of a small diameter Luneberg lens the values of A and B should be chosen such that the overall dielectric constant of the lens be increased. Also A and B should satisfy the necessary condition for the convergence of the solution for the function W_n .

The effect of the constants A and B , in equation (4.1), on the dielectric constant profile of the modified Luneberg lens can be explained further by referring to Fig. 4.2 which illustrates different profiles associated with different values of A and B as follows:

a) A = B = 1; which is the ordinary Luneberg lens case. The value of the dielectric constant changes from 2 at the lens centre to 1 on the surface.

b) A = 1; the effect of A and B is the same as adding a biasing effect (constant value) to the curve. In this case equation (4.1) can be expressed as

$$\kappa = 2B - \left(\frac{r}{a}\right)^2$$

$$= (2B - 2) + \left[2 - \left(\frac{r}{a}\right)^2\right] \qquad (4.27)$$

The second term of this equation gives the same profile as an ordinary Luneberg lens, while the first term presents an offset term of the value $(2B-2)$. This offset has to be positive to increase the total dielectric constant of the modified Luneberg lens.

Then $2B - 2 > 0$

or $B > 1$

It is also expected that the value of B should be kept below a certain value in order to preserve the characteristic profile of the Luneberg lens. This is due to the fact that the results reported by Mason [6] for a homogeneous sphere shows that the lens performance deteriorates if the dielectric constant is increased beyond 3.

c) $B = 1$; then

$$\kappa = 2 - A^2\left(\frac{r}{a}\right)^2 \qquad (4.28)$$

The value of A has to be less than unity to improve the lens behaviour. Curve C also indicates that unless the value of A is much smaller than unity no appreciable change in lens performance can be expected. On the other hand, a very small value of A will cause a large change in the dielectric contant profile which may cancel any improvement expected by this modification.

d) $A^2 = B$; This is another interesting case. It involves both values

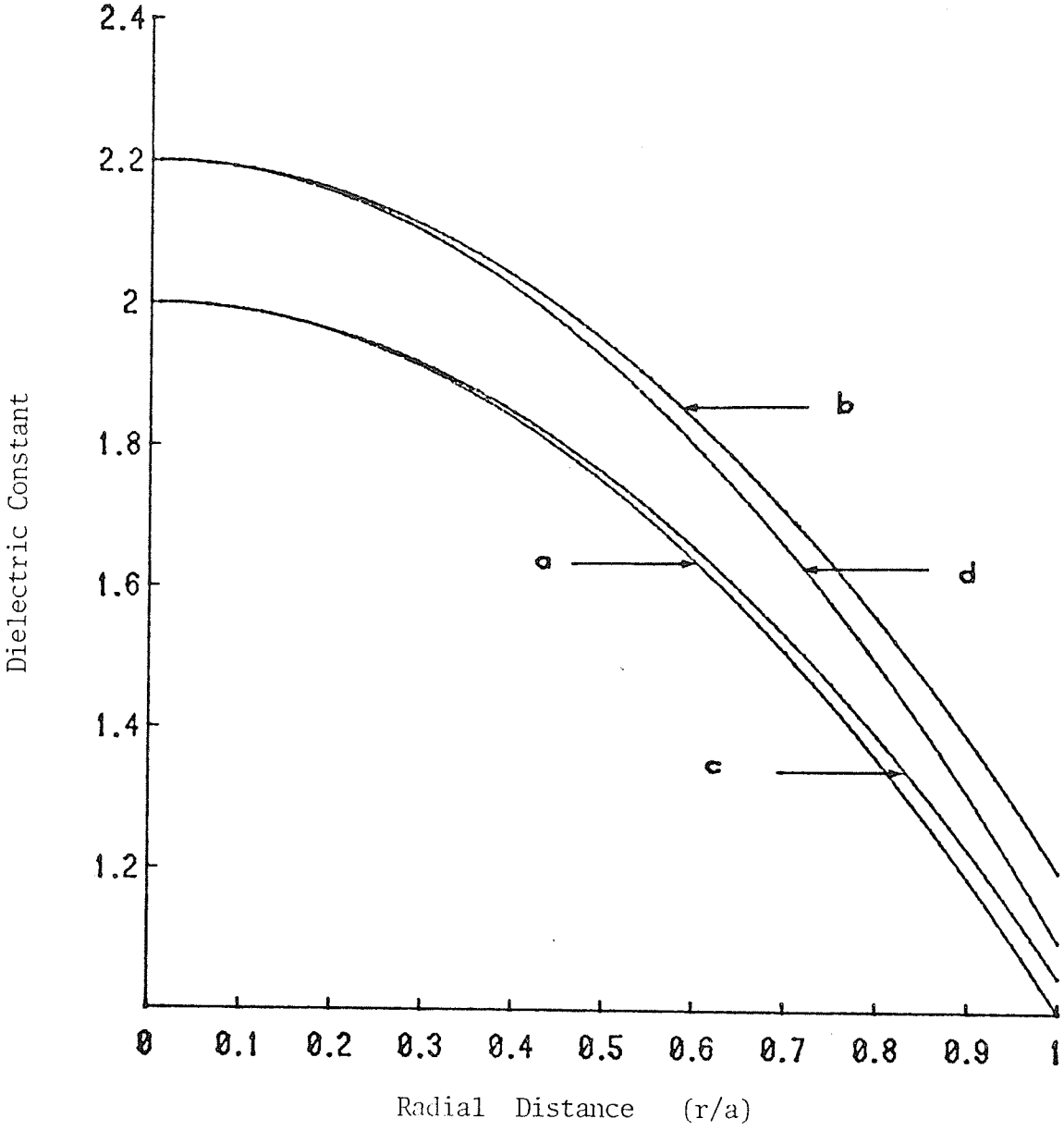

Fig. 4.2 Dielectric constant profile of the modified Luneberg lens; a) A = B = 1; b) A = 1, B = 1.1; c) A^2 = 0.95, B = 1; d) A^2 = B = 1.1

of A and B , while still satisfying the condition for convergence of the radial function $T_n(r)$. It is not expected that the performance of this modified design will be much different than that of the case b, since there is only a small difference between the two profiles. Although it may have the advantage of having a lower dielectric constant on the lens surface. This low surface dielectric constant may improve the matching between the lens and its feed if it is an air filled waveguide.

4.4 Results and Discussion

Here, we will investigate the proposed modifications and evaluate their effect on the radiation characteristic of a Luneberg lens. The modified Luneberg lens shall be fed by a Huygens' source located on its surface. Radiation characteristics such as directivity, beam width and the level of the first side lobe will be computed for the electric field in both principal planes.

Numerical calculations of the radiation characteristics of the new modified lens are shown in Figures 4.3 to 4.6. These figures show that the proposed modifications have enhanced the radiation characteristics of the Luneberg lens. The modified lens produces higher directivity and narrower beams than the ordinary Luneberg lens. The improvement is more visible in small diameter lenses and decreases as the lens diameter increases. This is expected, hence lenses with diameters of several wavelength approach their optical behaviour. In the following section we will present a discussion of the radiation characteristics of the modified lens.

4.4.1 Directivity

For the two dielectric constant profile cases corresponding to $A = 1$ and $B = A^2$, the value of B will be changed in increments of 0.01 and the directivity of the modified Luneberg lens when fed by a Huygens' source will be calculated for lens diameters from 2λ to 10λ.

The results for the first case, $A = 1$, are presented in Fig. 4.3. For all diameters the directivity increases with increasing B up to a certain limiting B value and then it decreases rapidly. When we compute the directivity beyond this limiting B value the lens demonstrate a resonance effect in the same manner as that for a homogeneous lens [6]. This indicates that beyond this limit the lens starts to behave as a homogeneous lens. The B limit decreases as the diameter of the lens is increased, which is also expected since as the lens diameter increases the performance of the lens approaches its optical behaviour.

With this first type of lens modification there is a noticeable increase in the directivity, particularly for smaller lenses; e.g. for a lens diameter of $D = 2\lambda$ an increase of 3db can be achieved with $B = 1.4$. This directivity increase is achieved over a reasonably wide range of B values. This is seen by the flat top shape of the directivity curve over a certain range B values. This phenomenon is very desirable since it allows for a large tolerance in the dielectric constant and therefore wider choice of dielectric material when manufcturing such a lens. Fig. 4.3 also shows that the improvement in directivity decreases as the lens diameter increases and the lens behaviour approaches that of an ideal one.

The directivity behaviour for the case $A^2 = B$ are presented

in Fig. 4.4. The lens performance in this case is approximately the same as for the case $A = 1$. The improvement in the directivity is lower; e.g., for a lens of 2λ diameter the directivity increases by about 2.3dB as compared to a 3db increase in the former case. Although this increase is more stable over a wider range of B values. This letter type of modification may be more desirable, especially since it provides an easier field match at its surface as discussed above.

It should be mentioned here that the proposed modifications have achieved a better lens performance at a smaller diameter than that for an ordinary Luneberg lens.

The percentage increase in the directivity versus the lens diameter are shown in Fig. 4.5. For the case of $A = 1$ the increase in the directivity will vary from approximately 91% to 14%, when the diameter increases from 2λ to 10λ respectively, while for $A^2 = B$ the corresponding increase is from approximately 61.0% to 10%. Fig. 4.6 shows the directivity of an ordinary Luneberg lens together with the two modified cases as a function of lens diameter.

4.4.2 Radiation patterns

The reason for the directivity enhancement caused by the lens modification may be explained by referring to Figures 4.7 and 4.8. The radiation pattern of two modified Luneberg lenses ($D = 2\lambda$, $D = 5\lambda$) fed by a Huygens' source are shown, together with the radiation patterns for the ordinary Luneberg lens. These curves show that for the modified case more power is concentrated in the main lobe with an accompanied reduction in the side lobes. This indicates an improvement to the lens focusing characteristic, which in turn leads to an improvement in the directivity of the modified lens gain.

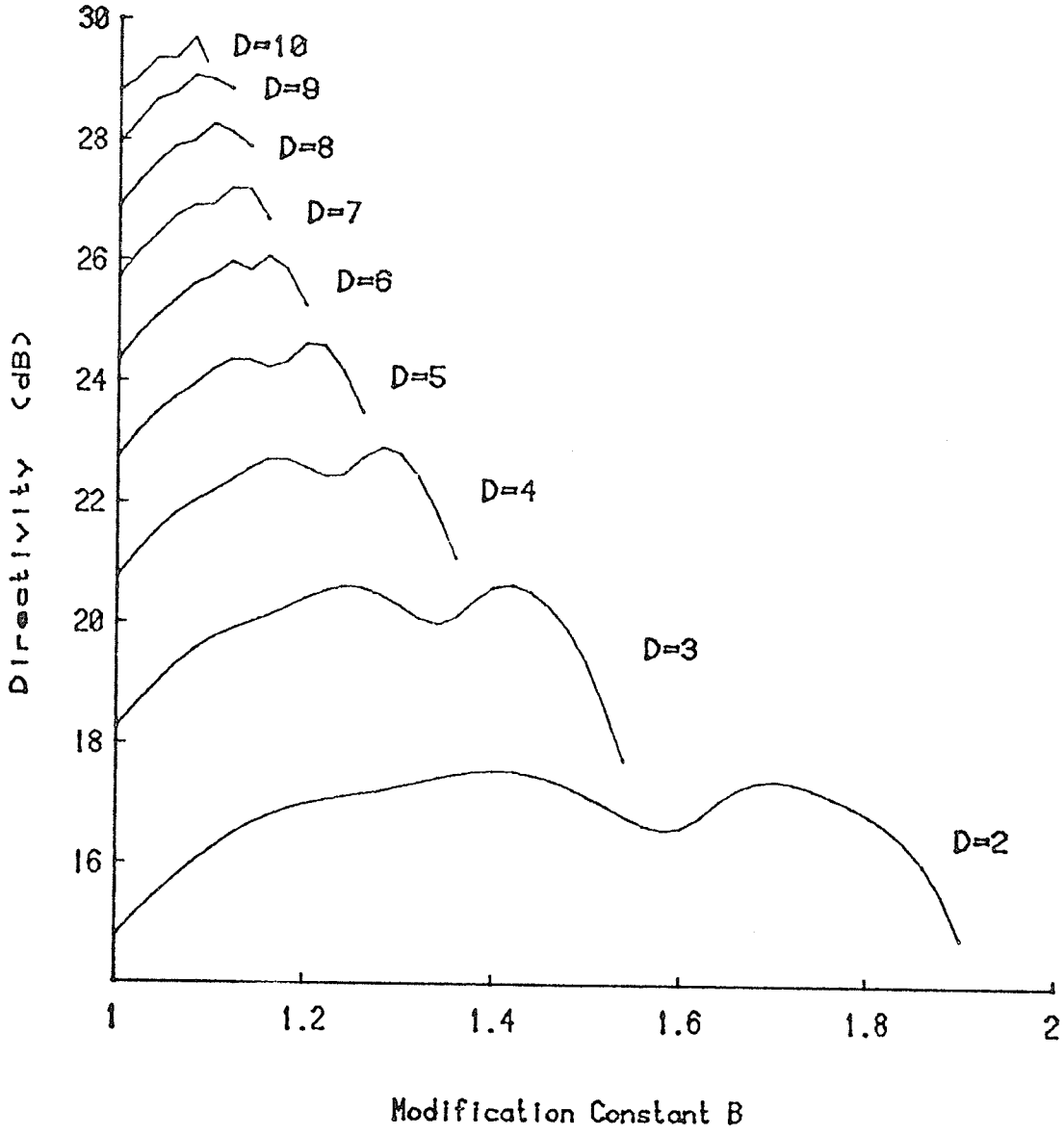

Fig. 4.3 Directivity of the modified Luneberg lens; A = 1

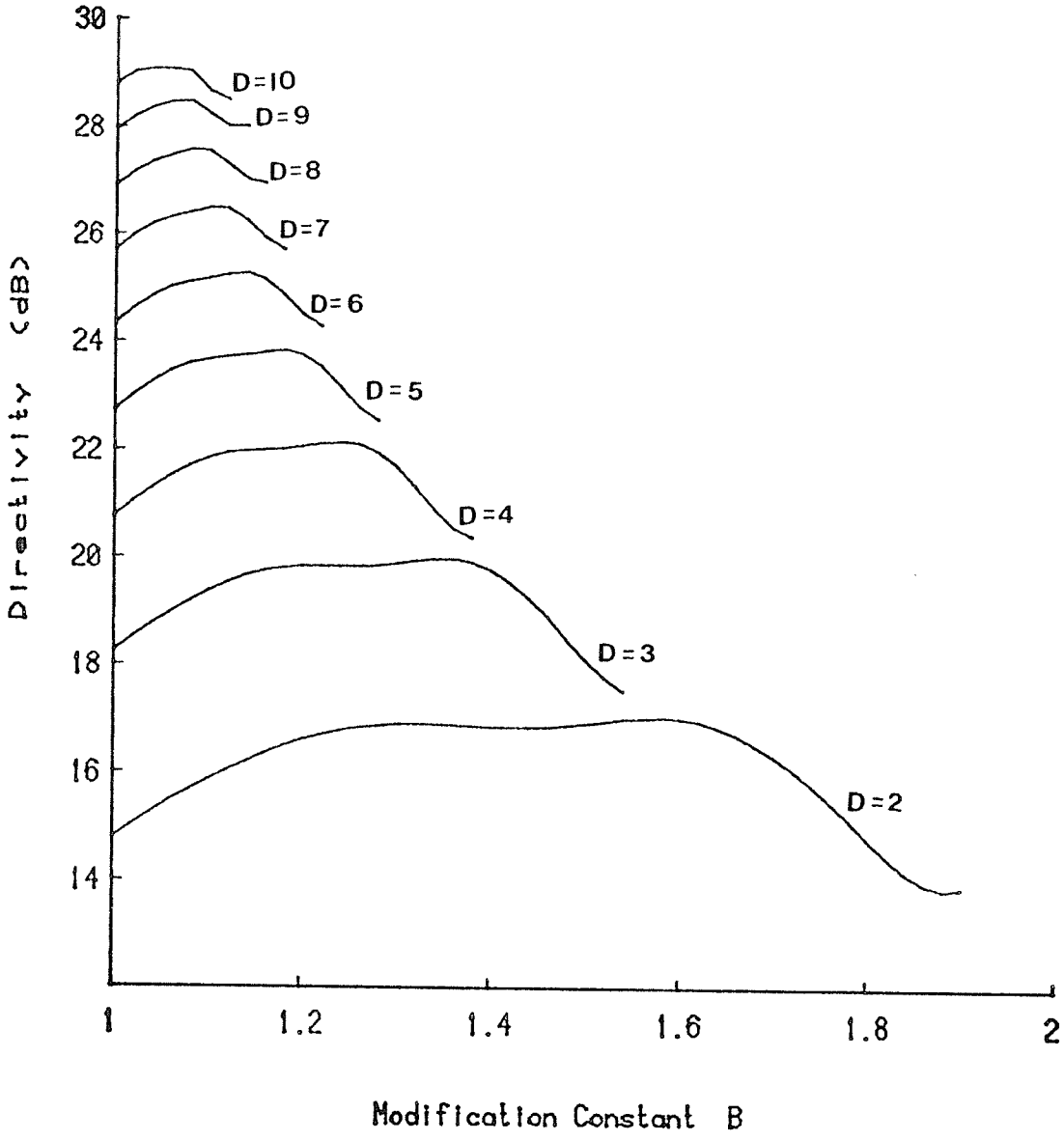

Fig. 4.4 Directivity of the modified Luneberg lens;A^2 = B

Table 4.1 is a summary of the radiation characteristics that is the Gain, beam width and the level of first side lobe for lens diameters from $D = 2\lambda$ to $D = 10\lambda$.

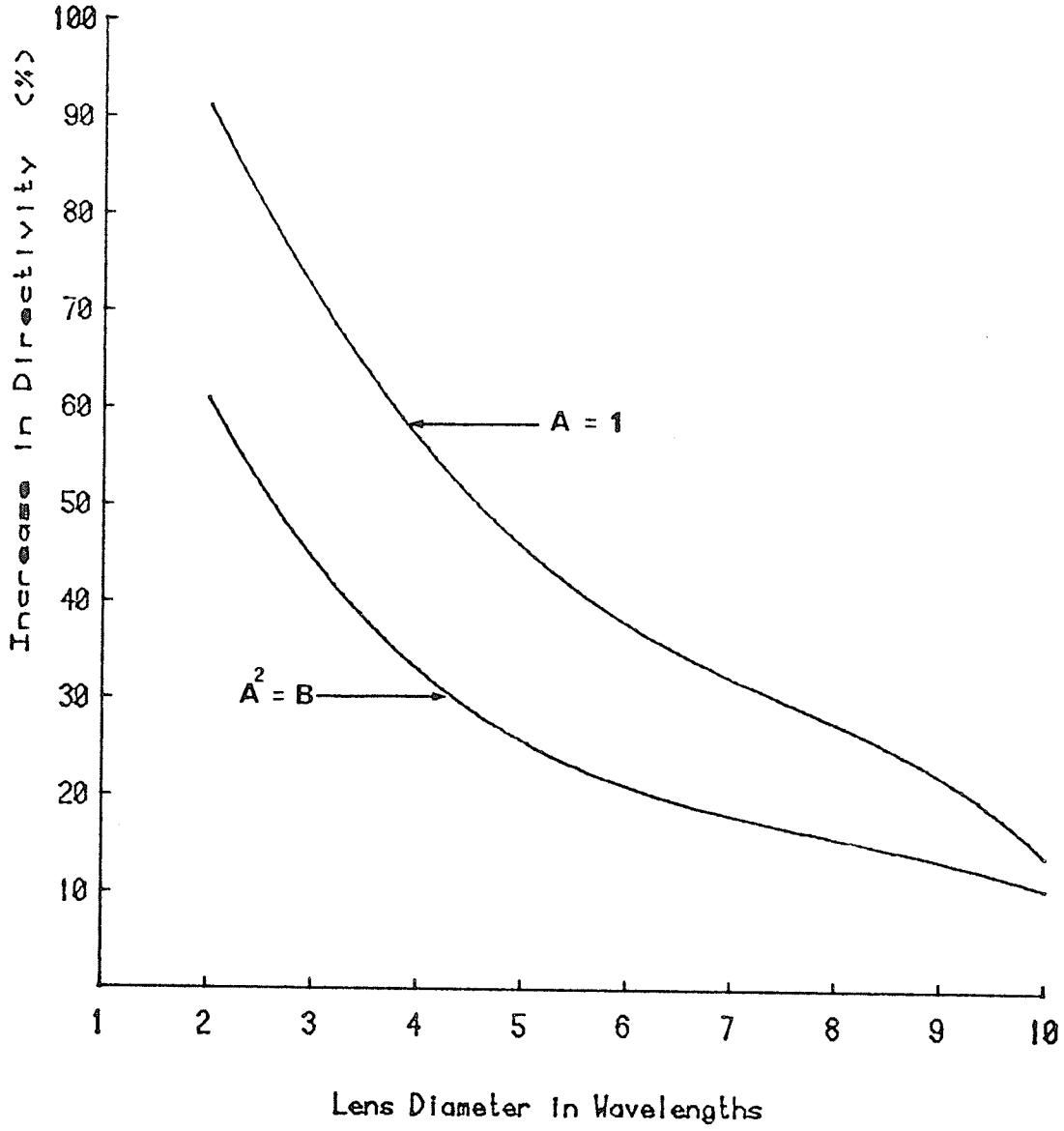

Fig. 4.5 Increase of the directivity of the modified Luneberg lens compared to the standard Luneberg lens

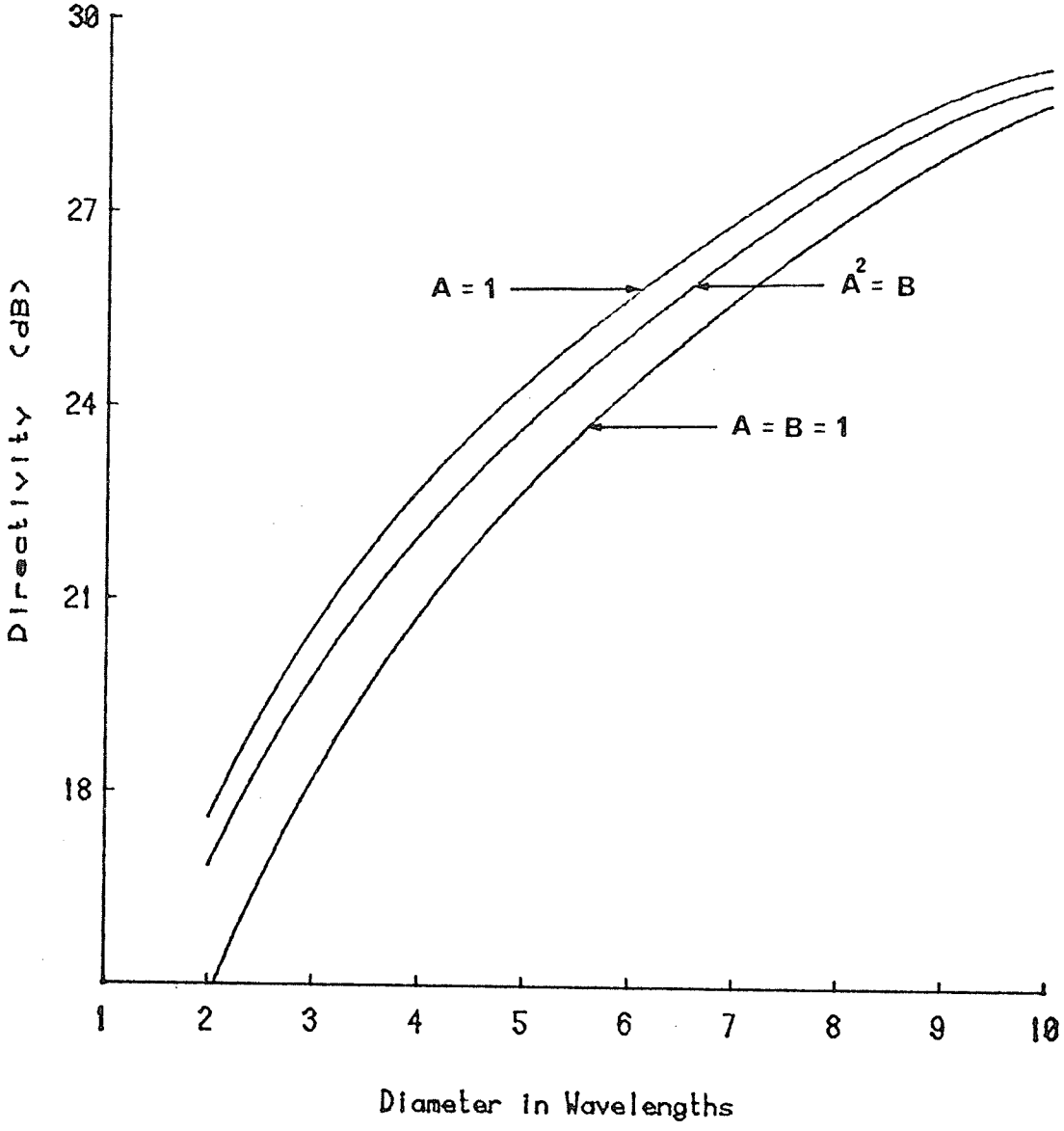

Fig. 4.6 Directivity of the modified Luneberg lens

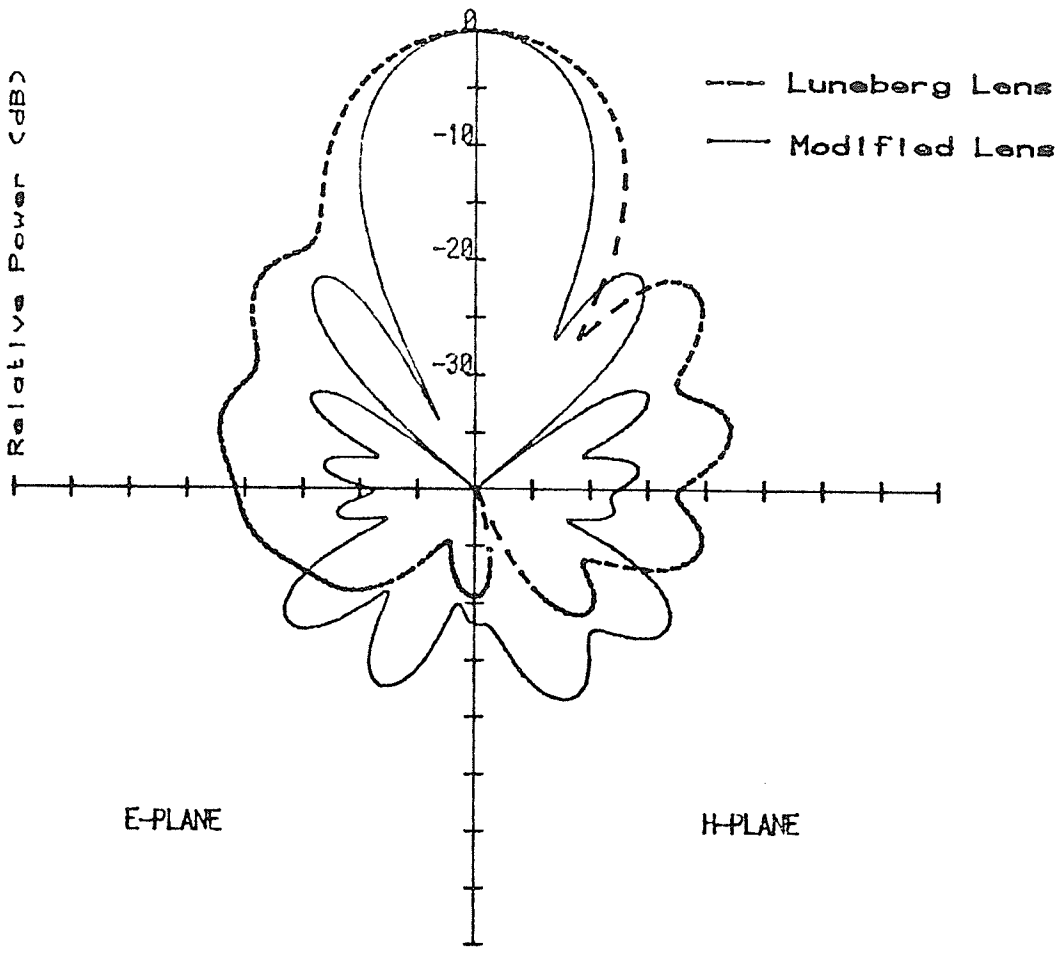

Fig. 4.7 Radiation pattern of a modified Luneberg lens;
Diameter D = 2λ

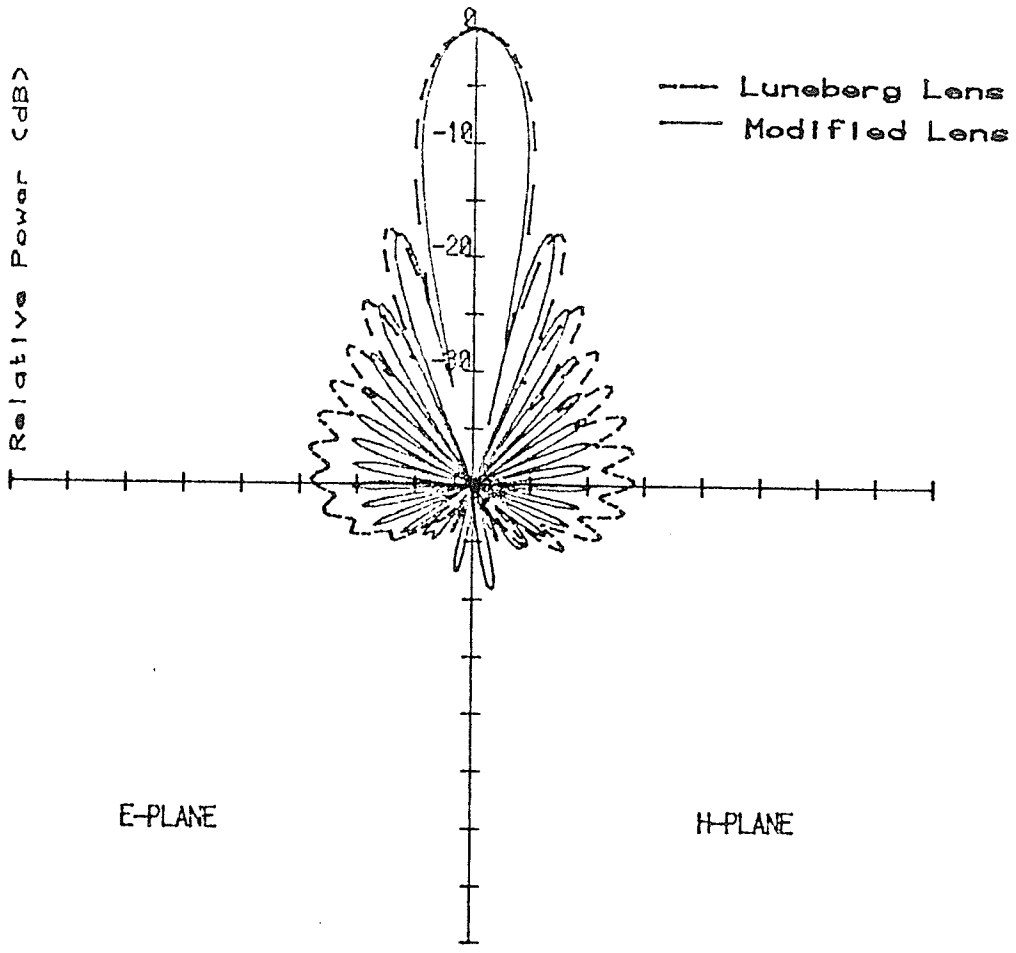

Fig. 4.8 Radiation pattern of a modified Luneberg lens; Diameter D = 5λ

TABLE 4.1

MODIFIED LUNEBERG LENS RADIATION PARAMETERS

Diameter in λ	B value	A = B = 1			A = 1			A^2 = B		
		Gain (dB)	Beam Width	1st side lobe level (dB)	Gain (dB)	Beam Width	1st side lobe level (dB)	Gain (dB)	Beam Width	1st side lobe level (dB)
2	1.4	14.79	30.2	-14.41	17.56	23.5	-17.15	16.85	24.0	-14.79
3	1.25	18.24	19.9	-15.78	20.60	16.7	-17.25	19.83	17.0	-15.6
4	1.16	20.761	15.1	-16.05	22.70	13.0	-16.9	22.0	13.25	-16.1
5	1.12	22.73	11.8	-16.74	24.37	9.5	-16.96	23.72	11.1	-16.32
6	1.1	24.34	9.8	-16.9	25.75	9.0	-16.97	25.17	9.1	-16.4
7	1.085	25.71	8.4	-17.0	26.91	7.6	-17.04	26.41	8.0	-16.47
8	1.075	26.90	7.3	-17.1	27.98	6.7	-17 .01	27.56	7.0	-16.6
9	1.06	27.94	6.5	-17.0	28.77	6.1	-16.7	28.47	6.2	-16.77
10	1.04	28.78	5.8	-16.35	29.35	5.5	-15.97	29.26	5.6	-16.81

CHAPTER 5

PERFORMANCE OF A LUNEBERG LENS WITH A PRACTICAL SOURCE ANTENNA

5.1 Introduction

A major use of the Luneberg lens, next to its use as a passive reflector, is as a broadband lens antenna. An open-ended waveguide or a feed horn may be employed as the actual source element. Such a relatively light weight feed can be moved rapidly over the lens surface to accomplish beam scanning. Alternatively, the moving feed may be replaced by an array of electronically switched feeds to eliminate bulky mechanical scanning system. Multiple frequency operation, using different feeds at different frequencies, is also feasible to improve feed bandwidth.

To simplify the analysis of the lens performance small aperture waveguides and horns are normally modelled by a single Huygens' source located at the feed aperture. However, such a representation of the feed with a single Huygens' source is generally inadequate and the computed lens characteristics do not agree satisfactorily with those obtained by experiment. To overcome this difficulty, we have represented an aperture feed element, such as an open ended rectangular waveguide, by a rectangular array of Huygens' sources. It is shown that by modifying the number of Huygens' source elements the radiation characteristics of any waveguide radiator can satisfactorily be represented by an array of Huygens' sources. Using this representation the radiation characteristics of Luneberg lenses illuminated by waveguide radiators is studied. Both standard and modified Luneberg lenses are

considered and their radiation patterns are computed.

To examine the quality of the radiated field both co-polar and cross-polar radiations are presented. It is shown that a Luneberg lens generally produces a high quality radiation with a relatively low level of cross-polarization. It is also found that modified lenses have better radiation characteristics than a Luneberg lens.

5.2 Waveguide Radiation Characteristics in the Presence of a Luneberg Lens

The radiation from a Luneberg lens of a few wavelengths in diameter, placed over the aperture of an open-ended waveguide is of practical interest since it exhibits properties suitable as transmitting and feed antennas. Since the exact analytical solution of a lens illuminated by a waveguide radiator is too difficult to obtain, previous investigators [6, 29] have used a Huygens' source to model the radiation of the waveguide.

Croswell et al [6] used a Huygens' source to model the waveguide aperture for excitation of a homogeneous dielectric sphere. They compared the theoretically computed normalized power patterns with the experimental results measured by Croswell and Chatterjee [5] for the radiation pattern of a plexiglass sphere centered against the flange of an open-ended waveguide. Although the agreement between the theoretical and the experimental results was good, the theoretical patterns have presented sharper nulls in the main beam and stronger back lobes than the measured patterns. They attributed the differences to scattering from the waveguide feed structure used in the measurements.

However, the Huygens' source radiation pattern shown in Fig. 3.2 is considerably different than the radiation pattern of a rectangular waveguide. Figure 5.1 illustrates these differences by showing both the normalized far field radiation characteristic of a Huygens' source together with the theoretical and experimental radiation patterns of a rectangular waveguide given by Silver [34]. It is clear that the 3 dB and 10 dB points of both the calculated and observed radiation patterns of the rectangular waveguide with $\frac{a}{\lambda} = 0.71$; $\frac{b}{\lambda} = 0.32$ are considerably narrower than that of a Huygens' source. Hence it is expected that the radiation patterns of the Huygens' source and the waveguide in the presence of a Luneberg lens will also be different.

In this section we will define a better model for the waveguide aperture. The electric and magnetic field distributions at the aperture suggests that a better model may be obtained by an array of Huygens' sources. We will then find a mathematical expression for the proposed model, calculate the radiation pattern for this array distribution and compare its data with the radiation pattern of a rectangular waveguide.

5.3 Rectangular Waveguide Model

5.3.1 Radiation pattern of a rectangular waveguide aperture

The tangential field components of TM and TE waves in the aperture of a rectangular guide, shown in Fig. 5.2, are given by [34]

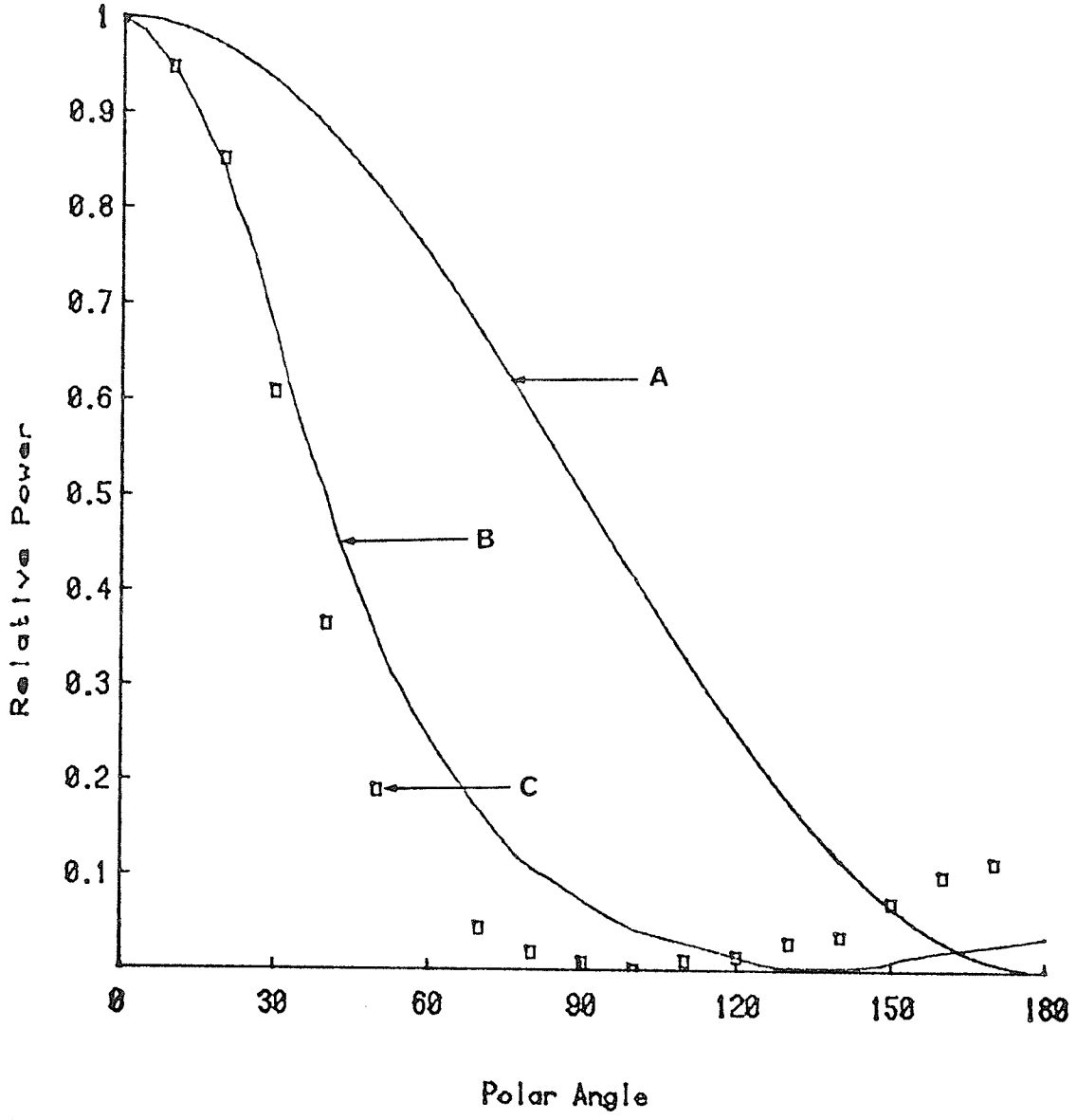

Fig. 5.1 Theoretical and observed radiation patterns of a rectangular waveguide (a = 0.7λ) [34], and the radiation pattern of a Huygens' source;
A) Huygens' source; B) Theoretical; C) Observed

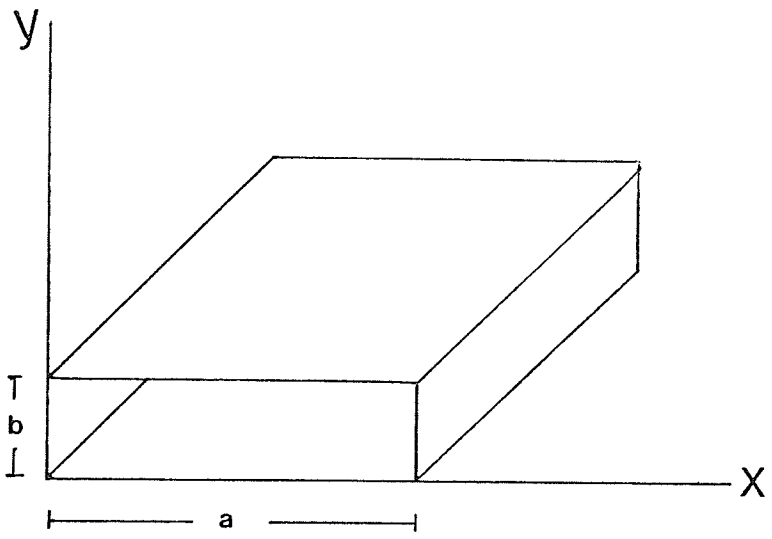

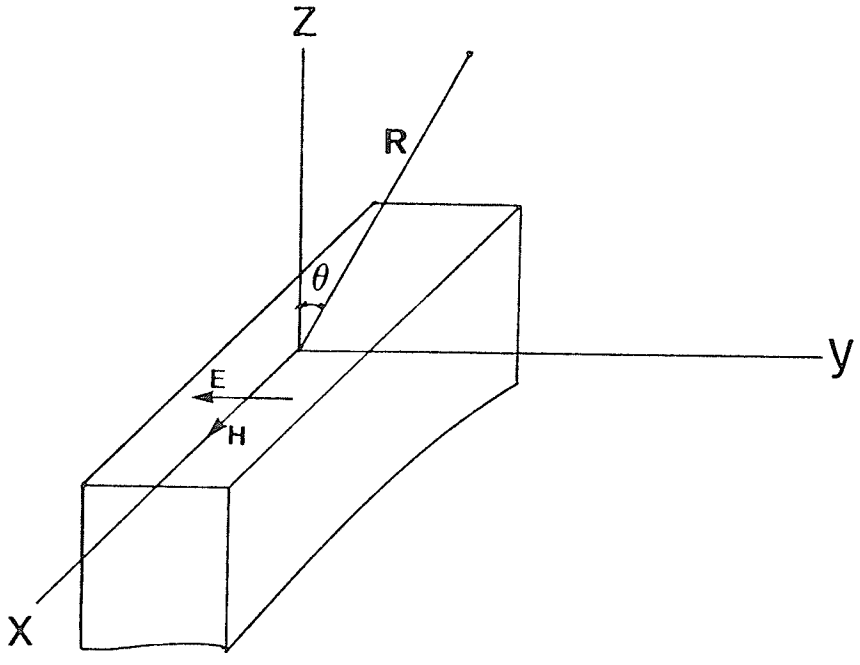

Fig. 5.2 Rectangular waveguide aperture

a. For TE-waves

$$H_x = -\frac{\gamma_{mn}}{i\omega\mu} \quad E_y = \frac{m\pi\gamma_{mn}}{k_{mn}^2 a} \sin\left(\frac{m\pi x}{a}\right) \cos\left(\frac{n\pi y}{b}\right)$$

$$H_y = \frac{\gamma_{mn}}{i\omega\mu} \quad E_x = \frac{n\pi\gamma_{mn}}{k_{mn}^2 b} \cos\left(\frac{m\pi x}{a}\right) \sin\left(\frac{n\pi y}{b}\right) \tag{5.1}$$

where $k_{mn}^2 = \left(\frac{m\pi}{a}\right)^2 + \left(\frac{n\pi}{b}\right)^2$

and propagation constant $\gamma_{mn} = (k_{mn}^2 - k^2)^{1/2}$

$$= \frac{2\pi}{\lambda g_{mn}}$$

where λg_{mn} is the waveguide wavelength.

b. For TM-waves

$$E_x = \frac{\gamma_{mn}}{i\omega\varepsilon} H_y = -\frac{m\pi\gamma_{mn}}{k_{mn}^2 a} \cos\left(\frac{m\pi x}{a}\right) \sin\left(\frac{n\pi y}{b}\right)$$

$$E_y = -\frac{\gamma_{mn}}{i\omega\varepsilon} H_x = -\frac{n\pi\gamma_{mn}}{k_{mn}^2} \sin\left(\frac{m\pi x}{a}\right) \cos\left(\frac{n\pi y}{b}\right) \tag{5.2}$$

The electric field over the aperture is polarized in the Y-direction and the electric-field components of the radiation field due to the TE_{mn} mode excitations are

$$E_\theta = -\left(\frac{\mu}{\varepsilon}\right)^{1/2} \frac{(\pi ab)^2 \sin\theta}{2\lambda^3 R k_{mn}^2} \left[1 + \frac{\beta_{mn}}{k} \cos\theta + \Gamma\left(1 - \frac{\beta_{mn}}{k} \cos\theta\right)\right]$$

$$\left[\left(\frac{m\pi}{a} \sin\phi\right)^2 - \left(\frac{n\pi}{b} \cos\phi\right)^2\right] \psi_{mn}(\theta,\phi) \ ,$$

$$E_\phi = -\left(\frac{\mu}{\varepsilon}\right)^{1/2} \frac{(\pi ab)^2 \sin\theta \sin\phi \cos\phi}{2\lambda^3 R}$$

$$\left[\cos\theta + \frac{\beta_{mn}}{k} + \Gamma\left(\cos\theta - \frac{\beta_{mn}}{k}\right)\right] \psi_{mn}(\theta,\phi) \ ,$$

where

$$\psi_{mn}(\theta,\phi) = \left[\frac{\sin\left(\frac{\pi a}{\lambda} \sin\theta \cos\phi + \frac{m\pi}{2}\right)}{\left(\frac{\pi a}{\lambda} \sin\theta \cos\phi\right)^2 - \left(\frac{m\pi}{2}\right)^2}\right]\left[\frac{\sin\left(\frac{\pi b}{\lambda} \sin\theta \sin\phi + \frac{n\pi}{2}\right)}{\left(\frac{\pi b}{\lambda} \sin\theta \sin\phi\right)^2 - \left(\frac{n\pi}{2}\right)^2}\right]$$

$$e^{i\left[kR - \frac{\pi}{\lambda} \sin\theta \ (a \cos\phi + b \sin\phi) - (m+n+1)\frac{\pi}{2}\right]} \qquad (5.3)$$

and Γ is the reflection coefficient at the waveguide aperture

For the TE_{10}-mode the radiation field reduces to

$$E_\theta^e = -\left(\frac{\mu}{\varepsilon}\right)^{1/2} \frac{\pi a^2 b}{2\lambda^2 R} \sin\phi \left[1 + \frac{\beta_{10}}{k}\cos\theta + \Gamma\left(1 - \frac{\beta_{10}}{k}\cos\theta\right)\right]$$

$$\left[\frac{\cos\left(\frac{\pi a}{\lambda}\sin\theta\cos\phi\right)}{\left(\frac{\pi a}{\lambda}\sin\theta\cos\phi\right)^2 - \left(\frac{\pi}{2}\right)^2}\right]\left[\frac{\sin\left(\frac{\pi b}{\lambda}\sin\theta\sin\phi\right)}{\left(\frac{\pi b}{\lambda}\sin\theta\sin\phi\right)}\right]$$

$$e^{i\left[kR - \frac{\pi}{\lambda}\sin\theta\,(a\cos\phi + b\sin\phi)\right]}$$

$$E_\phi = -\left(\frac{\mu}{\varepsilon}\right)^{1/2} \frac{\pi a^2 b}{2\lambda^2 R}\cos\phi\left[\cos\theta + \frac{\beta_{10}}{k} + \Gamma\left(\cos\theta - \frac{\beta_{10}}{k}\right)\right]$$

$$\left[\frac{\cos\left(\frac{\pi a}{\lambda}\sin\theta\cos\phi\right)}{\left(\frac{\pi a}{\lambda}\sin\theta\cos\phi\right)^2 - \left(\frac{\pi}{2}\right)^2}\right]\left[\frac{\sin\left(\frac{\pi b}{\lambda}\sin\theta\sin\phi\right)}{\frac{\pi b}{\lambda}\sin\theta\sin\phi}\right]$$

$$e^{i\left[kR - \frac{\pi}{\lambda}\sin\theta(a\cos\phi + b\sin\phi)\right]}$$

If the origin is shifted to the centre of the aperture, as shown in Fig. 5.2, the phase factor transforms into kR, R now being measured from the origin. In the case of large apertures $\Gamma \simeq 0$, therefore, the space factor is real and the waveguide is a directive point-source feed, the centre of the feed being the centre of the aperture. In small apertures where Γ is complex, there is no exact centre of the feed and the waveguide is only approximately a point source, from the point of view of the equiphase surfaces of the radiation pattern.

As shown in Fig. 5.2 the electric field over the aperture is

polarized in the y-direction so that the yz-plane is the E-plane of the system, while the xz-plane is the H-plane. The radiation patterns in the two principal planes are

for the E-plane,

$$E_\theta = 2\left(\frac{\mu}{\varepsilon}\right)^{1/2} \frac{a^2 b}{\pi\lambda^2 R}\left[1 + \frac{\beta_{10}}{k}\cos\theta + \Gamma\left(1 - \frac{\beta_{10}}{k}\cos\theta\right)\right]$$

$$\frac{\sin\left(\frac{\pi b}{\lambda}\sin\theta\right)}{\frac{\pi b}{\lambda}\sin\theta} e^{ikR}$$

and for the H-plane,

$$E_\phi = -\left(\frac{\mu}{\varepsilon}\right)^{1/2} \frac{\pi a^2 b}{2\lambda^2 R}\left[\cos\theta + \frac{\beta_{10}}{k} + \Gamma\left(\cos\theta - \frac{\beta_{10}}{k}\right)\right]$$

$$\frac{\cos\left(\frac{\pi a}{\lambda}\sin\theta\right)}{\left(\frac{\pi a}{\lambda}\sin\theta\right)^2 - \frac{\pi^2}{4}} e^{ikR} \qquad (5.5)$$

It is observed that the predominant factors in the patterns

$$\sin\left(\frac{\pi b}{\lambda}\sin\theta\right)/\frac{\pi b}{\lambda}\sin\theta \quad \text{and}$$

$$\cos\left(\frac{\pi a}{\lambda}\sin\theta\right)/\left[\left(\frac{\pi a}{\lambda}\sin\theta\right)^2 - \frac{\pi^2}{4}\right]$$

are determined by the dimension of the aperture in each respective plane. This illustrates that the patterns in the two principal planes

are independent and are determined by the aperture dimension in the respective plane.

The above discussion suggests that the waveguide aperture may be modelled by a rectangular array of Huygens' sources located in the plane of the aperture as presented in the next section.

5.3.2 Rectangular array of Huygens' sources

Consider the rectangular array of discrete Huygens' source elements in the xy plane as shown in Fig. 5.3, where the central element is chosen at the coordinate origin. If we select $2N_x+1$ elements in each column parallel to the x axis with an equal spacing d_x and $2N_y+1$ elements in each row parallel to the y axis with a common spacing d_y, the entire array will have $N_x \cdot N_y$ elements. The array becomes a square array when $N_x = N_y$ and $d_x = d_y$.

The field at a distant point P in free space contributed by the array column coincident with the x axis is then [21]

$$E_o = f(\theta,\phi) \sum_{m=-N_x}^{N_x} I_{mo} \exp[i(m\, k\, d_x \sin\theta \cos\phi + \alpha_x)] \qquad (5.6)$$

where $f(\theta,\phi)$ is the element pattern function, I_{mo} is the amplitude excitation of the mth element (counting from the origin) in the column $y = 0$, α_x is the associated phase excitation, and $k = \frac{2\pi}{\lambda}$. When the amplitude excitation for elements in other columns are proportional to those for corresponding elements on the x axis then

$$I_{mn} = I_{mo}\, I_{on}$$

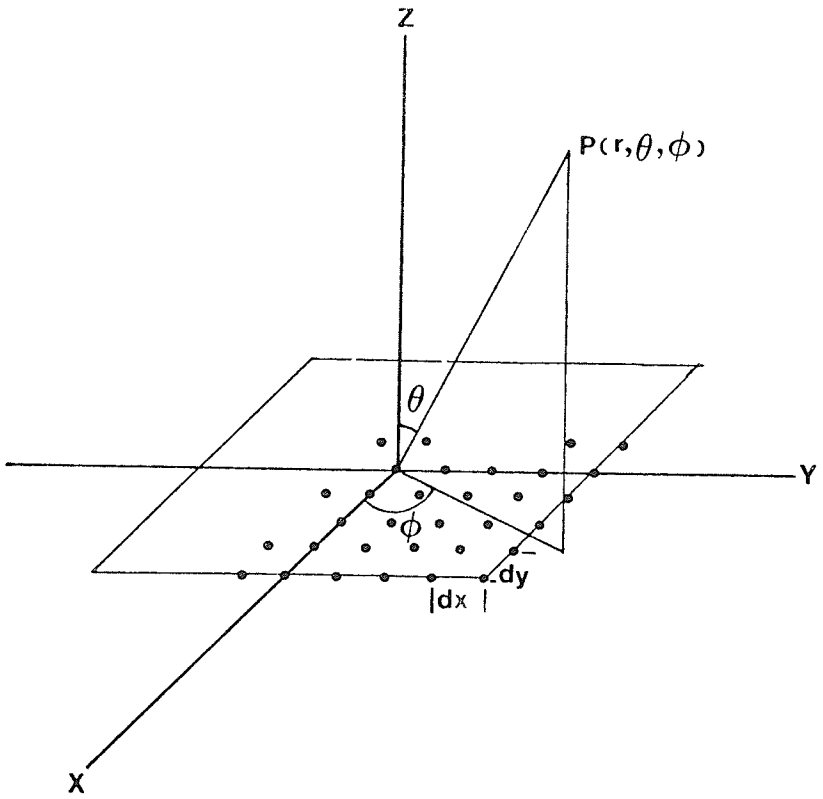

Fig. 5.3 Rectangular array of Huygens' sources

and we can sum up the total contribution from the array as

$$E(\theta,\phi) = \sum_{n=-N_y}^{N_y} E_n$$

$$= f(\theta,\phi) \sum_{m=-N_x}^{N_x} \sum_{n=N_y}^{N_y} I_{mn} \exp[i(m\, k\, d_x \sin\theta \cos\phi + \alpha_x)]$$

$$\cdot \exp[i(n\, k\, d_y \sin\theta \sin\phi + \alpha_y)]$$

$$= f(\theta,\phi)\, S_x\, S_y \qquad (5.7)$$

where $$S_x = \sum_{m=-N_x}^{N_x} I_{mo} \exp[i(m\, k\, d_x \sin\theta \cos\phi + \alpha_x)]$$

$$S_y = \sum_{n=-N_y}^{N_y} I_{on} \exp[i(n\, k\, d_y \sin\theta \sin\phi + \alpha_y)] \qquad (5.8)$$

It is clear from (5.7) that the pattern of the rectangular array is the product of the array factors of two linear arrays.

Now to calculate the field in the E-plane as defined in Chapter 3 for $\phi = 0$ where $\alpha_x = \alpha_y = 0$, i.e., element excitations are in phase, equations (5.8) can be written as

$$S_x = \sum_{m=-N_x}^{N_x} I_{mo} \exp[i(m\, k\, d_x \sin\theta)]$$

$$S_y = \sum_{n=-N_y}^{N_y} I_{on} \qquad (5.9)$$

Similarly for the H-plane for $\phi = 90°$

$$S_x = \sum_{m=-N_x}^{N_x} I_{mo}$$

$$S_y = \sum_{n=-N_y}^{N_y} I_{on} \exp[i(n\, k\, d_y)] \qquad (5.10)$$

Since in equations (5.9) and (5.10) S_y and S_x are constant respectively, the far field in the two principal planes is dependent only on the array distribution in each corresponding plane.

5.3.3 Huygens' source model of the waveguide

To calculate the far field of a rectangular array in the E and H-planes it is sufficient to calculate the field due to the linear array in the E or H planes. Hence the waveguide aperture may be modelled by two perpendicular arrays of Huygens' sources coinciding with the two principle axes as shown in Fig. 5.4.

We shall study the effect of the number of elements in each

array on the radiation characteristics, and identify a minimum number of Huygens' sources to model the aperture. This simple model may prove to be particularly desirable for more involved problems. According to equations (5.9) and (5.10) the far field of the array can be found by separately calculating the field due to individual array elements and summing their fields at any point in space.

Since we are interested primarily in calculating the radiation characteristics of a waveguide aperture in the presence of a Luneberg lens, the two arrays can be located on the surface of a large sphere with a diameter greater than several wavelengths (Fig. 5.5). Without loss of generality, this is acceptable since the waveguide wide dimension "a" is less than one wavelength, which is very small compared to the circumference of the sphere. This assumption will also make it possible to use all the equations deriven in Chapter 3.

Now, considering the array located on the xz or yz planes with $(2N_x+1)$ x $(2N_y+1)$ elements, respectively, with equal angular spacing of $\Delta\theta$ equations (5.7) and (5.8) may then be written as

$$E(\theta) = \sum_{m=-N_x}^{N_x} E_m(\theta) \qquad (5.11)$$

For the E-plane

$$E(\theta) = \sum_{n=-N_y}^{N_y} E_n(\theta) \qquad (5.12)$$

and the H-plane

where $E_m(\theta)$ and $E_n(\theta)$ are the field of elements m and n respectively

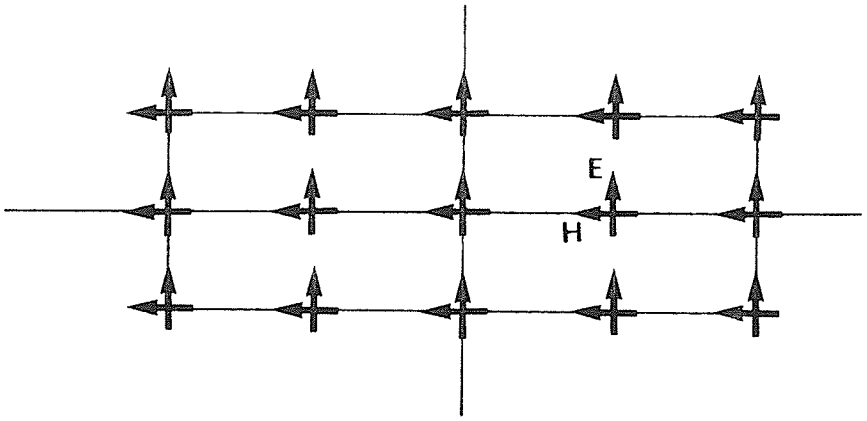

Fig. 5.4 Waveguide aperture representation by two linear arrays of Huygens' sources

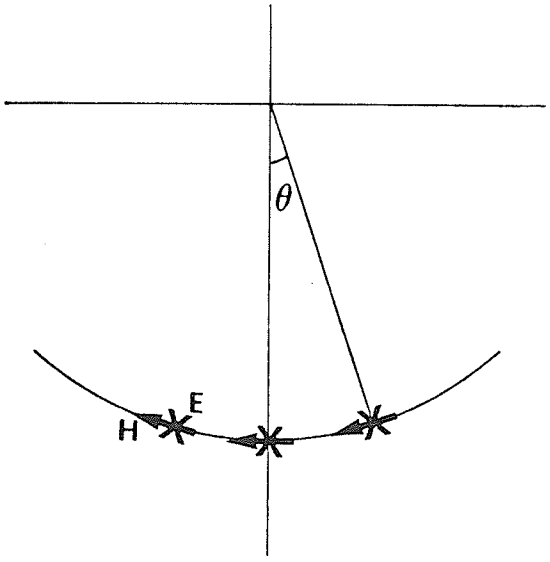

Fig. 5.5 Huygens' source array on the surface of a Luneberg lens

at a distant point of an angle θ .

If the far field is calculated at an angular interval equal to $\Delta\theta$, we can then denote the field at a point p of $\theta = \ell\Delta\theta$ due to a particular element n or m by $E(n, \ell)$ and $E(m, \ell)$. The total field at p can then be expressed as

$$E(\ell) = \sum_{m=-N_x}^{N_x} E(m, m+\ell) \tag{5.13}$$

for the E-plane, and

$$E(\ell) = \sum_{n=-N_y}^{N_y} E(n, n+\ell) \tag{5.14}$$

for the H-plane.

Using equation (5.13) and (5.14) together with the results obtained for a single Huygens' source in Chapter 3 we have found the radiation pattern; first for waveguide aperture in free space and then for a waveguide aperture in the presence of a Luneberg lens. The results are presented in section 5.6 of this chapter.

5.4 Cross-polarization

The use of two orthogonal polarizations to provide two communication channels for each frequency band has led to interest in the polarization purity of antenna patterns. The cross-plarization is considered in the case of three applications: 1) an antenna system to achieve nearly orthogonal polarization everywhere in some coverage region in order to create two communication channels for each frequency band; 2) a feed system for a paraboloidal reflector which will in turn

be used for the first application; and 3) a feed system for a paraboloidal reflector in which the objective is to maximize the aperture efficiency of the reflector.

In this section we will study the cross-polarization introduced by the Luneberg lens, and the possibility of using the lens to reduce cross-polarization of feeds with higher cross-polarization level, such as a dipole radiator.

5.4.1 Definition of the cross-polarization

The IEEE standard [37] defines the cross-polarization as the polarization orthogonal to a reference polarization. This definition has led to three alternative definitions [19]: 1) in rectangular coordinate system, one unit vector is taken as the direction of the reference polarization, and another as the direction of cross polarization [34]; 2) in spherical coordinate system the same definition applies using the unit vectors tangent to a spherical surface; and 3) reference and cross-polarization are defined to be what one measures when antenna patterns are taken in the usual manner. The third definition will be used in this section. Using this definition Ludwig [19] has shown that the measured co-polar and cross-polar patterns are given by, respectively,

$$R(\theta,\phi) = E(\theta,\phi) \cdot \{\cos\phi\ \hat{\theta} - \sin\phi\ \hat{\phi}\} \qquad (5.15)$$

$$C(\theta,\phi) = E(\theta,\phi) \cdot \{\sin\phi\ \hat{\theta} + \cos\phi\ \hat{\phi}\} \qquad (5.16)$$

For evaluating secondary patterns for the applications of orthogonal channels, we postulate the following ideal case: the

transmitting antenna has two ports, which radiate two patterns that are orthogonal at every pattern angle in the coverage region. Clearly, it is then possible to receive the two channels without any interference anywhere in the coverage region.

5.4.2 Cross-polarization of a Huygens' source in free space

Huygens' source is formed by a combination of an electric dipole and a magnetic dipole at 90° angular seperation. If the electric dipole is in the x direction and the magnetic dipole in the y direction, the far-zone electric field radiated by the Huygens' source is given by:

$$\bar{E}_H = -\frac{i\omega\mu_o C_e}{4\pi}\frac{e^{ikR}}{R}(\cos\phi\ \hat{\theta} - \sin\phi\ \hat{\phi})(1 - \cos\theta) \qquad (5.17)$$

where C_e is the electric dipole moment,

ω the angular frequency

μ_o the free space permittivity, and

k the propagation constant

From equation (5.16) the cross polarization field $C(\theta,\phi)$ is

$$C(\theta,\phi) = \bar{E}_{H\theta}\sin\phi + \bar{E}_{H\phi}\cos\phi$$

$$= \frac{-iw\mu_o C_e}{4\pi}\frac{e^{ikR}}{R}(1 - \cos\theta)\cdot(\sin\phi\cos\phi - \sin\phi\cos\phi)$$

$$= 0$$

This means that the cross polarization of a crossed Huygens' source is

identically zero. This presents an interesting concept, since by using a Huygens' source as the feed for any antenna system and by calculating the cross-polarization field, we directly calculate the cross-polarization introduced by the antenna system. This concept will be used later in this chapter to find the cross polarization introduced by the Luneberg lens.

5.4.3 Cross-polarization of an electric dipole in free space

To illuminate a Luneberg lens by a dipole source, we may assume the dipole is located at the coordinate origin and directed along the x-axis. Its far field can be found from the magnetic vector potential $\bar{A}_x$, which in spherical coordinates may be assumed to be

$$\begin{aligned} \bar{A}_r &= \bar{A}_x \cos\phi \sin\theta \\ \bar{A}_\theta &= \bar{A}_x \cos\phi \cos\theta \\ \bar{A}_\phi &= -\bar{A}_x \sin\phi \end{aligned} \tag{5.18}$$

where $\bar{A}_x = \frac{C_e}{4\pi r} \cdot e^{ikr}$, and C_e is the dipole moment. Then the magnetic field can be expressed as

$$H_\theta = \text{Curl}_\theta \bar{A} = \left[\frac{1}{r \sin\theta} \cdot \frac{\partial A_r}{\partial \phi} - \frac{1}{r} \frac{\partial (r A_\phi)}{\partial r}\right] \tag{5.19}$$

$$H_\phi = \text{Curl}_\phi \bar{A} = \frac{1}{r}\left[\frac{\partial}{\partial r}(rA_\theta) - \frac{\partial A_r}{\partial \theta}\right] \tag{5.20}$$

Evaluating equations (5.19) and (5.20) and ignoring terms of $1/r^2$ and

$1/r^3$ for the far field components, the electric fields in the θ and ϕ directions can be shown to be

$$E_\theta = \frac{-i\omega\mu_o C_e}{4\pi} \frac{e^{jkR}}{R} \cos\theta \cos\phi \tag{5.21}$$

$$E_\phi = \frac{i\omega\mu C_e}{4\pi} \frac{e^{jkR}}{R} \sin\phi \tag{5.22}$$

The expressions for the reference and cross polarization fields for an electric dipole in space can then be written as

$$R(\theta,\phi) = \frac{-i\omega\mu C_e}{4\pi} \frac{e^{ikR}}{R} \left[\cos\theta \cos^2\phi + \sin^2\phi\right]$$

$$= \frac{-i\omega\mu C_e}{4\pi} \frac{e^{ikR}}{R} \left[1 + \cos^2\phi(\cos\theta - 1)\right] \tag{5.23}$$

$$C(\theta,\phi) = \frac{-i\omega\mu C_e}{4\pi} \frac{e^{ikR}}{R} \left[\sin\phi \cos\theta \cos\phi - \sin\phi \cos\phi\right]$$

$$= \frac{-i\omega\mu C_e}{4\pi} \frac{e^{ikR}}{R} \sin\phi \cos\phi\left[\cos\theta - 1\right] \tag{5.24}$$

Equations (5.23) and (5.24) present the reference and cross-polarizations of an electric dipole located at the origin in the x direction. For the two principal planes $\phi = 0$, $\phi = 90$ equation (5.23) simplifies to the following:

In the E-plane for $\phi = 0$,

$$R(\theta,0) = \frac{-i\omega\mu C_e}{4\pi} \frac{e^{ikR}}{R} \cos\theta \qquad (5.25)$$

This equation will produce the familiar figure eight shape, with its maximum at $\theta = 0°$ and minimum at $\theta = 90°$.

In the H-plane for $\phi = 90°$

$$R(\theta,\pi) = \frac{-i\omega\mu C_e}{4\pi} \frac{e^{ikR}}{R} \quad , \qquad (5.26)$$

i.e. the field is constant and is independent of θ .

The cross polarization is identically zero in both principal planes due to the term $\sin\phi \cos\phi$ in equation (5.24). On the other hand, the cross-polarization will have a maximum value at $\phi = 45°$ as follows

$$C(\theta,\phi) = \frac{-i\omega\mu C_e}{4\pi} \frac{e^{ikR}}{R} \sin\phi \cos\phi \, [\cos\theta - 1]$$

$$= \frac{-i\omega\mu C_e}{4\pi} \frac{e^{ikR}}{R} \cdot \frac{1}{2} \sin 2\phi \, [\cos\theta - 1] \qquad (5.27)$$

which is maximum at the $\phi = 45°$ plane, and given by

$$C(\theta, \tfrac{\pi}{4}) = \frac{-i\omega\mu C_e}{8\pi} \frac{e^{ikR}}{R} \, [\cos\theta - 1] \qquad (5.28)$$

This equation shows that in the $\phi = \frac{\pi}{4}$ plane the cross-polarization has

the same shape as the reference polarization in the E-plane, although it is shifted by 90°. Figure 5.6 shows the reference and cross-polarization fields in the three planes discussed above. It is clear from this figure that the electric dipole has a substantial cross-polarization level, which increases rapidly with increasing pattern angle. The cross-polarization level is only 10 dB below the reference polarization level at the beam half power points.

5.5 Cross-polarization of a Luneberg Lens

In this section we will derive an expression for the cross-polarization introduced by a Luneberg lens. This can be achieved by calculating the cross-polarization field of a Luneberg lens fed by a Huygens' source, since Huygens' source does not introduce any cross-polarization.

The cross-polarization of a Luneberg lens fed by an electric dipole is also an interesting case, to investigate whether the lens can reduce the large cross-polarization level of the dipole antenna.

5.5.1 Cross-polarization of a Huygens' source in the presence of a Luneberg lens

The far electric field for a Huygens' source in the presence of a Luneberg lens has been derived in Chapter 3 and is

$$\bar{E}_H(R) = \frac{-i\omega\mu C_e}{4\pi} \frac{e^{ikR}}{R} \sum_{n=1}^{\infty} \frac{2n+1}{n(n+1)} (-i)^n$$

$$\{-i(A_n + D_n)\, \bar{m}_{oln} + (B_n + C_n)\, \bar{n}_{eln}\} \qquad (5.29)$$

where A_n, B_n, C_n and D_n are defined in Chapter 3 and the vector wave functions $\bar{m}_{oln}$, n_{eln} are given by

$$\bar{m}_{oln} = \frac{P_n^l(\cos\theta)}{\sin\theta} \cos\phi \, \hat{\theta} - \frac{\partial P_n^l(\cos\theta)}{\partial\theta} \sin\phi \, \hat{\phi}$$

$$\bar{n}_{eln} = \frac{\partial P_n^l(\cos\theta)}{\partial\theta} \cos\phi \, \hat{\theta} - \frac{P_n^l(\cos\theta)}{\sin\theta} \sin\phi \, \hat{\phi}$$

Then the far field can be written as

$$\bar{E}_H(\theta,\phi) = \bar{E}_{H1}(\theta) \cos\phi \, \hat{\theta} - \bar{E}_{H2}(\theta) \sin\phi \, \hat{\phi} \qquad (5.30)$$

where

$$\bar{E}_{H1}(\theta) = \frac{-\omega\mu C_e}{4\pi\varepsilon} \frac{e^{ikR}}{R} \sum_{n=1}^{\infty} \frac{2n+1}{n(n+1)} (-i)^n$$

$$\left\{ -i(A_n + D_n) \frac{P_n^l(\cos\theta)}{\sin\theta} + (B_n + C_n) \frac{\partial P_n^l(\cos\theta)}{\partial\theta} \right\}$$

$$\bar{E}_{H2}(\theta) = \frac{-\omega\mu C_e}{4\pi\varepsilon} \frac{e^{ikR}}{R} \sum_{n=1}^{\infty} \frac{2n+1}{n(n+1)} (-i)^n$$

$$\left\{ -i(A_n + D_n) \frac{\partial P_n^l(\cos\theta)}{\partial\theta} + (B_n + C_n) \frac{P_n^l(\cos\theta)}{\sin\theta} \right\}$$

Substituting equation (5.30) in equation (5.16) we can write the cross-polarization as follows:

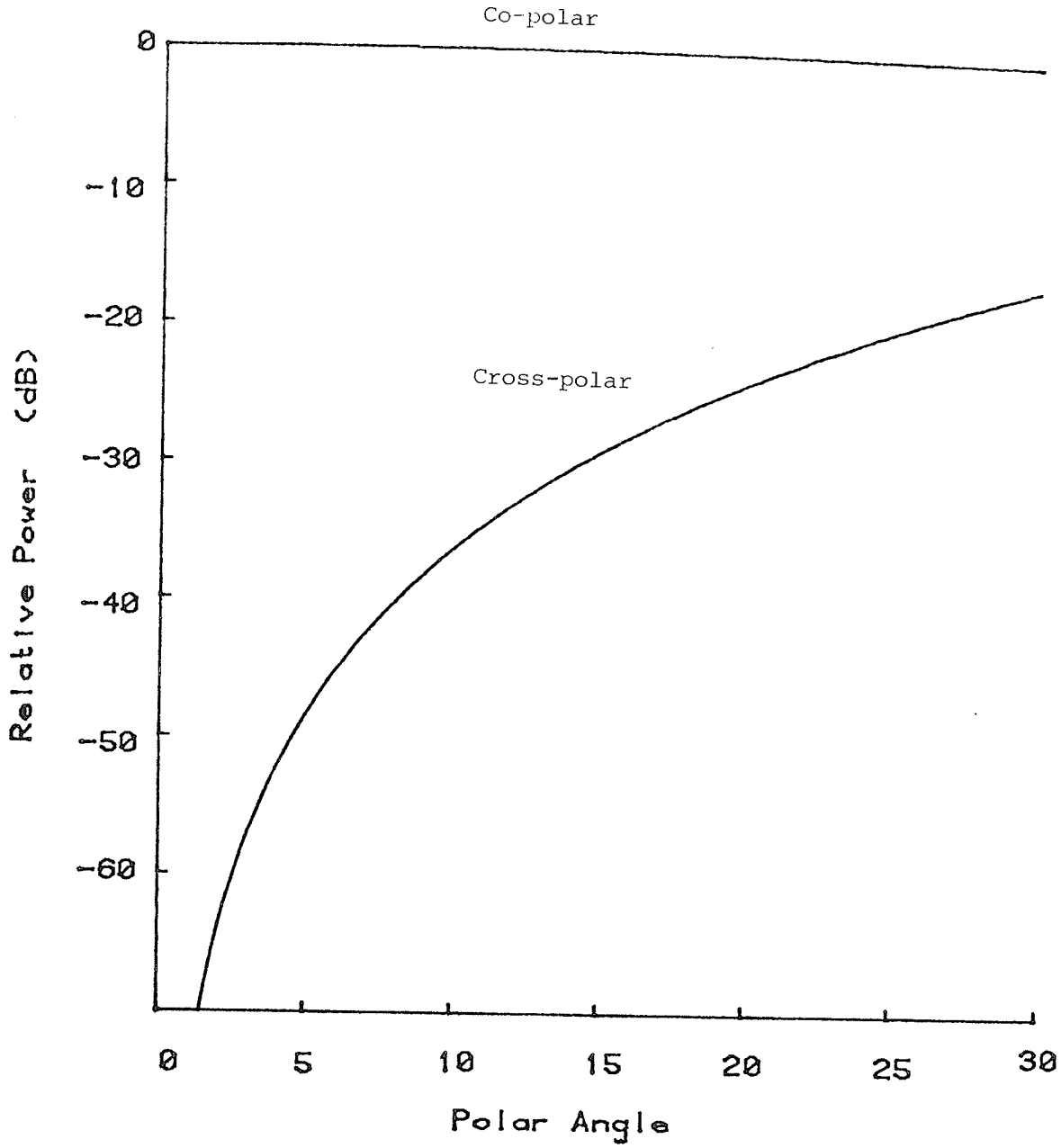

Fig. 5.6 Co-polar and cross-polar patterns of an electric dipole

$$C_H(\theta,\phi) = E_H(\theta,\phi) \cdot \left[\sin\phi\ \hat{\theta} + \cos\phi\ \hat{\phi}\right]$$

$$= \frac{1}{2} \sin 2\phi \left[\bar{E}_{H1}(\theta) - \bar{E}_{H2}(\theta)\right] \qquad (5.31)$$

The fields $\bar{E}_{H1}$ and $\bar{E}_{H2}$ are the fields in the two principal E and H-planes respectively.

Using equation (5.31) the maximum cross-polarization in the plane $\phi = \frac{\pi}{4}$, and for a certain polar angle θ can simply be obtained by subtracting the value of the electric field in one principal plane at the angle θ from the value of the electric field at the other principal plane at the same angle θ.

5.5.2 Cross-polarization of an electric dipole in the presence of a Luneberg lens

According to the definition of the cross polarization presented above the electric dipole produces a considerable cross-polarization level which increases with increasing pattern angle θ. It is interesting to investigate the effect of the Luneberg lens on the cross-polarization field of such a dipole. The far electric field of a dipole located at the surface of a Luneberg lens, with its centre at the origin is given by

$$\bar{E}_D(R) = \frac{-\omega\mu C_e}{4\pi} \frac{e^{ikR}}{R} \sum_{n=1}^{\infty} \frac{2n+1}{n(n+1)} (-i)^n$$

$$\left[-iA_n \bar{m}_{o1n} + B_n \bar{n}_{e1n} \right] \tag{5.32}$$

Then the far field can be expressed as in the Huygens' source case, as

$$\bar{E}_D(\theta) = \bar{E}_{D1}(\theta) \cos\phi \; i_\theta - \bar{E}_{D2} \sin\phi \; i_\phi \tag{5.33}$$

where

$$\bar{E}_{D1}(\theta) = \frac{-\omega\mu C_e}{4\pi} \frac{e^{ikR}}{R} \sum_{n=1}^{\infty} \frac{2n+1}{n(n+1)} (-i)^n$$

$$\left[-iA_n \frac{P_n^1(\cos\theta)}{\sin\theta} + B_n \frac{\partial P_n^1(\cos\theta)}{\partial\theta} \right]$$

and

$$\bar{E}_{D2}(\theta) = \frac{-\omega\mu C_e}{4\pi} \frac{e^{ikR}}{R} \sum_{n=1}^{\infty} \frac{2n+1}{n(n+1)} (-i)^n$$

$$\left[-i\, A_n \frac{\partial P_n^1(\cos\theta)}{\partial\theta} + B_n \frac{P_n^1(\cos\theta)}{\sin\theta} \right]$$

Following the same procedure used for the Huygens' source in the previous section the cross-polarization can be expressed as

$$C_D(\theta,\phi) = \frac{1}{2} \sin 2\phi \left[\bar{E}_{D1}(\theta) - \bar{E}_{D2}(\theta) \right] \tag{5.34}$$

where $\bar{E}_{D1}$ and $\bar{E}_{D2}$ are the H-plane and E-plane far fields respectively.

5.6 Results and Discussion

To investigate the validity of the waveguide model derived in the preceding sections, the far field of various waveguide models represented by different number of array elements will be calculated. this procedure will also help to identify the minimum array (array with minimum number of elements) that may correctly model the waveguide aperture.

5.6.1 Radiation pattern of a rectangular waveguide aperture in free space

The H-plane radiation patterns of a waveguide with a dimension $a = 0.7\lambda$ are shown in Fig. 5.7, together with the radiation patterns reported by Silver [34]. The radiation patterns are shown for three different model arrays having 9, 5 and 3 elements in the H-plane. The angular separation of the adjacent elements in the array are given by 0.5, 1 and 2 degrees respectively. It should be noted that the number of elements is always odd since we have chosen one of the elements to be at the centre of the aperture. All three distributions have presented a good model for the waveguide, judging by the far field radiation pattern, when compared with the reported patterns of the waveguide with the same dimension. It is particularly interesting to notice that the third case, an array with three sources, had produced a pattern very close to the measured pattern of the waveguide. This means that the waveguide aperture can be modeled by three Huygens' sources with equal strength, one located at the centre and the others

at each side of the aperture.

To further check the validity of the three source model, this model was used to calculate the radiation pattern for waveguide apertures of dimensions a = 0.5λ to a = 0.87λ. The calculated patterns are illustrated in Fig. 5.8. The width of the radiation lobe decreases as the dimension "a" of the waveguide increases, which is consistant with the observed waveguide aperture radiation characteristics. This again confirms that the three source array is a valid model for the rectangular waveguide aperture.

5.6.2 Radiation pattern of a rectangular waveguide aperture in the presence of a Luneberg lens

In the preceding section we have shown that the waveguide aperture can be modeled by an array of three Huygens' sources. In this section we will find the radiation pattern of a rectangular waveguide in the presence of a Luneberg lens, and point out the differences between this pattern and the patterns for a single Huygens' source presented in Chapter 3.

The radiation patterns of a rectangular waveguide aperture with the broad dimension a = 0.7λ located at the surface of a Luneberg lens of diameter D = 5λ and D = 10λ are presented in Figures 5.9 and 5.10 respectively. Compared to the radiation patterns of a single Huygens' source, the waveguide radiation pattern presented a slightly wider major lobe, while the minor lobes are largely suppressed. For the Luneberg lens with diameter D = 5λ the half power point beam width has increased by approximately two degrees while the side lobes have been reduced by 8dB. For the Luneberg lens with a diameter D = 10λ the beam width has increased by one degree, and the side lobes have

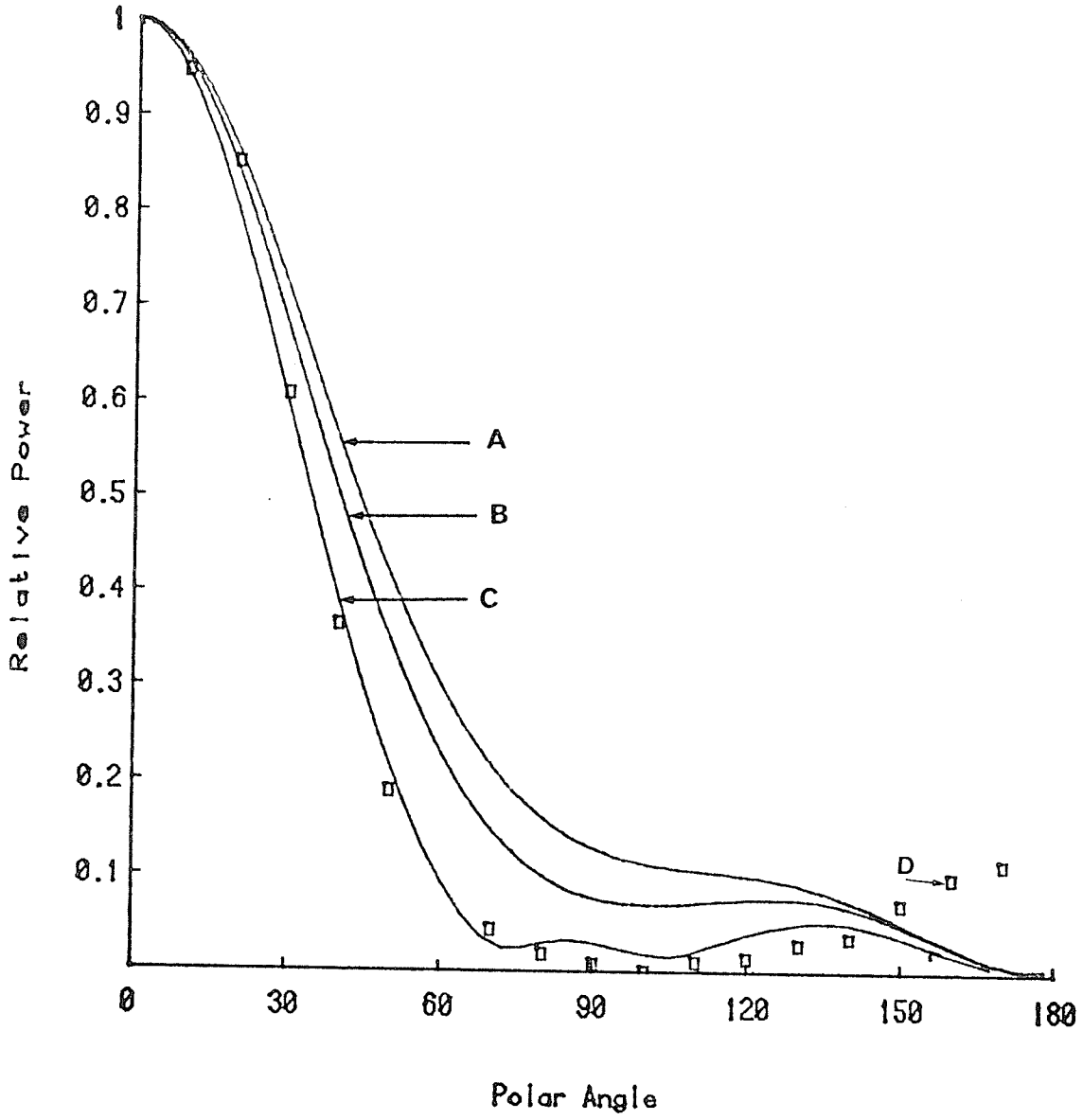

Fig. 5.7 Generation of the radiation characteristics of a rectangular waveguide by an array of Huygens' sources; A) 9 elements; B) 5 elements; C) 3 elements; D) measured (34).

decreased by 8 dB.

Finally, we will present the radiation pattern for a waveguide aperture in the presence of a modified Luneberg lens, as described in Chapter 4. Only a lens with a diameter D = 5λ has been considered since for larger diameters the improvement in the Luneberg lens is small. The radiation pattern for the above case is presented in Fig. 5.11. The major lobe presented the same characteristics as in the case of an ordinary Luneberg lens in Fig. 5.9 although the improvement in the side lobe is better.

5.6.3 Cross-polarization of an electric dipole

The electric dipole presents a significant cross-polarization level. It is therefore interesting to study the cross-polarization fields of a dipole radiator in the presence of a Luneberg lens.

The reference and cross-polarization fields for an electric dipole in the presence of a Luneberg lens are shown in Figures 5.12 and 5.13. The maximum cross-polarization field level at the main beam half power points is -22 dB, compared to the corresponding level of -10 dB for a dipole in free-space. This means that the Luneberg lens has reduced the cross-polarization level by 12 dB. This indicates that a combination of a dipole and a Luneberg lens may be used as a feed for a parabolic reflector antenna. The combination will reduce the cross-polarized currents on the surface of the paraboloid and hence increase the aperture efficiency. It should also be noted that the maximum cross-polarization level is -14 dB compared to 0 dB for a dipole in free space. That indicates that the Luneberg lens not only reduces the cross-polarization level in the coverage area, but also reduces the total power of the cross-polarization field.

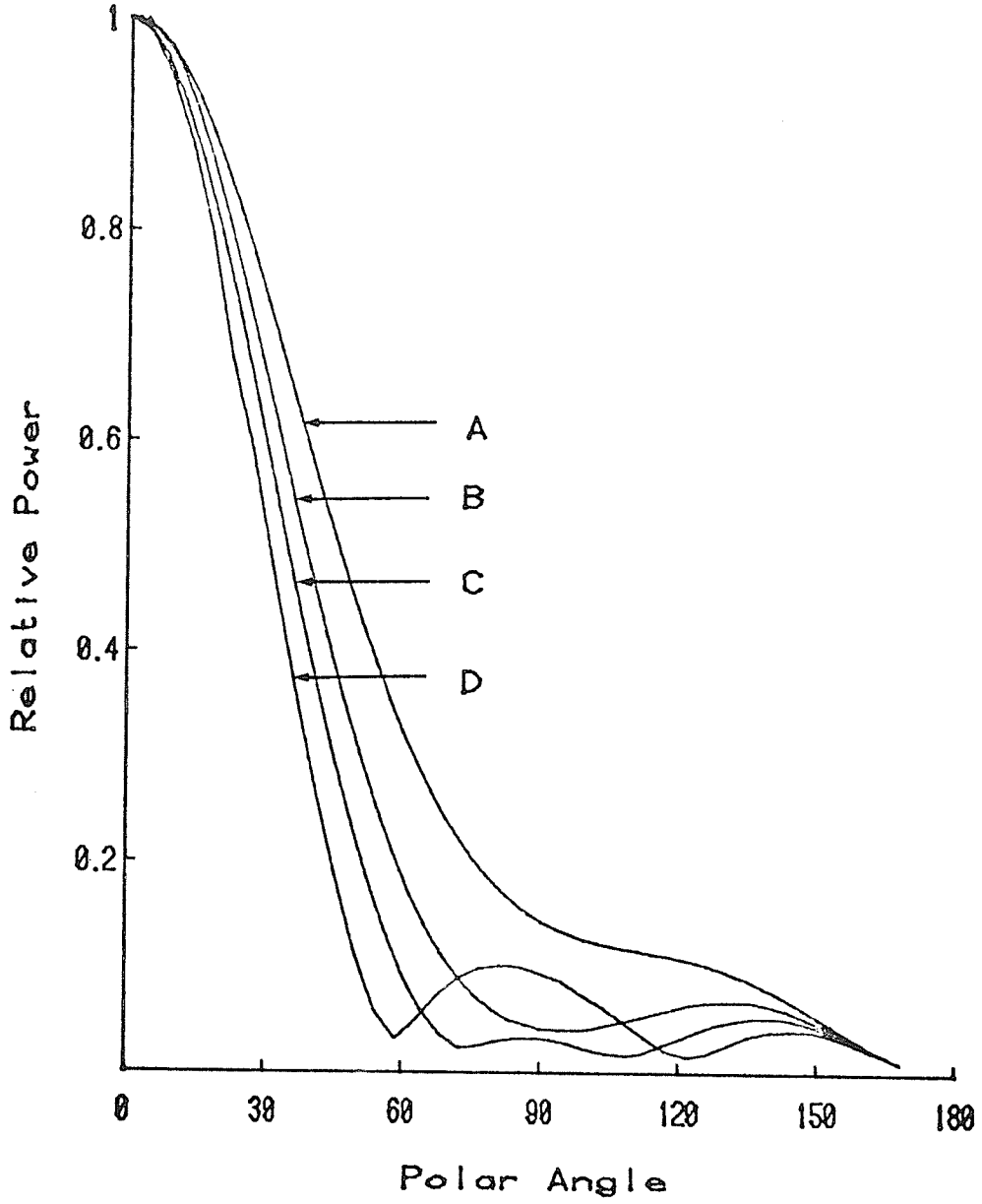

Fig. 5.8 Generation of the rectangular waveguide radiation characteristics by a 3 element array of Huygens' sources, waveguide dimension; A) $a = 0.52\lambda$; B) $a = 0.65\lambda$; C) $a = 0.7\lambda$; D) $a = 0.78\lambda$

5.6.4 Cross-polarization of a Luneberg lens

By definition, Huygens' source produce no cross-polarization field components in free space. Hence the cross-polarization field of a Luneberg lens may be evaluated by calculating the cross-polarization field of a Huygens' source in the presence of a Luneberg lens. The cross-polarization fields when the source is located on the surface of the sphere are shown in Figs. 5.14 and 5.15. A summary of the cross-polarization levels at the beam half power points, for lens diameters from $D = 2\lambda$ to $D = 10\lambda$ are shown in Table 5.1. The table also shows the corresponding values for the modified Luneberg lens introduced in Chapter 4. This table shows that the modified lens of $A = 1$ produced a considerable reduction of cross polarization level in the beam area of coverage. Also the modified lens has reduced the total power of the cross-polarization field, as shown in Fig. 5.16.

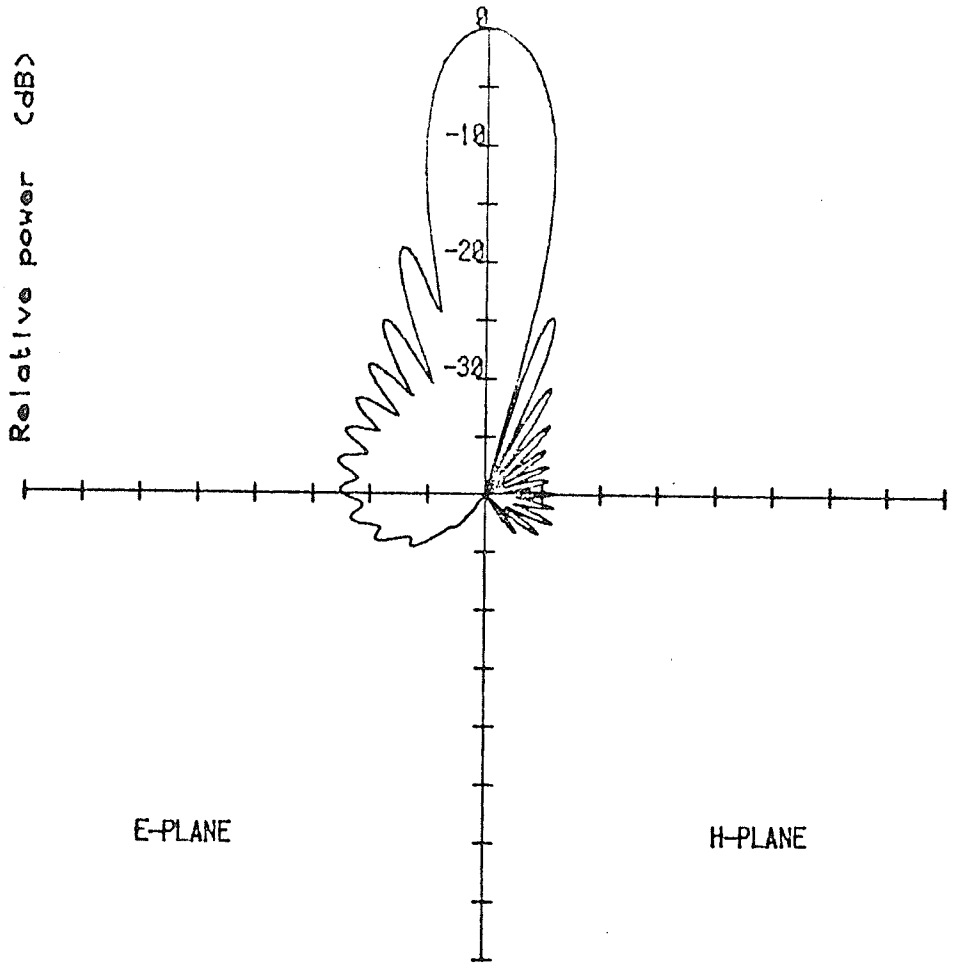

Fig. 5.9 Radiation pattern of a rectangular waveguide in the presence of a Luneberg lens; Diameter D = 5λ

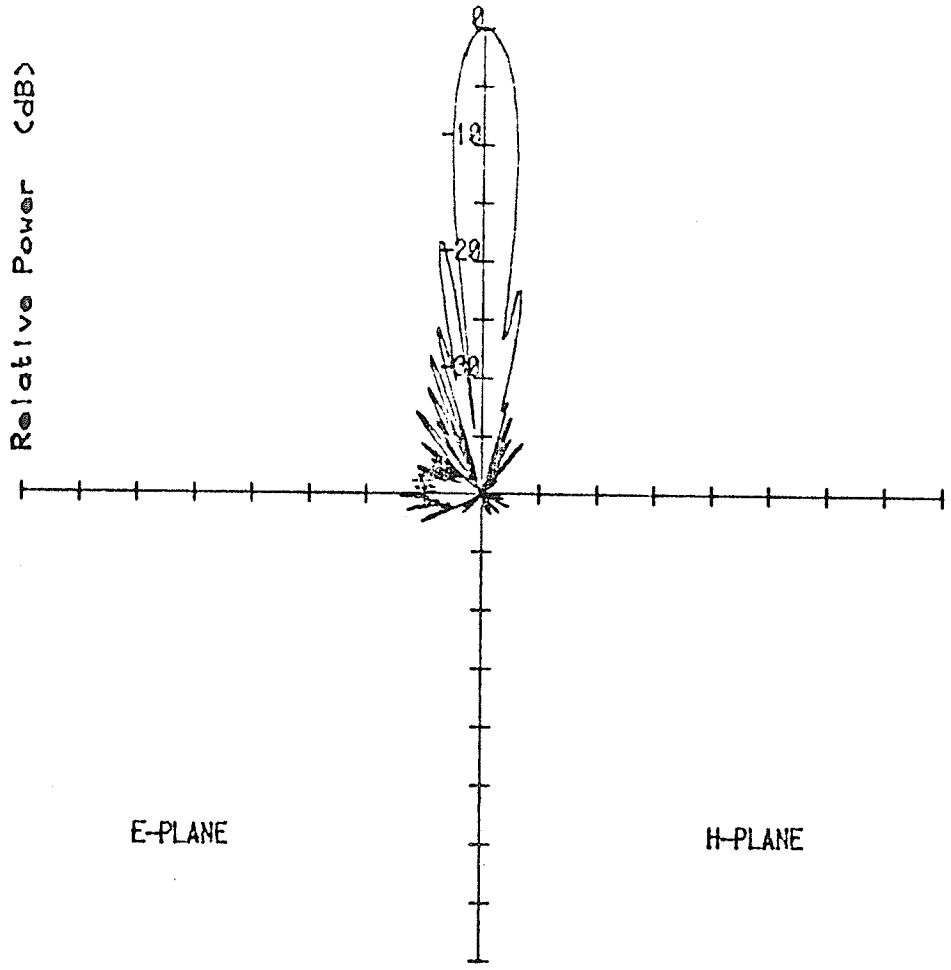

Fig. 5.10 Radiation pattern of a rectangular waveguide in the presence of a Luneberg lens; Diameter D = 10λ

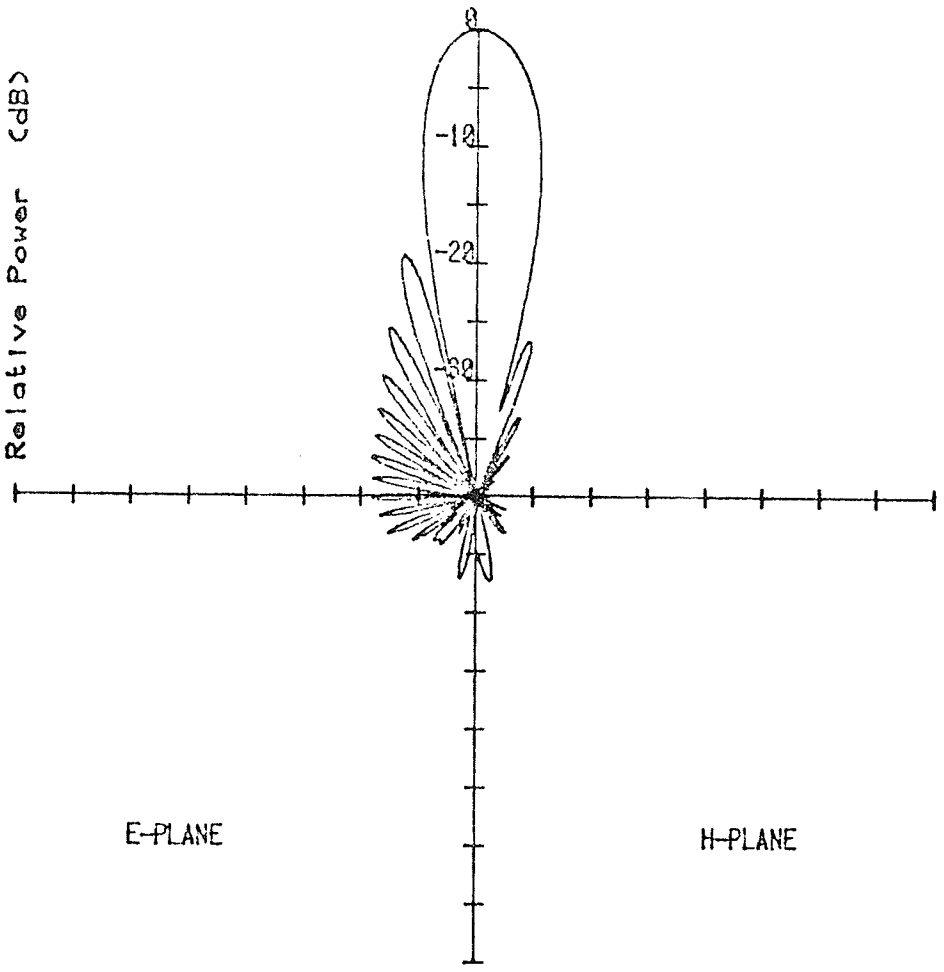

Fig. 5.11 Radiation pattern of a rectangular waveguide in the presence of a modified Luneberg lens; Diameter D = 5λ

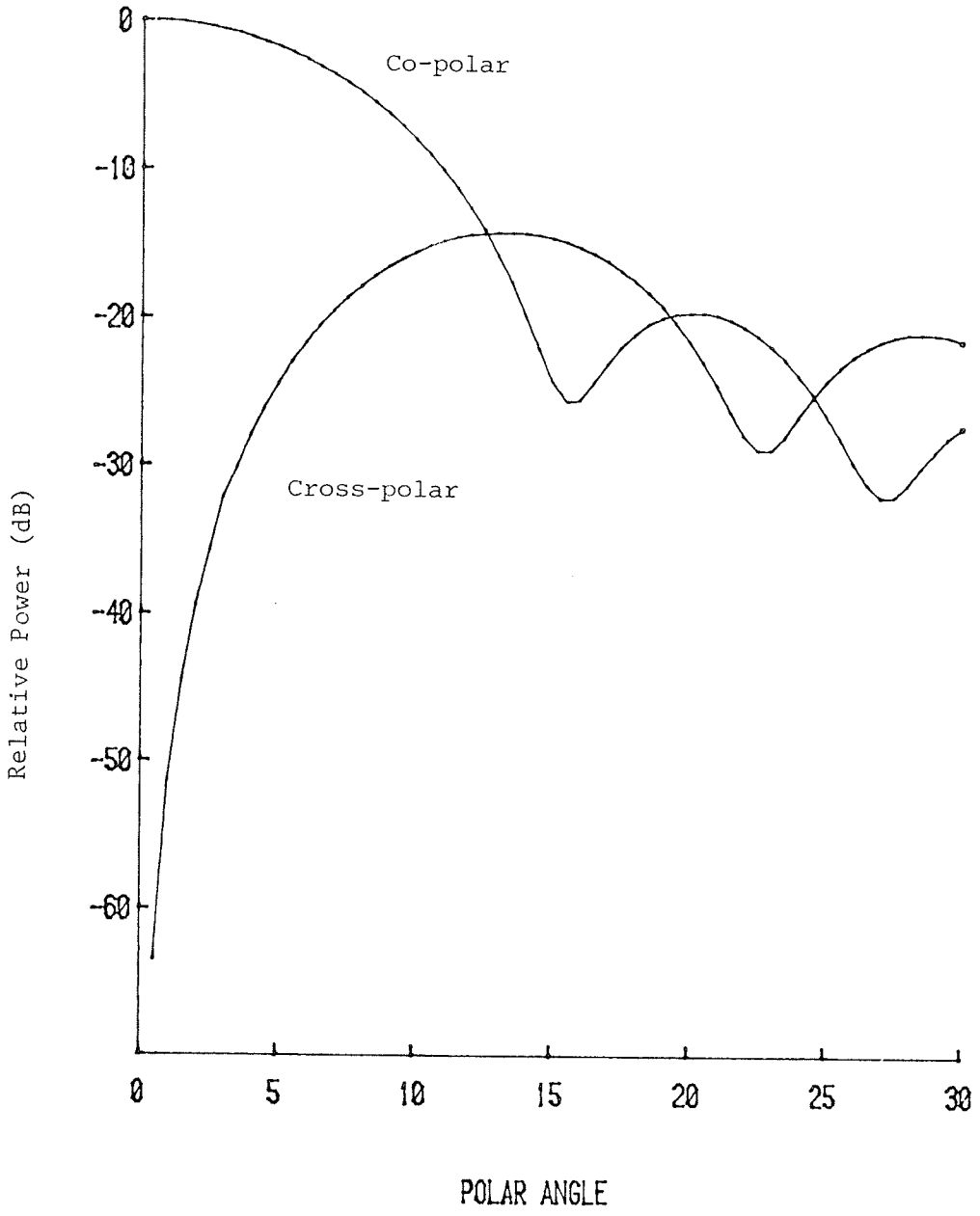

Fig. 5.12 Co-polar and cross-polar radiation patterns of an electric dipole in the presence of a Luneberg lens; Diameter D = 5λ

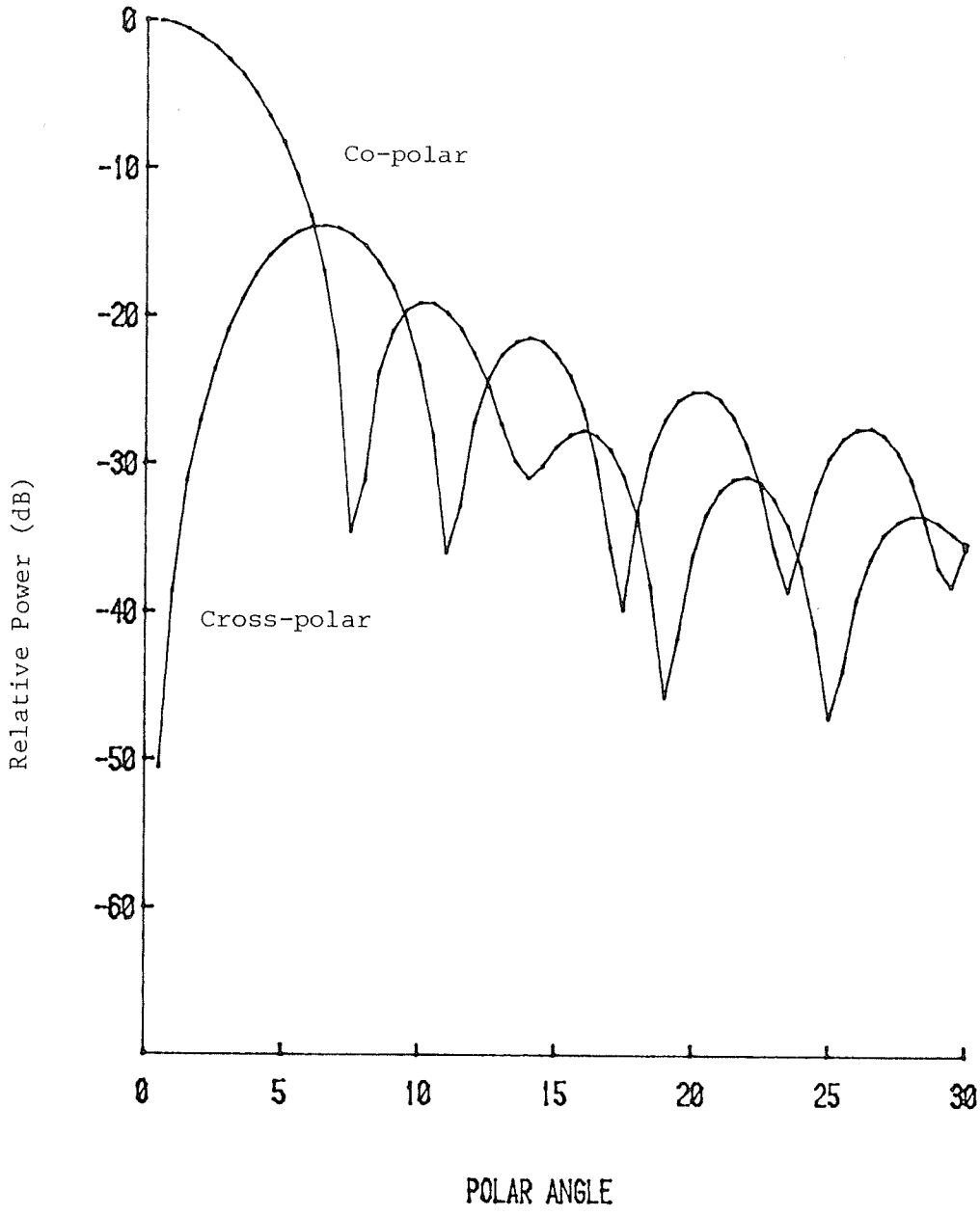

Fig. 5.13 Co-polar and cross-polar radiation patterns of an electric dipole in the presence of a Luneberg lens; Diameter D = 10λ

TABLE 5.1

Luneberg Lens Cross-Polarization

at Beam Half-Power Point: $\phi = 45°$

	Cross-Polarization (dB)		
Diameter (λ)	Luneberg Lens	Modified Luneberg Lens	
		A = 1	$A^2 = B$
2	-27.44	-40.35	-29.62
3	-31.33	-40.52	-32.81
4	-33.9	-39.81	-35.18
5	-36.13	-40.43	-36.98
6	-37.78	-40.99	-38.26
7	-39.17	-41.35	-39.60
8	-40.42	-41.69	-40.87
9	-41.50	-42.40	-41.83
10	-43.26	-43.41	-42.54

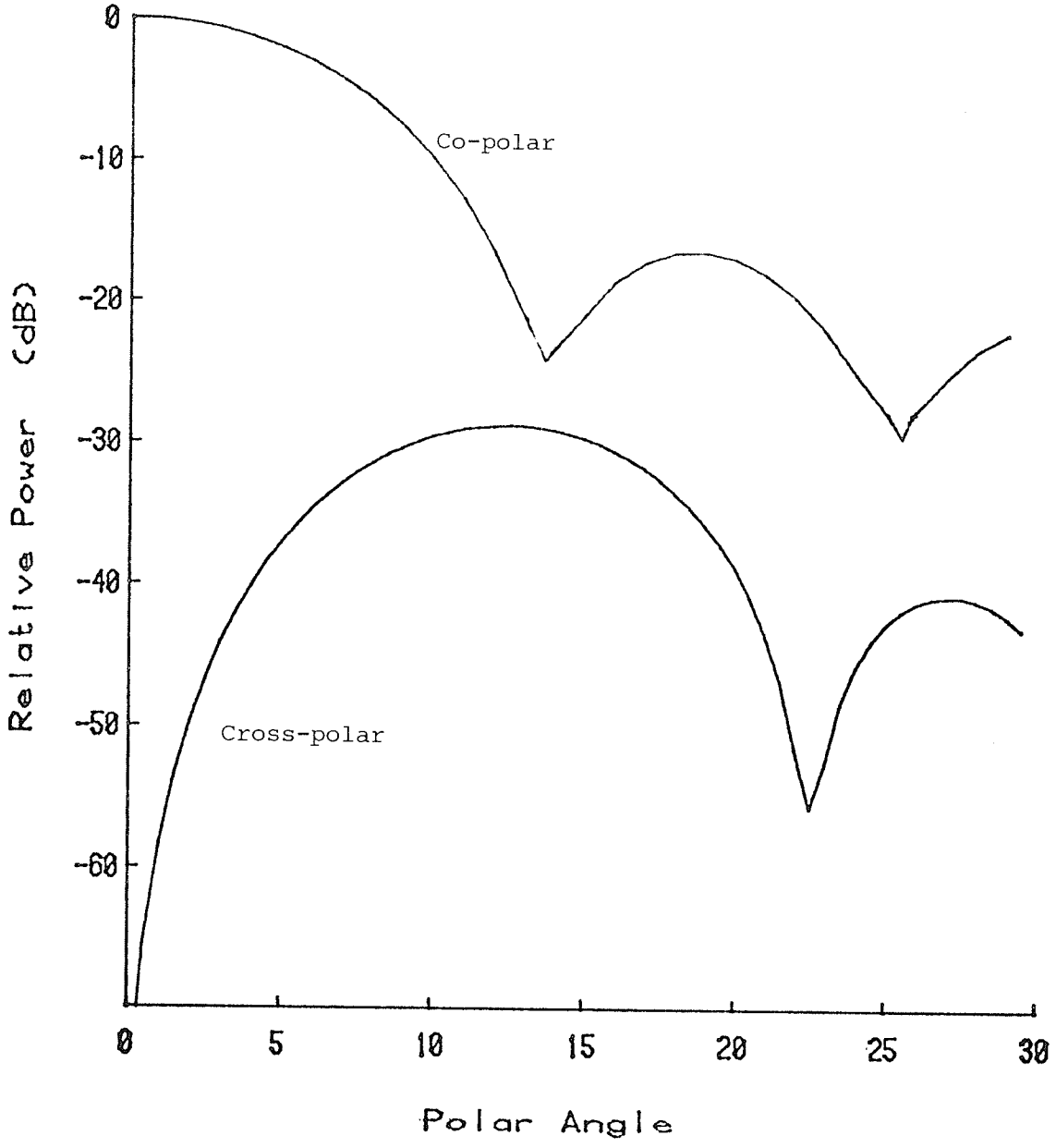

Fig. 5.14 Co-polar and cross-polar radiation patterns of a Huygens' source in the presence of a Luneberg lens; Diameter D = 5λ

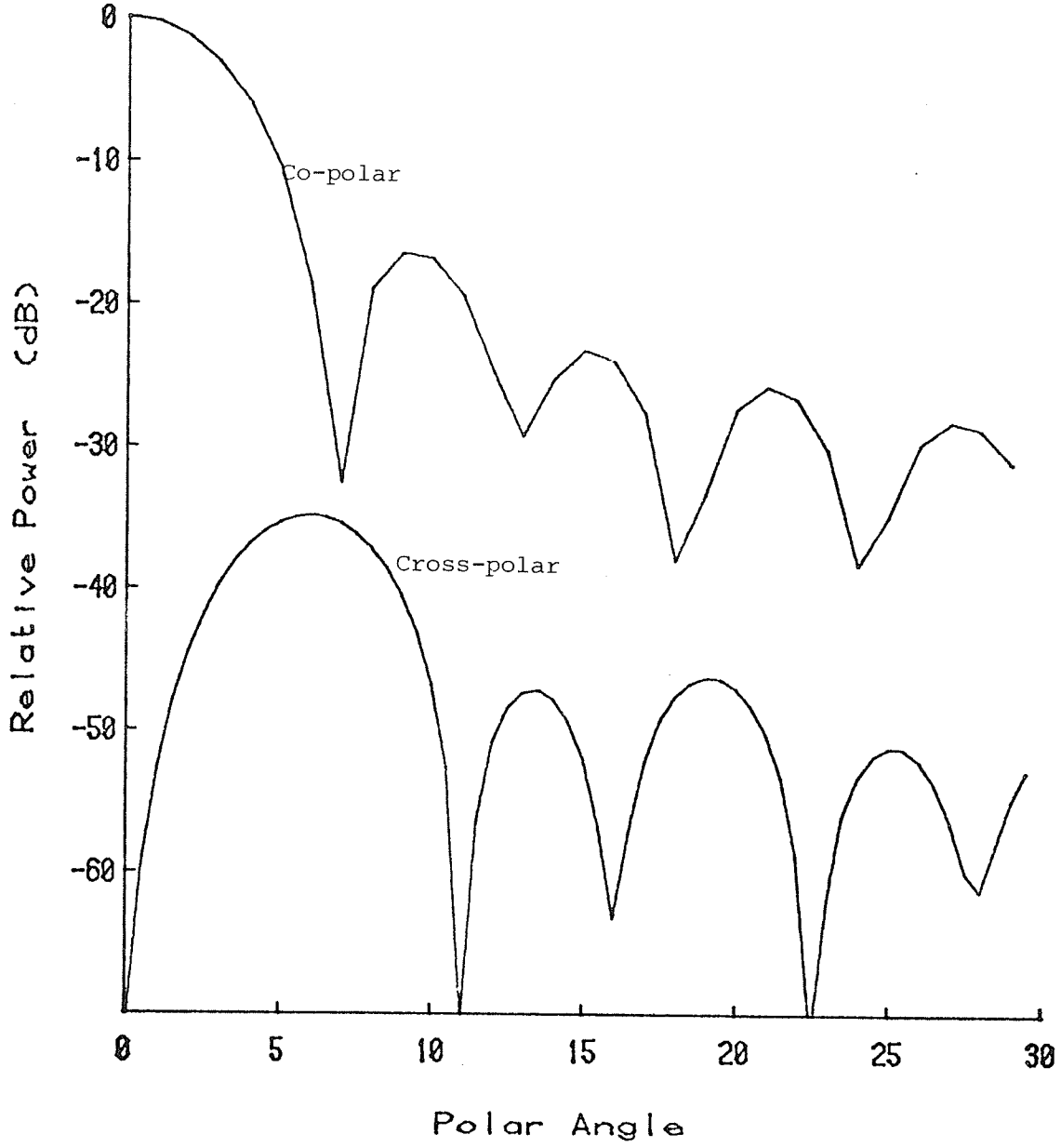

Fig. 5.15 Co-polar and cross-polar radiation patterns of a Huygens' source in the presence of a Luneberg lens; Diameter D = 10λ

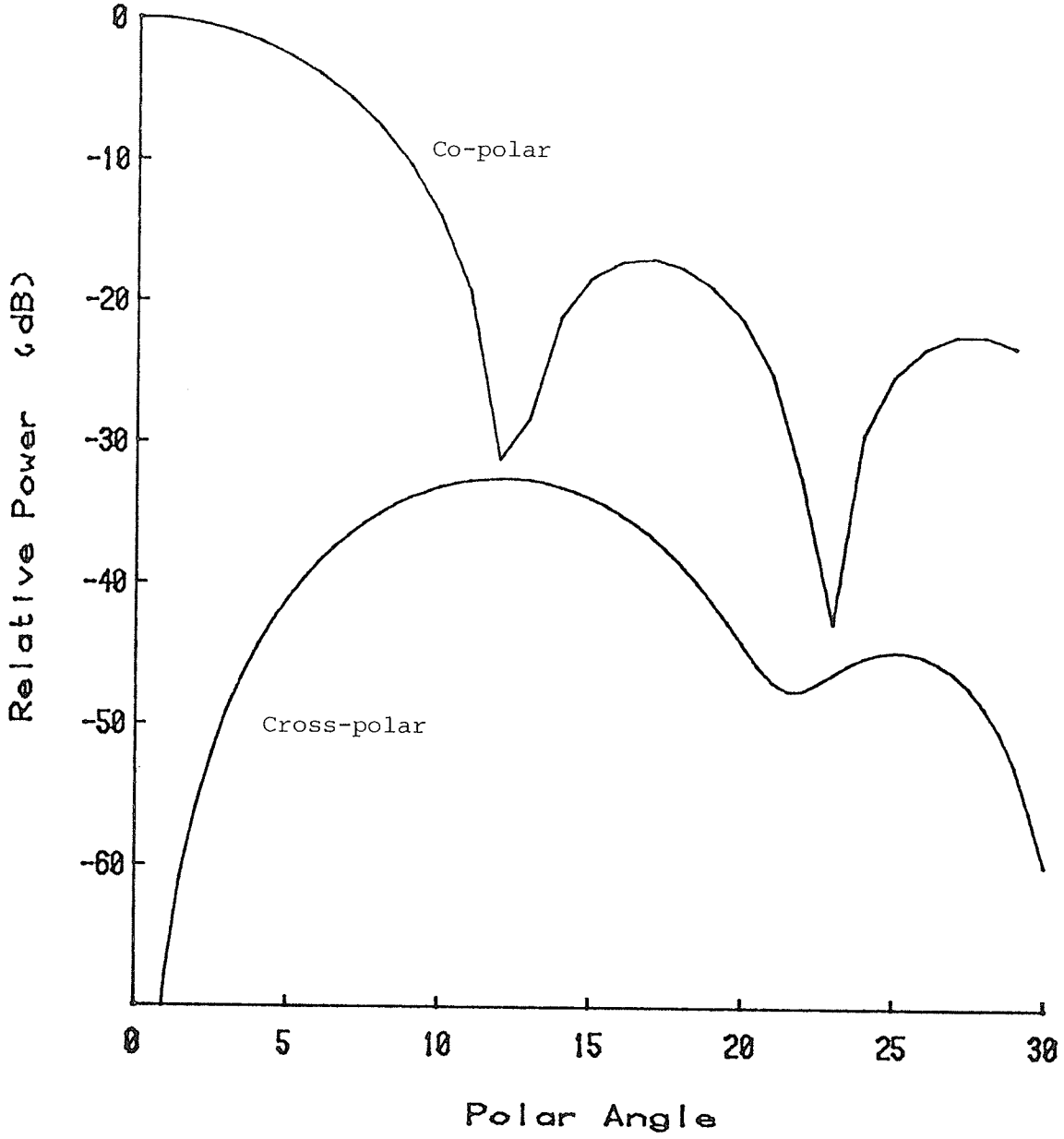

Fig. 5.16 Co-polar and cross-polar radiation patterns of a Huygens' source in the presence of a modified Luneberg lens; D = 5λ

CHAPTER 6

CONCLUSION

6.1 Summary of the Results

A solution for the electromagnetic fields in the presence of a radially stratified spherical lens was used to study the radiation characteristics of Luneberg lenses. The distribution of the total power among the modes and the directivity of the lens, as a function of its size, were examined. It was found that a Luneberg lens does not exhibit the resonant property of a homogeneous sphere and the modal power distribution shows a smoother behaviour. Furthermore, the percentage power content of the higher order modes reduced rapidly beyond a certain mode number $M \simeq ka - 1$, where a is the lens radius and k is the propagation constant of the wave. Similarly, the directivity of a Luneberg lens showed a smooth variation with the lens size and asymptotically approached the directivity of a uniformly illuminated aperture. However, at the low frequency end it decreased continuously below that of a uniformly illuminated aperture.

To enhance the directivity of the lens at low freqeuncies three new lens profiles were considered. Their permittivity profiles were assumed similar to a Luneberg lens, but with larger average dielectric constants. Examination of the radiation characteristics of the modified Luneberg lenses indicated that their focusing properties can be controlled by modifying their dielectric profile, but generally, showed better directivities at low frequencies than a standard Luneberg lens. The electromagnetic field solution of these modified lenses were

obtained by utilizing the spherical wave expansion method, which was developed to account for the assumed variations of the dielectric profiles.

The performance of a Luneberg lens with a practical source antenna was also investiaged. We represented an open-ended rectangular waveguide, by a rectangular array of Huygens' sources. It was shown that by modifying the number of Huygens' source elements the radiation characteristics of any waveguide radiator can be satisfactorily represented. Using this representation the radiation characteristics of both standard and modifed Luneberg lenses, illuminated by a waveguide radiator were studied.

To examine the quality of the radiated field both co-polar and cross-polar radiations were presented. It was shown that the Luneberg lens generally produced a high quality radiation with a relatively low level of cross-polarization. It was also found that the radiation patterns of the modified Luneberg lenses have lower side lobe levels and produce more symmetrical patterns. This latter property resulted in low cross-polar radiation level for the modified lens.

6.2 Suggestions for Further Work

1. All through the present and previous investigations, only the case of a lossless Luneberg lens has been considered. It may be interesting to study the effect of introducing a loss factor into the dielectric constant and study its impact on the radiation characteristics of the lens.

2. We have attributed the increase of the directivity of the modified Luneberg lens to the increase of the average permittivity of the lens. However, the investigation of the near field may also shed some light on the improved behaviour of the modified lens. Such a study may indicate the degree of field concentration at the focal point and show the actual location of the focal point that an exciting source may be located to yield a better radiation field.

REFERENCES

1. Born, M. and Wolf, E., "Principles of Optics," Pergamon Press, Oxford, 1959.

2. Braun, E.N., "Radiation Characteristics of the Spherical Luneberg lens," IRE, Trans. Antennas and Propagation, AP4, P132, 1956.

3. Brown, J., "Microwave Wide Angle Scanner," Wireless Eng., Vol. 30, No. 10, P250, 1953.

4. Buckley, E.F., "Stepped-Index Luneberg Lenses," Electronic Design, P86, April 13, 1960.

5. Croswell, W.F. and Chatterjee, J.S, "Waveguide Excited Dielectric Spheres as Feeds," IEEE Trans. Antenna and Propagation," AP-20, P206, 1972.

6. Croswell, W.F. Chatterjee, J.S., Mason, V.B. and Tai, C.T., "Radiation from a Homogeneous Sphere Mounted on a Waveguide Aperture," IEEE Trans. Antenna and Propagation, AP-23, P647, 1975.

7. Daniele, V., Uslenghi, P.L.E. and Zich, R., "A Note on the Generalized Luneberg lenses," Estratto da'Alta Frequenza, vol. 39, no. 5, P5400, 19700.

8. Eaton, T.E., "An Extension of the Luneberg-type Lenses," Naval Research Lab, Report 4110, 1953.

9. Garbacz, R.J., "Electromagnetic Scattering by Radially Inhomogeneous Spheres," Antenna Lab, Ohio State University, Columbus, Report No. 1223-3.

10. Gunderson, L.C. and Holmes, G.T., "A Microwave Luneberg Lens", Appl. Optics, vol. 7, P801, 1968.

11. Gunderson, L.C. and Kaufman, J.F., "A High Temperature Luneberg Lens," Proceedings of the IEEE, no. 56, P883, 1968.

12. Gutman, A.S., "Modified Luneberg Lens," J. Appl. Phys., vol. 25, no. 7, P855, 1954.

13. Hizal, A. and Tosun, H., "State-Space Formulation of Scattering with Applications to Spherically Symmetric Objects," Can. J. Phys., 51, P549, 1973.

14. Huynen, J.R., "Theory and Design of a Class of Luneberg Lenses", IRE Wescon Convention Records, 2, 1958.

15. Jasik, H., "Antenna Engineering Handbook," McGraw-Hill Book Co., 1959.

16. Jasik, N., "The Electromagnetic Theory of the Luneberg Lens," Dissertation, Dept. of Electrical Engineering, Polytechnical Institute of Brooklyn, New York, 1954.

17. Kay, A.F., "Spherically Symmetric Lenses," IRE Trans. Antenna and Propagation, AP-7, P32, 1959.

18. Kemble, E.C., "Fundamental Principles of Quantum Mechanics," McGraw-Hill Book Co., 1937.

19. Ludwig, A.C., "The Definition of Cross-Polarization," IEEE Trans. Antenna and Propagation, AP-21, P116, 1973.

20. Luneberg, R.K., "Mathematical Theory of Optics," University of California Press, 1966.

21. Ma, M.T., "Theory and Application of Antenna Arrays," John Wiley and Sons, 1973.

22. Morgan, S.P., "General Solution of the Luneberg Lens Problem," Journal of Applied Physics, vol. 29, no. 9, P1358, 1958.

23. Onoe, M., Hasebe, N. and Zama, T., "Radar Reflector with Controllable Reflection," Trans. Inst. Electron. and Commun. Eng. Japan, vol. E63, no. 3, P227, 1980.

24. Peeler, G.O.M. and Archer, O.H., "A Two-dimensional Microwave Luneberg Lens," Naval Research Lab, Rept. 4115, 1953.

25. Peeler, G.O.M. and Colman, H.P., "Microwave Stepped-Index Luneberg Lenses," IRE Trans. Antennas and Propagation, AP-6, P202, 1958.

26. Peeler, G.O.M., Kelleher, K.S. and Coleman, H.P., "Virtual Source Luneberg Lenses," Naval Research Lab, Rept. 4194, 1953.

27. Rainville, E.D., Intermediate Differential Equations," MacMillan Book Co., 1964.

28. Rinehand, R.F., "A Solution of the Rapid Scanning Problem for Radar Antenna," J. Appl. Phys., vol. 19, P868, 1948.

29. Rozenfeld, P., "The Electromagnetic Theory of Three-Dimensional Inhomogeneous Lenses," IEEE Trans. Antennas and Propagation, AP-1976.

30. Ryan, C.E. Jr., and Cain, F.L., "Design Consideration for the Constant Index Lenses," Abst. 21st Annual Symp. USAF Antenna Res. and Dev. Prog., U. of Illinois.

31. Sarap, B.K. and Bhattacharya, P.K., "Radiation Pattern of Open-Ended Waveguide Fed Luneberg Lens," J. Instn. Electronics and Telecom. Engrs., vol. 21, no. 11, P594, 1975.

32. Shafai, L., "Scattering by Spherically Symmetric Objects," Can. J. Phys., vol. 50, P749, 1972.

33. Tai, C.T., "The Electromagnetic Theory of the Spherical Luneberg Lens," Appl. Sci. Res., Section B, vol. 7, P113, 1958.

34. Silver, S., "Microwave Antenna Theory and Design," Dover Publications, 1965.

35. Warren, F.G.R. and Pinnell, S.G.A., "Tin Hat Scanning Antennas," RCA Victor Co., Montreal, Canada.

36. Webiter, R.E., "Radiation Patterns of a Spherical Luneberg Lens with Simple Feeds," IRG Trans. Antennas and Propagation, AP-6, P301, 1958.

37. "IEEE Standard Definition of Terms for Antennas", IEEE Trans. Antennas and Propagation, vol. AP-17, P262, 1969.